공학박사 학위논문

Development of 3D CFD models and observation system design for wind environment assessment over a clear-cut in mountainous region

산악지역 내 개벌지 풍환경 평가를 위한 3차원 CFD 모델 개발과 관측시스템 설계

2018년 2월

서울대학교 대학원

생태조경·지역시스템공학부 지역시스템공학전공

하 태 환

Development of 3D CFD models and observation system design for wind environment assessment over a clear-cut in mountainous region

산악지역 내 개벌지 풍환경 평가를 위한 3차원 CFD 모델 개발과 관측시스템 설계

지도 교수 이 인 복

이 논문을 공학박사 학위논문으로 제출함

2018년 2월

서울대학교 대학원

생태조경·지역시스템공학부 지역시스템공학전공

하 태 환

하태환의 공학박사 학위논문을 인준함

2018년 2월

위 원 장 _____ (인)

부위원장 _____ (인)

위 원 _____ (인)

위 원 _____ (인)

위 원 _____ (인)

DEVELOPMENT OF 3D CFD MODELS AND OBSERVATION SYSTEM DESIGN FOR WIND ENVIRONMENT ASSESSMENT OVER A CLEAR-CUT IN MOUNTAINOUS REGION

A DISSERTATION

SUBMITTED TO THE DEPARTMENT OF LANDSCAPE ARCHITECTURE AND RURAL SYSTEMS ENGINEERING AND THE COMMITTEE ON GRADUATE STUDIES OF SEOUL NATIONAL UNIVERSITY IN PARTIAL FULFILLMENT OF THE REQUIREMENTS FOR THE DEGREE OF

DOCTOR OF PHILOSOPHY

BY

TAEHWAN HA

FEBRUARY 2018

I certify that I have read this dissertation and that in my opinion it is fully adequate, in scope and quality, as dissertation for the degree of Doctor of Philosophy.

Chairman

I certify that I have read this dissertation and that in my opinion it is fully adequate, in scope and quality, as dissertation for the degree of Doctor of Philosophy.

Vice-Chairman

I certify that I have read this dissertation and that in my opinion it is fully adequate, in scope and quality, as dissertation for the degree of Doctor of Philosophy.

I certify that I have read this dissertation and that in my opinion it is fully adequate, in scope and quality, as dissertation for the degree of Doctor of Philosophy.

I certify that I have read this dissertation and that in my opinion it is fully adequate, in scope and quality, as dissertation for the degree of Doctor of Philosophy.

Abstract

Installation of meteorological observation system in mountain region is important to aid effective monitoring of mountainous meteorology, predictions of mountain disasters such as fires and landslides, and the dispersion of pollutants or airborne viruses. International organizations, which include the World Meteorological Organization (WMO) and the Canadian Forest Sservice (CFS) recommend that weather observation system in mountain area should be located in clear-cut area where forest cover has been cleared or felled, and the distance from the system to any obstacle should be more than 10 times greater than maximum height of any nearby trees. In addition, the height of an anemometer to monitor wind environment in mountain region should be at least 10 m higher than the tallest trees, when the construction of clear-cut was limited. In addition, there is a method to install the meteorological observation system on the flat land in the Republic of Korea, but there are no installation standards of a mountain meteorological observation system.

In case of the installation methods of international standards, excessively wide clear-cuts are difficult to find and tall observation masts cost more and may not be as safe as 10 m mast. Therefore, research to determine an appropriate installation methods for the meteorological observation system in mountain region in the Republic of Korea should be conducted. Because of limitations of a field experiment such as difficulty to acquire results due to unstable and unpredictable environmental conditions, high time- and labor costs, and a great deal of capital for a variety of experimental conditions, many researchers have used computational fluid dynamics (CFD).

In this thesis, as a first step, comprehensive literature reviews on “Meso-scale numerical weather prediction modelling”, “Micro-scale numerical weather prediction modelling” and “Air resistance of trees” were intimately conducted to build the foundation and to suggest the appropriateness of the study

In Chapter 3, a 3D micro-scale CFD model was developed in order to simulate the wind environment in mountain region using ANSYS, one of the generally used commercial CFD software, and proposed methods to apply the air resistance of trees to the CFD model. Proposed methods of applying air resistance of trees using commercial CFD software were a method of designing canopy regions of trees that is distributed in mountain terrain while designing the CFD model and a method of using a UDF (user defined function) in a computation process of the CFD model without dividing canopy regions of trees. Because the method of dividing the canopy regions of the trees was distorted about the boundary of forest regions in process of designing the CFD model, it was determined that it is appropriate to apply the air resistance coefficient of the trees to meshes where the canopy regions are located using the UDF.

In Chapter 4, a 3D micro-scale open-source CFD model was also developed in order to simulate the wind environment in mountain region using OpenFOAM, one of the generally used open-source CFD software, and proposed a method to apply the air resistance of trees to the open-source CFD model. First of all, a 3D mountain topography model was designed without dividing domains for the forest regions distributed in the target area. The air resistance coefficients of the trees were applied to each group of meshes corresponding to the forest region of the designed open-source CFD model using developed code. The CFD simulation models developed in Chapter 3 and 4 were validated using the wind environment data monitored in the

field and the reliability of the CFD models were secured.

In Chapter 5, appropriate installation methods of meteorological observation system in mountain region according to the type of trees, the air-resistance of trees, the tree height, the size of the clear-cut, etc. were proposed based on analysis of wind environment in the clear-cut. In addition, conversion factors for estimating the reference wind speed which is not influenced by the surrounding trees, was derived in order to compensate the cases of not satisfying the appropriate height of the meteorological observation system and the size of the clear-cut in mountain region.

Keywords : Clear-cut, Mountainous region, Observation system design, Open-source CFD, Tree porosity, Wind environment

Student Number : 2014-30403

Contents

Chapter 1. Introduction 1

1.1. Study Background 1

1.2. Objective of thesis 4

Chapter 2. Literature review 6

2.1. Numerical weather prediction 6

2.1.1. Meso-scale numerical weather prediction modelling 7

2.1.2. Micro-scale numerical weather prediction modelling 14

2.2. Air resistance of trees 20

Chapter 3. Development of a micro-scale CFD model to predict wind environment on mountain terrain using a commercial CFD package 28

3.1. Introduction 28

3.2. Materials and methods 28

3.2.1. The study area 28

3.2.2. Computational fluid dynamics (CFD) 30

3.2.3. Porosity of the trees 32

3.2.4. Modelling procedure 36

3.2.4.1. Topographical modelling 36

3.2.4.2. Tree porosity modelling 38

3.2.4.2.1. Porosity modelling using separated geometry volume based on forest type classification 39

3.2.4.2.2. Porosity modelling using a UDF code based on a digitized forest type classification 41

3.2.4.3. Methodology for validation of the CFD model 43

3.3. Results and discussions 45
3.3.1. Wind environment analysis of the study area 45
3.3.2. Validation of the CFD simulation model 47
3.3.2.1. Horizontal wind verification 47
3.3.2.2. Vertical wind verification 50
3.4. Conclusions 53
Chapter 4. Development of a micro-scale CFD model to predict wind environment in mountain terrain using an open-source CFD package 54
4.1. Introduction 54
4.2. Materials and methods 55
4.2.1. The study area 55
4.2.2. Experimental trees for evaluating porosity coefficient 56
4.2.3. Open-source CFD 57
4.2.4. Experimental procedure 60
4.2.4.1. Evaluating the inertial resistance coefficient of trees 61
4.2.4.2. Design of 3D open-source CFD model 64
4.2.4.3. Methodology for validation of the open-source CFD model 68
4.3. Results and discussions 71
4.3.1. Inertial resistance coefficient of experimental trees 71
4.3.2. Validation of the open-source CFD model 74
4.4. Conclusions 78
Chapter 5. Recommendation of installation method for meteorological observation system in mountain region based on open-source CFD simulations 79

5.1. Introduction 79

5.2. Materials and methods 79

5.2.1. Design of open-source CFD model for suggesting the appropriate installation method 79

5.2.2. CFD simulation cases for evaluating the appropriate installation method 81

5.3. Results and discussions 83

5.3.1. Wind environment in clear-cut according to type of tree 86

5.3.2. Wind environment in clear-cut according to the inertial resistance coefficient of the canopy 90

5.3.3. Proper height for wind environment monitoring 98

5.3.4. Conversion factor for the reference wind speed 105

5.4. Conclusions 123

Chapter 6. Summary and concluding remarks 124

6.1. Summary 124

6.2. Concluding remarks 127

References 129

Appendix I. UDF code for porosity modelling of FLUENT 137

Appendix II. OpenFOAM codes 141

A. System 141

A.1. blockMeshDict 141

A.2. controlDict 144

A.3. decomposeParDict 145

A.4. fvSchemes 146

A.5. fvSolution 148

A.6. meshQualityDict 150
A.7. sampleDict 152
A.8. snappyHexMeshDict 153
A.9. surfaceFeatureExtractDict 162
A.10. topoSetDict 164
B. constant 166
B.1. porosityProperties 166
B.2. transportProperties 169
B.3. turbulenceProperties 170
C. boundary conditions and initial conditions 171
C.1. ABLConditions 171
C.2. initialConditions 171
C.3. epsilon 172
C.4. k 174
C.5. nut 176
C.6. p 178
C.7. U 180
국 문 초 록 182

List of Figures

Figure 1 PM_{10} emission distribution (a) and simulated PM_{10} concentration in Beijing in July (b) and August (c) 2008 (Cheng et al., 2007)..... 9

Figure 2 Surface wind field at 2100 UTC 6 September 2002 using MC2 model with 0.25° resolution (a) and MC2 model with 0.167° resolution (b) (Ren and Perrie, 2006) 10

Figure 3 Spatial distribution change of simulated precipitation (mm day^{-1}) and temperature (°C) for spring (Cabré et al., 2016)..... 11

Figure 4 Averaged air temperature (a) and wind velocity (b) simulated by WRF (1, 5-12, 14 August 2007) (Takane et al., 2013)..... 13

Figure 5 Satellite image of the study area (left) and 3D computational domain of the developed topographical model (right) (Hong et al., 2011a) ... 16

Figure 6 Satellite photograph showing the wooden area around the livestock farm area (left) and the simplification process using topographical classification. (Seo et al., 2014) 18

Figure 7 Schematic diagram of the field experiment for monitoring wind velocity and stem deflection (Koizumi et al., 2010) 25

Figure 8 Schematic diagram of the wind tunnel experiment with measurement points at windward and leeward (Bitog et al., 2011)..... 26

Figure 9 Variation of shape of the Emerald Cedar (a ~ e) and Japanese Holly (f ~ i) according to pruning. (a) initial shape of the Emerald Cedar, (b) 1st pruning of the Emerald Cedar, (c) 2nd pruning of the Emerald Cedar, (d) 3rd pruning of the Emerald Cedar, (e) 4th pruning of the Emerald Cedar, (f) initial shape of the Japanese Holly, (g) 1st pruning of the Japanese Holly, (h) 2nd pruning of the Japanese Holly, (i) 3rd pruning of the Japanese Holly (Cao et al., 2012) 27

Figure 10 (a) Satellite image of the study area and (b) the contour image of the study area. 29

Figure 11 Points at which tree heights were measured near the GCK (left) and GDK (right) towers 30

Figure 12 Simulation procedure of a 3D CFD modelling 31

Figure 13 Calculated inertial resistance coefficient according to the conifer tree density using raw data from Bitog et al. (2012) 34

Figure 14 Research process for this study of the development of a micro-scale 3D CFD model 36

Figure 15 Design procedure for the 3D complex topography CFD model 38

Figure 16 Two methods for simulating a pressure drop by tree porosity 39

Figure 17 Land use classification of study area (left) and simplified land use classification (right)..... 40

Figure 18 (a) Forest type map of the target region provided by the Korea Forest Service (KFS), (b) surface classification of the target region according to tree type, (c) digitized surface classification data converted to 5 m grid size (each black has 5 m ×5 m gr id size) with red box area of (b) enlarged, (d) image applied forest type in the 3D CFD model using the UDF. 41

Figure 19 Flow chart for the procedure for the implementation of the tree porosity to CFD model. 43

Figure 20 Wind environments of (a) GCK tower and (b) GDK tower in 2015.. 45

Figure 21 (a) Normalized wind speed distribution at GCK tower according to the height of the anemometers in a west wind condition, (b) normalized wind speed distribution at GCK tower according to the height of the anemometers in an east wind condition. 46

Figure 22 (a) Picture looking west direction from the GCK tower, (b) picture looking east direction from the GCK tower. 47

Figure 23 (a) Comparison of the measured wind speed and the simulated wind speed according to the height of anemometers in a west wind condition, (b) Comparison of the measured wind speed and the simulated wind speed according to the height of anemometers in an east wind condition..... 52

Figure 24 (a) Forest type map of the target region provided by the Korea Forest Service (KFS), (b) forest type map of the study area reclassified as coniferous forest, deciduous forest, and mixed forest. 56

Figure 25 (a) Picture of coniferous tree (Abies holophylla) which was used to field experiment (37°46′01.8″N, 127°10′45.7″E), (b) Picture of deciduous tree (Quercus serrata) which was used to field

experiment(37°46′01.8″N, 127°10′45.7″E)..... 57

Figure 26 Simulation procedure of a 3D open-source CFD modelling..... 59

Figure 27 Simulation case structure of the OpenFOAM..... 60

Figure 28 (a) Experimental schematic side view, (b) experimental schematic top view, (c) experimental pictures for evaluating air-resistance of the coniferous tree and (d) the deciduous tree..... 62

Figure 29 CFD simulation domain for deriving inertial resistance coefficient of experimental trees, where H is the tree height..... 64

Figure 30 OpenFOAM code for design a primary grid..... 64

Figure 31 OpenFOAM code to extract feature lines..... 65

Figure 32 design procedure of 3D complex terrain CFD model using OpenFOAM CFD package..... 66

Figure 33 3D complex terrain CFD models for grid independence test (mesh size near the interested experimental ground surface: (a) 3.12 m, (b) 6.25 m, and (c) 12.5 m))..... 66

Figure 34 OpenFOAM code of 'topoSetDict' function to set the forest region. 68

Figure 35 Measured wind speed reduction according to wind speed of windward by field experiment during August 10 to September 6 (a : Coniferous tree 1, b : coniferous tree 2, c : deciduous tree 1, d : deciduous tree 2)..... 71

Figure 36 Relationship between the wind speed reduction ration (α) and inertial resistance coefficient (C_i) of tree..... 73

Figure 37 Results of grid independence test of the 3D open-source CFD model under the west wind condition..... 75

Figure 38 Results of grid independence test of the 3D open-source CFD model under easterly wind conditions..... 76

Figure 39 Schematic diagram of the 3D open-source CFD model; (a) top view of the model, (b) side view of the deciduous case, and (c) side view of the coniferous case..... 81

Figure 40 Vertical distribution of wind speed when the height of tree was 30 m

according to type of tree; (a) Coniferous tree, (b) Deciduous tree (shaded green region was the canopy of the tree region) 89

Figure 41 Vertical distribution of wind speed when the height of the coniferous tree was 30 m using an inertial resistance coefficient of (a) 0.3 m^{-1}, (b) 0.5 m^{-1}, and (c) 0.7 m^{-1} 91

Figure 42 Vertical distribution of wind speed when the height of the deciduous tree was 30 m using an inertial resistance coefficient of (a) 0.3 m^{-1}, (b) 0.5 m^{-1}, and (c) 0.7 m^{-1} 95

Figure 43 Appropriate height for wind environment monitoring when the inertial resistance coefficient of the coniferous tree was 0.3 m^{-1}. 99

Figure 44 Appropriate height for wind environment monitoring when the inertial resistance coefficient of the deciduous tree was 0.3 m^{-1}. 99

Figure 45 Appropriate height for wind environment monitoring when the inertial resistance coefficient of the coniferous tree was 0.5 m^{-1}. .. 102

Figure 46 Appropriate height for wind environment monitoring when the inertial resistance coefficient of the deciduous tree was 0.5 m^{-1}. ... 102

Figure 47 Appropriate height for wind environment monitoring when the inertial resistance coefficient of the coniferous tree was 0.7 m^{-1}. .. 103

Figure 48 Appropriate height for wind environment monitoring when the inertial resistance coefficient of the deciduous tree was 0.7 m^{-1}. ... 103

Figure 49 Appropriate height for wind environment monitoring when the inertial resistance coefficient of the coniferous tree was 0.9 m^{-1}. .. 104

Figure 50 Appropriate height for wind environment monitoring when the inertial resistance coefficient of the deciduous tree was 0.9 m^{-1}. ... 104

Figure 51 Vertical distribution of wind speed when the inertial resistance of coniferous tree was 0.3 m^{-1} with 50 m clear-cut; (a) wind speed at boundary condition of inlet : 1.0 m s^{-1}, (b) 3.0 m s^{-1}, and (c) 6.0 m s^{-1}, and normalized vertical wind speed when the inertial resistance of coniferous tree was 0.3 m^{-1} with 50 m clear-cut; (d) wind speed at boundary condition of inlet : 1.0 m s^{-1}, (e) 3.0 m s^{-1}, and (f) 6.0 m s^{-1} 106

Figure 52 CFD modeling for wind environment simulation over mountainous region..... 124

List of Tables

Table 1 Characteristics of meso-scale numerical weather prediction modelling and micro-scale numerical weather prediction modelling..... 6

Table 2 Summary of the ARPS, MC2, MM5, and WRF meso-scale models..... 8

Table 3 Summary of the micro-scale numerical weather prediction modelling for simulation of airflow over complex terrain. 15

Table 4 Drag coefficient of various coniferous trees from various studies..... 22

Table 5 Drag coefficient of various deciduous trees from various studies..... 23

Table 6 Characteristics of tree of the study area 30

Table 7 The measured data from the GCK and GDK towers when wind boundary condition was an east wind considering 95% confidence interval (C.I.). 48

Table 8 The simulated results of the CFD model according to various turbulence models when the wind boundary condition was an east wind. 48

Table 9 The measured data from the GCK and GDK towers when wind boundary condition was an west wind considering 95% confidence interval (C.I.). 49

Table 10 The simulated results of the CFD model according to various turbulence models when the wind boundary condition was an west wind. 50

Table 11 summary of commercial CFD and open-source CFD 54

Table 12 Input data of the 3D open-source CFD model..... 70

Table 13 Wind speed reduction derived from the CFD simulation according to inertial resistance coefficient and wind speed of the windward side (wind speed of windward side – wind speed of leeward side)..... 72

Table 14 Inertial resistance coefficient of coniferous tree and deciduous tree... 74

Table 15 RMSE of turbulence model test of the 3D open-source CFD model under the west wind condition 75

Table 16 RMSE of turbulence model test of the 3D open-source CFD model under easterly wind conditions..... 77

Table 17 Threshold values of the mesh quality and finally designed mesh quality of 3D open-source CFD model. 80

Table 18 Experimental cases for the 3D open-source CFD simulation..... 82

Table 19 Recommended height of the anemometer for observing wind environment located in small clear-cut (Lawson and Armitage, 2008). 83

Table 20 Simulated reference wind speed (m s^{-1}) at the reference height (H + 10 m) according to the type of tree and the inertial resistance coefficient (Ci) of tree 85

Table 21 Simulated wind speeds at the recommended height by the CFS (Table 19) where the inertial resistance coefficient of the deciduous tree canopy was 0.3 m^{-1} (wind speed difference from wind speed at reference height in control condition) 86

Table 22 Simulated wind speeds at the recommended height by the CFS (Table 19) where the inertial resistance coefficient of the coniferous tree canopy was 0.3 m^{-1} (wind speed difference from wind speed at reference height in control condition) 87

Table 23 Simulated wind speeds at the recommended monitoring height by the CFS (Table 19) using an inertial resistance coefficient for a coniferous canopy of 0.5 m^{-1} (wind speed difference from wind speed at reference height in control conditions)..... 92

Table 24 Simulated wind speeds at the recommended monitoring height by the CFS (Table 19) using an inertial resistance coefficient for a coniferous canopy of 0.7 m^{-1} (wind speed difference from wind speed at reference height in control conditions)..... 93

Table 25 Simulated wind speeds at the recommended monitoring height by the CFS (Table 19) using an inertial resistance coefficient for a coniferous canopy of 0.9 m^{-1} (wind speed difference from wind speed at reference height in control conditions)..... 94

Table 26 Simulated wind speeds at the recommended monitoring height by the CFS (Table 19) using an inertial resistance coefficient for a

deciduous canopy of 0.5 m^{-1} (wind speed difference from wind speed at reference height in control conditions)..... 95

Table 27 Simulated wind speeds at the recommended monitoring height by the CFS (Table 19) using an inertial resistance coefficient for a deciduous canopy of 0.7 m^{-1} (wind speed difference from wind speed at reference height in control conditions)..... 96

Table 28 Simulated wind speeds at the recommended monitoring height by the CFS (Table 19) using an inertial resistance coefficient for a deciduous canopy of 0.9 m^{-1} (wind speed difference from wind speed at reference height in control conditions)..... 97

Table 29 appropriate heights for wind environment monitoring when the inertial resistance coefficient of the coniferous trees was 0.3 m^{-1}.. 100

Table 30 appropriate heights for wind environment monitoring when the inertial resistance coefficient of the deciduous trees was 0.3 m^{-1}... 100

Table 31 Conversion factor (α) for the reference wind speed using observed wind speed at 10 m height using an inertial resistance coefficient for coniferous trees of 0.3 m^{-1} 108

Table 32 Conversion factor (α) for the reference wind speed using observed wind speed at 10 m height using an inertial resistance coefficient for coniferous trees of 0.5 m^{-1} 108

Table 33 Conversion factor (α) for the reference wind speed using observed wind speed at 10 m height using an inertial resistance coefficient for coniferous trees of 0.7 m^{-1} 109

Table 34 Conversion factor (α) for the reference wind speed using observed wind speed at 10 m height using an inertial resistance coefficient for coniferous trees of 0.9 m^{-1} 109

Table 35 Conversion factor (α) for the reference wind speed using observed wind speed at 10 m height using an inertial resistance coefficient for deciduous trees of 0.3 m^{-1}..... 110

Table 36 Conversion factor (α) for the reference wind speed using observed wind speed at 10 m height using an inertial resistance coefficient for deciduous trees of 0.5 m^{-1}..... 110

Table 37 Conversion factor (α) for the reference wind speed using observed wind speed at 10 m height using an inertial resistance coefficient for deciduous trees of 0.7 m^{-1}..... 111

Table 38 Conversion factor (α) for the reference wind speed using observed wind speed at 10 m height using an inertial resistance coefficient for deciduous trees of 0.9 m^{-1} 111

Table 39 Constants of polynomial regression equation of normalized wind speed for the height when the height of coniferous tree was 10 m 113

Table 40 Constants of polynomial regression equation of normalized wind speed for the height when the height of coniferous tree was 15 m 114

Table 41 Constants of polynomial regression equation of normalized wind speed for the height when the height of coniferous tree was 20 m 115

Table 42 Constants of polynomial regression equation of normalized wind speed for the height when the height of coniferous tree was 25 m 116

Table 43 Constants of polynomial regression equation of normalized wind speed for the height when the height of coniferous tree was 30 m 117

Table 44 Constants of polynomial regression equation of normalized wind speed for the height when the height of deciduous tree was 10 m. 118

Table 45 Constants of polynomial regression equation of normalized wind speed for the height when the height of deciduous tree was 15 m. 119

Table 46 Constants of polynomial regression equation of normalized wind speed for the height when the height of deciduous tree was 20 m. 120

Table 47 Constants of polynomial regression equation of normalized wind speed for the height when the height of deciduous tree was 25 m. 121

Table 48 Constants of polynomial regression equation of normalized wind speed for the height when the height of deciduous tree was 30 m. 122

Chapter 1. Introduction

1.1. Study Background

Over 65% of the Republic of Korea's territory is forestland, and the atmospheric environment over mountain areas is characterized by different phenomena as compared to flatlands, due to the airflow resistance of forest and its dynamic changes in topography and altitude. The Korean government plans to construct 200 mountain meteorological observation systems until 2017. Using these, the Korean government expects to provide better information about mountain weather and to aid effective predictions of mountain disasters such as fires and landslides, and the dispersion of pollutants or airborne viruses. The Weather Observation Standardization Act of the Republic of Korea was revised in 2017, and methods for installation of meteorological observation system in the flatlands were addressed in the enforcement ordinance. However, despite the increasing numbers of meteorological observation system located in mountain areas, no standards exist for the installation of a mountain meteorological observation system.

International organizations, which include the World Meteorological Organization (WMO) and the Canadian Forest Service (CFS) recommend that weather observation system in mountain area should be located in clear-cut area where forest cover has been cleared or felled, and the distance from the system to any obstacle should be more than 10 times greater than maximum height of any nearby obstacles (Jarraud, 2008; NRFA, 2010). The Canadian guidelines for a Remote Automated Weather Station (RAWS) have a standard similar to those recommended for a weather observation system in mountain areas by the WMO, but

additional standards for an observation system installed in areas that are not clear-cut. The height of an anemometer to monitor wind environment in mountain region should be at least 10 m higher than the tallest trees (Lawson and Armitage, 2008).

Construction of an excessively wide clear-cut or a tall observation mast are required to install an observation system in mountain area. However, excessively wide clear-cuts are difficult to find and tall observation masts cost more and may not be as safe as 10 m mast. Therefore, research to determine an appropriate location, size, and height for the observation system should be conducted, because no criteria for assessing the installation method exist. It is possible to use empirical data measured in field experiment, but field experiments have critical limitations; 1) results are difficult to acquire due to unstable and unpredictable environmental conditions, 2) experimental conditions are difficult to change once the experiment has been set up, 3) time- and labor- costs are high, and 4) a great deal of capital is necessary for a variety of experimental conditions such as the location and height of observation system and size of the clear-cut (Bournet et al., 2010; Kwon et al., 2015; Li et al., 2006). Compared to a field experiment, a numerical simulation such as Computational Fluid Dynamics (CFD) has the following advantages; 1) relatively low cost to investigate various experimental conditions, 2) experiments can be easily repeated, again with a low cost and within a short time, 3) a quantitative and qualitative visualization of an invisible air flow pattern is possible, and 4) results under hypothetical experimental conditions can be predicted (Hong et al, 2011; Kim and Baik, 1999, 2001; Liu and Barth, 2002; Seo et al., 2015; Sini et al., 1996; Xueling and Fei, 2005).

Commercial software packages such as CFD-ACE+, CFX, Flow-3D, and Fluent are widely used as tools for CFD simulations. These commercial software

packages have been continuously improved in terms of their GUI interfaces so that users can use them more easily. They also provide pre-processing modules for the design the mesh of domain, main-processors for the numerical analysis, and post-processors for visualizing the simulated result. However, a license fee must be paid in order to use these programs, and massive parallel simulations can often be prohibitively expensive. On the other hand, open-source CFD software such as OpenFOAM has the advantage that there is no license fee for use of the main solver. In addition, thanks to the flexibility of this software, researchers can modify the main solver or develop a new solver for their own purposes.

The results computed by commercial CFD simulation software and by open-source CFD simulation software show similar results because the governing equations for calculating fluid flow are largely the same. Therefore, the commercial CFD simulation software and open-source CFD simulation software can be selectively used according to their respective advantages depending on the purpose of the research.

1.2. Objective of thesis

In this study, high resolution CFD models for mountain topographic terrain were developed using both a commercial CFD simulation package and an open source CFD simulation package in order to more precisely predict the micro-climate in complex forest terrain. Then, a methodology for simulating the air-resistance of the trees distributed in the mountain area was suggested. The developed 3D CFD models were validated by comparison with field data in order to ensure the reliability of the predicted data by the developed CFD models. Finally, the wind environments were analyzed according to various environmental conditions such as the air-resistance of trees, tree height, size of the clear-cut, etc., and proper installation method for mountain meteorological observation system to monitor wind environment was proposed based on the simulated results.

- The thesis is organized into five chapters. As a first step of compromising the mentioned issues, Chapter 2 provides a comprehensive literature review that provides the foundation of the study and highlights to importance of the issues being addressed. The review covers literature on meso-scale weather prediction modelling in order to predict meso-scale weather phenomena with a horizontal resolution of several kilometers, micro-scale weather prediction modelling in order to predict micro-scale weather phenomena with a horizontal resolution of 100 m or less, and the air-resistance effects of trees on airflow.

- Chapter 3 discusses how to develop 3D micro-scale CFD model that simulates the wind environment in complex mountain terrains using commercial CFD simulation

software, and how to apply the air-resistance of trees to the CFD model. The suggested methods to apply air-resistance of the trees into the CFD model are 1) separately designing the canopy region of the trees distributed in the mountain area during the design of the CFD model, and 2) applying the air-resistance of trees in the computation process using user defined function (UDF). The developed 3D CFD model was validated using wind environment data measured in field.

- Chapter 4 follows the same structure as Chapter 3, but focuses on the use of open-source, rather than commercial, CFD models.

- Chapter 5 discusses proper installation method for weather station in mountain region. The wind environment in the clear-cut was analyzed according to various environmental conditions such as the type of trees, the air-resistance of trees, the tree height, the size of the clear-cut, etc. Finally, the appropriate height of anemometer, the size of clear-cut, and the conversion factor that can be used to convert the reference wind speed using the wind speed observed at 10 m were proposed using the analyzed wind environment results by the open-source CFD model.

Chapter 2. Literature review

2.1. Numerical weather prediction

Meso-scale and micro-scale numerical weather prediction modelling can be used to predict weather in mountain terrain. The meso-scale modelling typically analyzes meso-scale meteorological phenomena for several hundreds of kilometers. In particular, the weather research and forecasting (WRF) model has the advantage that prediction results can be derived for various resolutions according to the purpose of the researcher. However, it is limited in terms of meteorological analysis of geographically complex areas such as urban and mountain regions, because the WRF model simulates meteorological phenomena by using relatively large and coarse grids with terrain-following hydrostatic-pressure vertical coordinates. Recently, micro-scale modelling such as computational fluid dynamics (CFD) has been actively used to overcome these limitations. Micro-scale modelling has advantages in that it can analyze the effects of more complex terrain using smaller size grid than those used in meso-scale modelling.

Table 1 Characteristics of meso-scale numerical weather prediction modelling and micro-scale numerical weather prediction modelling

	Meso-scale numerical weather prediction modelling	Micro-scale numerical weather prediction modelling
Time interval	1 hour / day / month	Hz (< a second) ~ seconds
Calculation speed	Fast	Slow
Predictable area	Relatively large	Relatively small
Geometry resolution	Low resolution (Limitations on information to realize)	High resolution (No limitations on information to realize)
Horizontal	3 – 100 km	Less than 100 m

meteorological scale	(Thunder storm, hurricane travel path)	(evaporation, dispersion of pollutant)

2.1.1. Meso-scale numerical weather prediction modelling

Since Bjerknes (1904) suggested new seven equations to determine the future state of the atmosphere, the technique and accuracy of Numerical Weather Prediction (NWP) has greatly improved. During the past two decades, meso-scale numerical modelling techniques have been actively developed, along with the development of computer technology, parallel architecture, and the proliferation of relatively inexpensive, but powerful, high-tech computers (Chow et al., 2012). Recently, various mes-oscale NWP models, such as the Advanced Regional Prediction Systems (ARPS), the Meso-scale Compressible Community model (MC2), the fifth-generation Penn State/NCAR meso-scale model (MM5), the Weather and Research Forecasting model (WRF), have been used to simulate atmospheric flow with a horizontal resolution of less than 10 km (Dudhia, 1993; Hodur, 1997; Xue et al., 2000). Specifically, the WRF model could simulate the atmospheric flow from a synoptic scale to a several-kilometer horizontal scale based on a global model. A WRF model can be used to consider terrain using the hydrostatic pressure vertical coordinate system proposed by Laprise (Laprise, 1992).

Table 2 Summary of the ARPS, MC2, MM5, and WRF meso-scale models.

	ARPS (advanced regional prediction systems)	MC2 (meso-scale compressible community)	MM5 (fifth-generation Penn State/NCAR meso-scale model)	WRF (weather research and forecasting) model
Development	1990	1993	1978	1990s
Model	Nonhydrostatic compressible model	Nonhydrostatic compressible model	Nonhydrostatic and hydrostatic model	Fully compressible Euler nonhydrostatic equations
Horizontal coordinate	Arakawa C-grid	Cartesian coordinate	Staggered grid	Arakawa C-grid
Vertical coordinate	Terrain following z-coordinate	Terrain following z-coordinate	σ-coordinate	η-coordinate
Horizontal resolution	> 1 km	> 1 km	> 5 km	> 1 km
Time interval	> 2 hrs	> 10 minutes	> several hours	> several hours
Purpose	Storm prediction, Simulation of monsoon depression, etc.	Simulation of Typhoon and fog formation, estimation of urban heat island and wind power potential, etc.	Precipitation forecast, katabatic wind simulation, assessment of climate change, etc.	Diffusion simulation of secondary organic aerosol, simulation of forest fire and wind environment, etc.
References	Xue et al. (2000, 2003), Vaidya et al. (2004), Cheng et al. (2007), Li et al. (2016), etc.	Bass et al. (2002), Ren and Perrie (2006), Gultepe and Milbrandt (2007), Waewsak et al. (2015), etc.	Anderson et al. (2000), Bromwich et al. (2001), Trusilova et al. (2007), Cabré et al. (2016), etc.	Jiang et al. (2012), Jiménez and Dudhia (2012), Coen et al. (2013), Takane et al. (2013), Mughal et al. (2017), etc.

The Center for Analysis and Prediction of Storms (CAPS) at the University of Oklahoma developed the ARPS as an effective tool for basic and applied research and as a system suitable for explicit prediction of convective storms as well as weather systems. The ARPS includes data ingest, quality control and objective analysis packages, a data assimilation system, the forward prediction component, and a post processing system (Xue et al., 2000). The ARPS model has been used in various studies. Xue et al. (2003) used the model to forecast watershed runoff by predicting rainfall on the Uruguay River, and Vaidya et al. (2004) used the model to predict monsoonal depression and tropical cyclone over Indian region. Cheng et al. (2007) analyzed the effect of various aerosols generated in China on PM10 concentration in Beijing by using MM5, ARPS and CMAQ models as shown in figure 1. Li et al. (2016) simulated two intense quasi-linear meso-scale convective systems in northern China using the WRF model and the ARPS model.

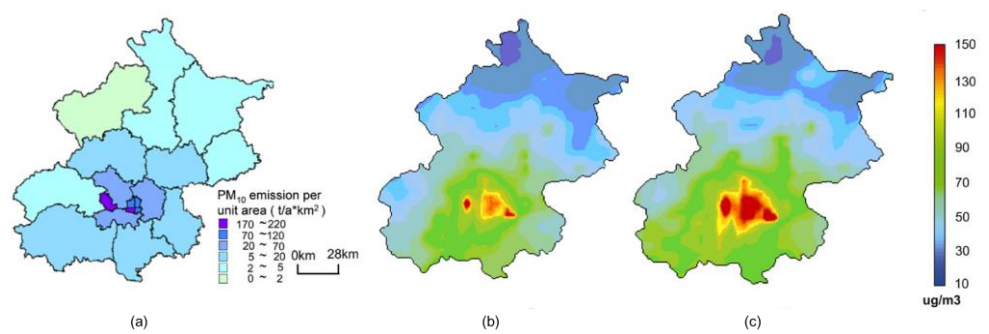

Figure 1 PM_{10} emission distribution (a) and simulated PM_{10} concentration in Beijing in July (b) and August (c) 2008 (Cheng et al., 2007)

The MC2 model, a non-hydrostatic model, was originally developed by Robert (1981, 1982) to demonstrate the advantages of using semi-Lagrangian advection in a semi-implicit limited area hydrostatic model. The model used a comprehensive

physical package that includes a planetary boundary layer based on turbulent kinetic energy, vertical dispersion, horizontal dispersion, and topographical surface characteristics (Mailhot et al. 1998). Bass et al. (2002) used the MC2 model to analyze the reduction of the roof temperature and the reduction of the urban heat island effect due to the placement of plants on the roofs of urban buildings, using model nested to a 1 km grid resolution from a 25 km grid resolution model. Ren and Perrie (2006) investigated the interactions between the atmosphere and the ocean during extreme weather conditions to analyze the sensitivity of hurricane development to sea level temperature reduction caused by typhoons using the MC2 model with a horizontal grid size of 0.25 degree. Gultepe and Milbrandt (2007) simulated the amount of the atmospheric water vapor in Ontario, Canada, using the MC2 model with the model nested to a 2 km grid resolution using the output from a 10 km simulation. (Waewsak et al., 2015) simulated the meso-scale wind speed in the area of the Gulf of Thailand in order to estimate wind power potential using the MC2 model.

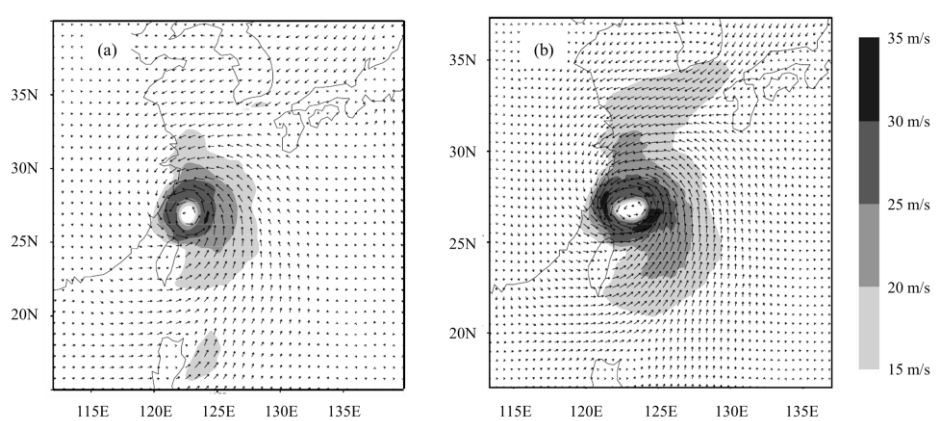

Figure 2 Surface wind field at 2100 UTC 6 September 2002 using MC2 model with 0.25˚ resolution (a) and MC2 model with 0.167˚ resolution (b) (Ren and Perrie, 2006)

The fifth-generation Penn State/NCAR meso-scale model (MM5) is the latest in a series of models that developed from a meso-scale model originally documented by Anthes and Warner (1978). The MM5 is a nonhydrostatic model developed to simulate or predict meso-scale and regional-scale atmospheric circulation over a limited area. Anderson et al. (2000) simulated the runoff in the Calaveras watershed, California, using a HEC-HMS runoff prediction model and the MM5 model. Bromwich et al. (2001) used a polar MM5 model modified from the original MM5 model to analyze the katabatic wind in Greenland. The temperature, pressure, wind speed, and wind direction in Greenland were simulated using the polar MM5 model with a 40 km horizontal grid, and the simulated results were compared with observed results. Trusilova et al. (2008) used the MM5 model to assess the urbanization impacts on the climate in Europe. Urbanization of the land surface was estimated to cause about a 19% decrease in precipitation in summer seasons and about a 8% increase in winter seasons. Cabré et al. (2016) used the MM5 model to evaluate the climate change under the SRES A2 emission scenario over southern South America.

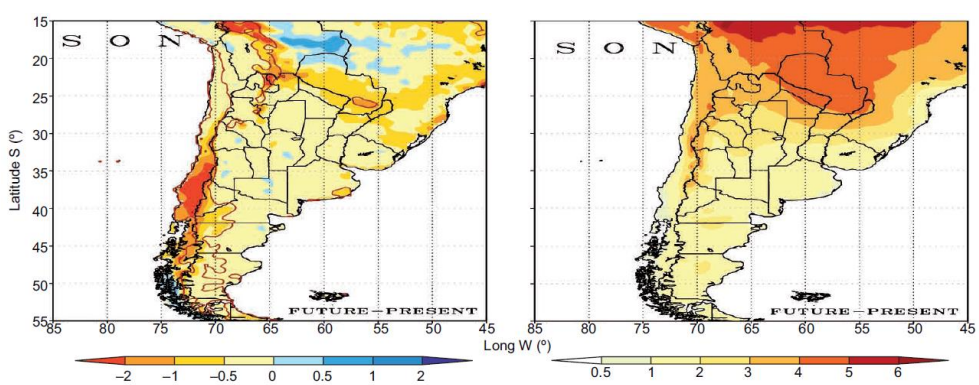

Figure 3 Spatial distribution change of simulated precipitation (mm day^{-1}) and temperature (℃) for spring (Cabré et al., 2016)

Many researchers have used the WRF model for meteorological simulations on urban and national scale. Jiang et al. (2012) analyzed the generation and diffusion of secondary organic aerosol (SOA) over China using a new generation air quality modelling system (WRF/Chem). The generation and diffusion of the SOA was simulated using the system comprising a horizontal grid of 45 km for a domain of 6075 x 4500 km, with 28 vertical layers from the ground up to a height of 100 hPa. Jiménez and Dudhia (2012) attempted to correct for a high surface wind speed bias over plains and valleys of the WRF model by parameterizing the effects of unresolved topographic features. The study was conducted for the area located in the north of Iberian Peninsula using the WRF model designed as a horizontal grid of 2 km. Coen et al. (2013) simulated forest fires using the WRF-Fire model, which combines the WRF model with the wildland fire model, to assess the factors affecting the spread of fire. The sensitivity analysis was carried out according to perimeter shape, fire intensity, wind speed, and fuel characteristics. It is important to design a model that can accurately simulate the wind environment near the ground, because the wind velocity near the ground has the greatest influence on the spread of fire. Takane et al. (2013) designed a simulation model with horizontal grid size of 2 km using the WRF model to analyze the high temperature phenomenon which has occurred between Osaka and Tokyo, Japan in the past. In addition, it is analyzed that the synoptic scale wind occurring in summer season contributes to the high temperature phenomenon of Osaka and Tokyo. Lee et al. (2014) designed a 90 m horizontal resolution numerical model to analyze wind environment in the valley of Gwangneung forest, Republic of Korea. They simulated a morning upslope wind and an evening downslope wind in the valley region. Mughal et al. (2017) estimated wind

speed and direction over the East African site of the Lake Turkana Wind Farm using the WRF model with the model nested to a 0.55 km horizontal grid resolution using the output from a 5 km resolution simulation.

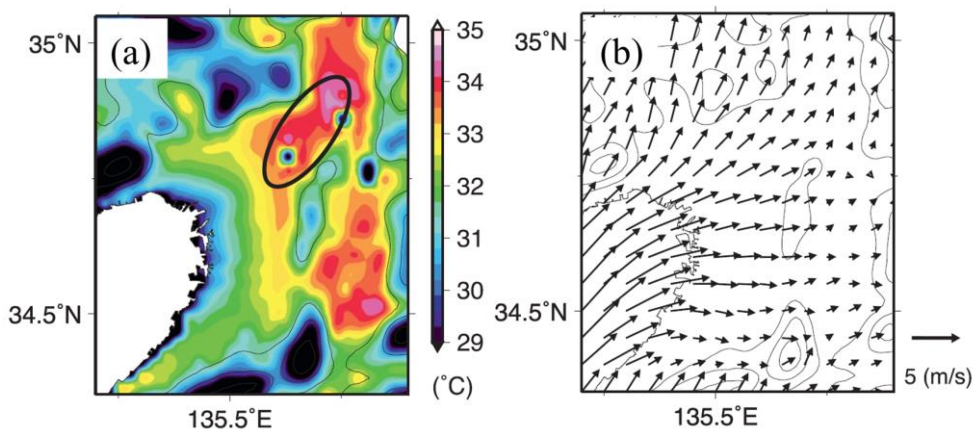

Figure 4 Averaged air temperature (a) and wind velocity (b) simulated by WRF (1, 5-12, 14 August 2007) (Takane et al., 2013)

The initial WRF model, which has been used for weather prediction, has presented a high surface wind speed bias over land (Cheng and Steenburgh, 2005; Skamarock and Klemp, 2008). However, this bias still persists in recent versions of the WRF model and it is a limitation in terms of accurate surface wind estimations required for research into areas such as wind energy applications or air quality studies (Bermardet et al., 2005; Mass and Ovens, 2010, 2011; Roux et al., 2009). This bias occurs partly because the ground shape in the WRF model is modelled smoothly. This bias can also be increased by plants distributed on the ground (Jiménez and Dudhia, 2012). Therefore, to reduce these biases, it is important to use a model that can consider characteristics of mountain terrain such as complex topographic shape, rough ground surface and increased plant cover.

2.1.2. Micro-scale numerical weather prediction modelling

Many researchers have attempted to predict the airflow using various CFD simulation packages with more precise meshes in order to overcome the limitations of meso-scale numerical weather prediction modelling. CFD simulation packages are used to predict the airflow in a relatively narrow area rather than the meso-scale or global-scale modelling, and the CFD model is designed with a grid of several tens of meters in the domain region in order to study the air-flow for urban areas or complex terrain.

Many researchers have studied the dispersion of pollutants such as aerosol, dust, and smoke, and of hazardous substances such as toxic gases in urban area(Baik et al., 2007; Choi et al., 2012; Cui et al., 2016; Di Sabatino et al., 2007, 2008; Gidhagen et al., 2004; Gousseau et al., 2011; Hang et al.1 2012; Hanna et al., 2009; Hefny and Ooka, 2009; Kang and Kim, 2015; Kim et al., 2015; Kim and Baik, 2004; Ko et al., 2015; Labovský and Jelemenský, 2013; Milliez and Carissimo, 2007; Park and Baik, 2007; Pontiggia et al., 2010, 2011; Pospisil et al., 2004; Salim et al., 2011; Xie et al., 2005; Xing et al., 2013), and the heat island phenomena in urban area and the impact of tall buildings on the urban wind environment (Ashie and Kono, 2011; Kim and Baik, 2005; Lee and Kim, 2011; Yang and Kim, 2015). In addition, the micro-scale modelling has also been used to evaluate the dispersion of gases or clouds in complex terrain and wind power generation (Bergeles et al., 1996; Blocken et al., 2015; Cattin et al. 2006; Dhunny et al., 2017; Forthofer, 2007; Gavelli et al., 2008; Hong et al., 2011b; Koo et al., 2009; Liu et al., 2016; McBride et al., 2001; Meroney, 2012; Seo et al., 2014; Riddle et al., 2004; Uchida and Ohya, 2003).

Table 3 Summary of the micro-scale numerical weather prediction modelling for simulation of airflow over complex terrain.

	Software	Resolution	Turbulence model	Objectives
Bergeles et al. (1996)	CFD solver code	-	-	Assessment of the applicability of a 3D Navier-stokes code
McBride et al. (2001)	CFX	15 m	k-ε model	The key parameter findings for the chlorine dispersion
Uchida and Ohya (2003)	RIAM-COMPACT	50 m	LES model	Prediction of turbulence airflow over complex terrain using the LES turbulence model
Riddle et al. (2004)	Fluent, ADMS 3	100 m	k-ε model, LES model	Prediction of the gas dispersion over the complex terrain
Cattine et al. (2006)	WindSim	-	-	Validation of CFD wind modelling over complex terrain
Forthofer (2007)	FARSITE model	40 m	RNG k-ε model	Simulation of airflow over complex terrain for the mountain fire spread
Gavelli et al. (2008)	Fluent	-	k-ε model	Proposal of CFD code as an alternate method for the prediction of flammable vapor cloud
Koo et al. (2009)	CFD_NIMR_SNU	7.5 m	-	Simulation of detailed wind flow over a locally heated mountain area
Hong et al. (2011b)	Fluent	5 m	LES model	Simulation of the odor dispersion over complex terrain
Meroney (2012)	Fluent	-	Realizable k-ε model	Simulation of dense gas cloud dispersion over irregular terrain
Seo et al. (2014)	OpenFOAM	5 m	-	Prediction of the spread of HPAI airborne virus
Blocken et al. (2015)	Fluent	-	Realizable k-ε model	Simulation of wind flow over natural complex terrain
Liu et al. (2016)	Fluent	2 m	k-ε model	Simulation of carbon dioxide dispersion over artificial complex environment
Dhunny et al. (2017)	WindSim		k-ε model	The key parameter findings for estimation of wind power over highly complex terrain

Pospisil et al. (2004) analyzed the diffusion of carbon monoxide and nitrogen monoxide, which are typical pollutants emitted from automobiles, in the Pisarky tunnel in Brno region and the downtown area in Hannover area using the StarCD CFD simulation software. They simulated the spread of air pollutants emitted from moving cars simulated by the Eulerian-Lagrangian model. Hanna et al. (2009) simulated the transport and dispersion of a dense chlorine cloud to assist in emergency response decisions and planning in case of releases of pressurized liquefied chlorine from railroad tank cars using the FLACS CFD simulation software package. The FLACS CFD model was designed with a grid size of $6\text{m} \times 6\text{m} \times 2\text{m}$ and the spread of chlorine gas was simulated according to various wind scenarios. Hong et al. (2011a, 2011b) evaluated the odor spread emitted from a livestock house located in a mountain area using the FLUENT 6.3 simulation software. They presented three methods for designing 3D CFD model of complex terrain using DEM (digital elevation model), DEM image, and contour lines for a domain area of 3.6 km in horizontal diameter and 2.5 km in height (Fig. 5). However, they did not consider the effect of the trees distributed in the mountain terrain on airflow.

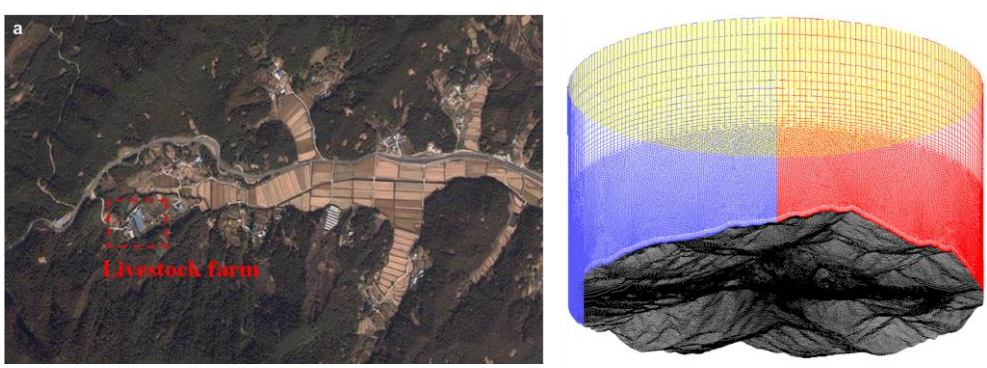

Figure 5 Satellite image of the study area (left) and 3D computational domain of the developed topographical model (right) (Hong et al., 2011a)

Salim et al. (2011) analyzed the wind environment and dispersion of pollutants in urban building canyon using the wind tunnel test and the CFD simulation using FLUENT 6.3. The influence of the grid size and the turbulence model on the simulation were evaluated. However, it had limitations in that they did not analyze the wind environment of building canyon located in actual urban area, but analyzed the wind environment between two blocks of 18 m height, 10 m width, and 180 m long. Labovský and Jelemenský (2013) implemented the actual shape of buildings in the downtown area of Žilina, Slovakia, and simulated the spread of chlorine gas into the city in case of liquid chlorine was released from the railway passing through the city. The digital map of urban building distribution was used to realize actual city shape, and the model was designed using the GAMBIT and FLUENT 6.3 CFD simulation software. The simulated results were compared with the estimated result by the ALOHA software, which is most commonly used to evaluate the spread risk of hazardous materials. Through this study, it was shown that CFD can overcome the limitations of the ALOHA software, which assumes that the hazardous materials will diffuse into a cone shape according to the wind velocity and diffusion coefficient, without consideration building shape. Seo et al. (2014) developed a CFD model to predict the spread of HPAI (highly pathogenic avian influenza) airborne viruses. They divided wooded areas into subparts on the CFD model and the divided subparts were assumed to be a porous media in order to consider an effect of air-resistance of wooded areas (Fig. 6). However, they simplified boundaries of the wooded areas because of realistic boundary design difficulties of wooded areas on the CFD model as the subparts.

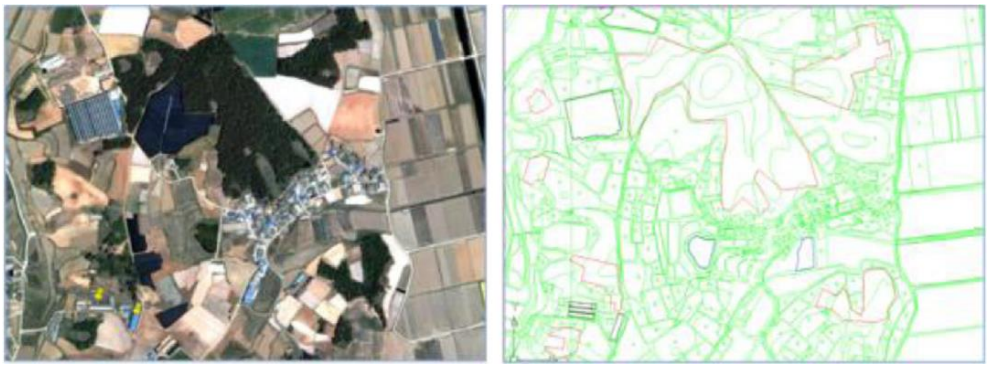

Figure 6 Satellite photograph showing the wooden area around the livestock farm area (left) and the simplification process using topographical classification. (Seo et al., 2014)

Blocken et al. (2015) used FLUENT 6.3 CFD software for wind environment analysis of a coastal area of $25\ \text{km} \times 20.5\ \text{km}$ containing a 250 m high hill. After simulating the wind environment for various wind directions, the simulated wind environment results were used as the input data for real time ship driving simulation.

It is very important to set boundary conditions carefully, since they can greatly affect the airflow in the domain, however, in the case of the CFD models designed to simulate external airflow, it is very difficult to design the boundary conditions. Recent studies have been conducted to simulate the airflow in complex terrains through the coupling of meso-scale and micro-scale weather prediction (Choi et al., 2012; Gopalan et al., 2014; Jeong et al., 2014; Kaoru et al., 2011; Kwak et al., 2015; Miao et al., 2013; Zheng et al., 2015). Choi et al. (2012) simulated the micro-scale atmospheric airflow of an urban area affected by buildings and analyzed the spread pattern and areal extent of pollutants in the case of a fire. Miao et al. (2013) linked the micro-scale model (OpenFOAM) and the meso-scale model (WRF model) to analyze airflow and pollutant dispersion in an urban area in Beijing, China. The boundary conditions for the micro-scale model were designed using the results of

the WRF model, which was a meso-scale weather prediction model simulated with grid size of 1 km. The dispersion of pollutants was analyzed according to four wind direction scenarios, but the model was not validated. Jeong et al. (2014) evaluated the accuracy improvement of airflow prediction in urban area through the implementation of UCP (urban canopy parameter). Zheng et al. (2015) conducted a sensitivity analysis of factors such as atmospheric boundary structure, wind speed, wind direction, and location of pollutant source and how they affected to airflow and pollutant spread in urban area in Shenyang, China.

Previous studies have focused on implementing the shape of complex terrains or buildings to simulate the wind environment in mountain regions or urban areas. However, distributions and characteristics of trees which affect the wind environment near the surface are not generally considered for CFD simulations. For example, Hong et al. (2011b) focused on realizing the complex mountain topographical shapes in order to estimate odor dispersion, but did not consider the aerodynamic resistance of trees distributed in the mountain area. On the other hand, although Seo et al. (2014) simulated airflow considering the air-resistance of the wooded area, it has the limitation that it cannot consider the actual distribution by simplifying the shape of the wooded area for the model design.

2.2. Air resistance of trees

Due to topographical factors such as altitude differences and the shape of valleys or hilly terrain, the direction, speed and turbulence of airflow in the forested areas are different from those found in, for example, plains areas. In addition, the physical characteristics of each tree constituting the forest, such as species, shape, and height of tree, greatly affect the turbulence of airflow in the forest. Therefore, it is important to simulate the physical characteristics of the trees distributed in the study area, as well as topographical factors when designing 3D terrain CFD models for mountain region. Various studies on the effect of trees on the airflow have been made largely focused on the effect of windbreak or on the drag force of tree.

Windbreak trees are mainly used to protect crops or livestock in rural area from strong wind, or to prevent the wind erosion and the movement of sand dunes. In recent years, it has also been used to reduce heat, noise, and odor (Lin et al., 2007; Slusher and Wallace, 1997; Zhu et al., 2004). Generally, windbreaks are installed in order to reduce damage caused by strong winds and to reduce soil movements due to strong winds. Therefore, the effect of windbreaks can be evaluated according to the wind speed reduction. The wind speed reduction effect of windbreaks is affected by the height, width, density, porosity, arrangement and location conditions of windbreak trees. The height and width of the windbreak forest are considered to be factors affecting the extent of the area protected from the wind and the porosity, determined by the arrangement of the windbreaks is suggested as a factor directly affecting to the wind flow (Heisler and Dewalle, 1988). Porosity is defined as the ratio of the area or volume of empty space to the area or volume of leaves and stems (Raine and Stevenson, 1977). The porosity is affected by species, leaf area index

(LAI), leaf thickness, and tree height. Many studies have shown that windbreak trees with low porosity affect to high wind velocity reduction and turbulence generation (Bitog et al, 2011; Cornelis and Gabriels, 2005). However, it is difficult to measure the porosity directly in the field due to the uneven size and shape of the trees, unstable ambient environmental conditions, and uncontrolled experimental conditions. In studies on wind environment, aerodynamic porosity or drag coefficient is often proposed as an alternative of the porosity in order to overcome the limitations of measuring the porosity in field experiment. The aerodynamic porosity is defined as the ratio of average wind speed immediately leeward of the windbreak to the average wind speed of an open field provided wind direction was perpendicular to the windbreak (Guan et al., 2003). In other words, the aerodynamic porosity of the windbreak determines the ratio between airflow that passes through the windbreak pore and airflow that diverges over the windbreak (Středová et al., 2012). The drag coefficient is defined as the ratio of the pressure difference between windward and leeward sides of the windbreak and the dynamic force (Bitog et al., 2011). There is a disadvantage to this approach in that aerodynamic porosity can be difficult to measure when experimental conditions are not easily controled. However, there is also an advantage in that the drag coefficient can be measured relatively easily using a pressure gauge. Therefore, many researchers have estimated the drag coefficients, not only using wind tunnel test, but also field experiment (Table 4 and 5).

Table 4 Drag coefficient of various coniferous trees from various studies

Tree	Drag coefficient (C_D, non-dimensional)	Inertial resistance coefficient (C_i, m^{-1})	Experimental method	Experimental wind speed ($m\ s^{-1}$)	Reference
Sitka spruce	0.72	-	Wind tunnel	9.1	Raymer (1962)
Scots pine	0.52			9.1	
Douglas fir	0.50			9.1	
Western hemlock	0.32			9.1	
Sitka spruce	0.74	-	Wind tunnel	9.4	Mayhead (1973)
Corsican pine	0.66			9.4	
Lodgepole pine	0.57			9.4	
Grand fir	0.88			9.4	
Lodgepole pine	0.35	-	Wind tunnel	26.0	Mayhead et al. (1975)
Scots pine	0.35			26.0	
Sitka spruce	0.40			26.0	
Abies alba (70%), Fagus sylvatica (15%), Picea abies (15%)	0.13	-	Field experiment (by measuring drag force)	1.39 ~ 6.19	Cescatti and Marcolla (2004)
Picea abies (85%), Pinus cembra (12%), Larix decirua (3%)	0.33			1.40 ~ 5.9	
Redcedar	0.9	-	Wind tunnel	4.0	Rudnicki et al. (2004)
Hemlock	1.1			4.0	
Pine	1.0			4.0	
Black pine	0.55 ~ 1.08	0.33 ~ 1.11	Wind tunnel	2.0 ~ 8.0	Bitog et al. (2011)

Table 5 Drag coefficient of various deciduous trees from various studies

Tree	Drag coefficient (C_D, non-dimensional)	Inertial resistance coefficient (C_i, m^{-1})	Experimental method	Experimental wind speed ($m\ s^{-1}$)	Reference
Platanus, Sugar maple, Whitebeam (with leaf)	0.841	-	Field experiment (by measuring tree deflection)	2.4 ~ 8.2	Roodbaraky et al. (1994)
Platanus, Sugar maple, Whitebeam (without leaf)	0.205	-	Field experiment (by measuring tree deflection)	1.5 ~ 9.1	
Paper birch	0.66 ~ 1.06	-	Wind tunnel	4.0	Vollsinger et al. (2005)
Black cottonwood	0.73 ~ 1.04			4.0	
Red alder	0.71 ~ 0.86			4.0	
Bigleaf maple	0.90 ~ 0.95			4.0	
Trembling aspen	0.87 ~ 0.89			4.0	
Red maple	0.59	-	Field experiment (using pickup truck)	20.0	Kane and Smiley (2006)
Black poplar (with leaf)	0.25	-	Field experiment (by stem deflection)	10.0	Koizumi et al. (2010)
Black poplar (without leaf)	0.133	-	Field experiment (by stem deflection)	10.0	

Roodbaraky et al. (1994) conducted field experiments to measure the aerodynamic characteristics of urban trees in Nottinghamshire. The deflection of trees was observed in high wind conditions and the variation of drag coefficient according to presence or absence of leaves was analyzed. Kane and Smiley (2006) measured the drag coefficient of Canadian maple trees to analyze the occurrence of overturning due to strong winds. The trees were fixed to a pickup truck and the truck accelerated steadily on a straight course up to a speed of 20 m s^{-1} in order to adjust the experimental wind speed. The drag force of the trees was estimated by measuring the pressure applied in front of the tree using a dynamometer when the truck accelerated. The drag coefficients of the trees were estimated to be 0.512 ~ 0.933. However, the results contained errors since the influence of ambient wind was not removed. In addition, the physical shape of canopy was classified into two shape: triangular and square; and no significant difference in drag coefficient between these two shape was found. Koizumi et al. (2010) monitored wind velocity and stem deflections simultaneously to evaluate the drag coefficient of actual-sized poplar trees (Fig. 7). They measured the stem deflection and stem stiffness using a self-made middle-ordinate gauge to calculate wind force acting on a crown and the drag coefficient was calculated using the calculated wind force and monitored wind velocity from following equations.

$$C_D = \frac{2 \times P_W}{\rho A U^2}$$

$$P_W = \frac{K\delta}{H_W - H_D}$$

where P_W is wind force, ρ is air density, A is the horizontally projected crown area,

U is wind velocity, K is stem stiffness, δ is stem deflection, H_W is the height of the wind pressure center, and H_D is the height of the deflection sensor.

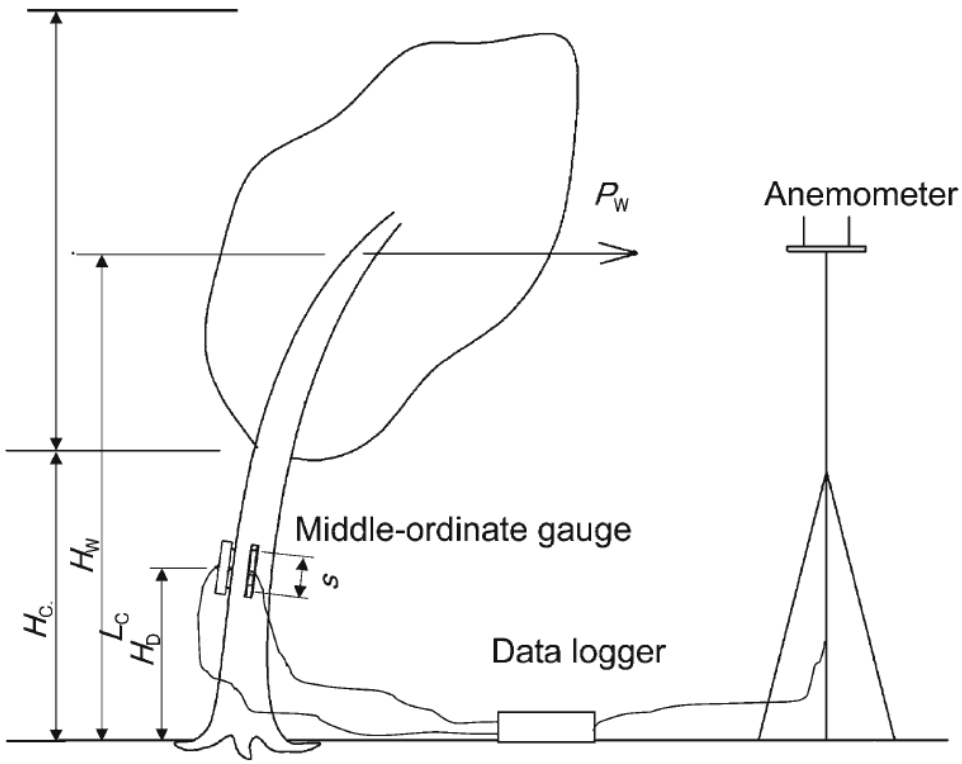

Figure 7 Schematic diagram of the field experiment for monitoring wind velocity and stem deflection (Koizumi et al., 2010)

Lee et al. (2010) measured the geometric characteristics of Arizona Cypress (*Cupressus arizonica var. arizonica*) using a laser scanning system equipped with a GPS receiver. In addition, the effect of tree geometry on wind speed reduction was investigated. However, they focused on measuring the geometric characteristics of trees by optical approach using the scanning system, and did not estimate a porosity or drag coefficient for the trees. Bitog et al. (2011) conducted wind tunnel tests in order to estimate the drag coefficient of medium-sized black pine trees (*Pinus*

thunbergii), which are typical coniferous trees in the Republic of Korea and are commonly used as a windbreak in coastal area because the tree is not much affected by external environmental changes. The drag coefficient of the trees was estimated by measuring the wind speed windward and leeward of the trees, while varying the tree density and tree combination (Fig. 8). The average drag coefficients found to be 0.55, 0.82, and 1.08 for one, two, and three trees, respectively. The determined drag coefficient of a single tree is comparable to the drag coefficient determined by Mayhead (1973) in wind tunnel experiments for *Pinus contorta* and *Pinus nigra*, which were 0.57 and 0.69, respectively.

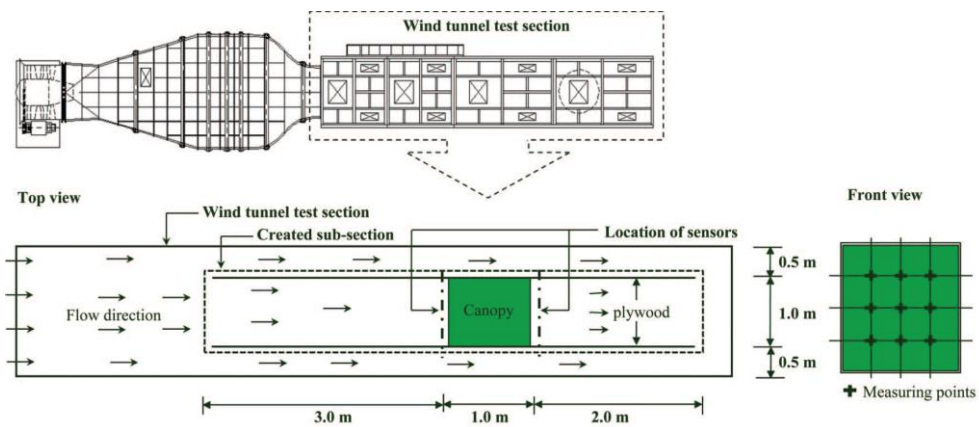

Figure 8 Schematic diagram of the wind tunnel experiment with measurement points at windward and leeward (Bitog et al., 2011)

Cao et al. (2012) measured drag forces and overturning moments of coniferous tree, Emerald Cedar (*Thuja occidentalis 'Smaragd'*), and the evergreen tree, Japanese Holly (*Ilex crenata*), under different wind speeds. After initial experiments, the Emerald Cedar was pruned in four steps and the Japanese Holy was pruned in three steps in order to investigate the effect of crown porosity (Fig. 9). Drag coefficients of the Emerald Cedar were 0.67 to 0.83, and drag coefficient of the Japanese Holly

were constant at around 0.79.

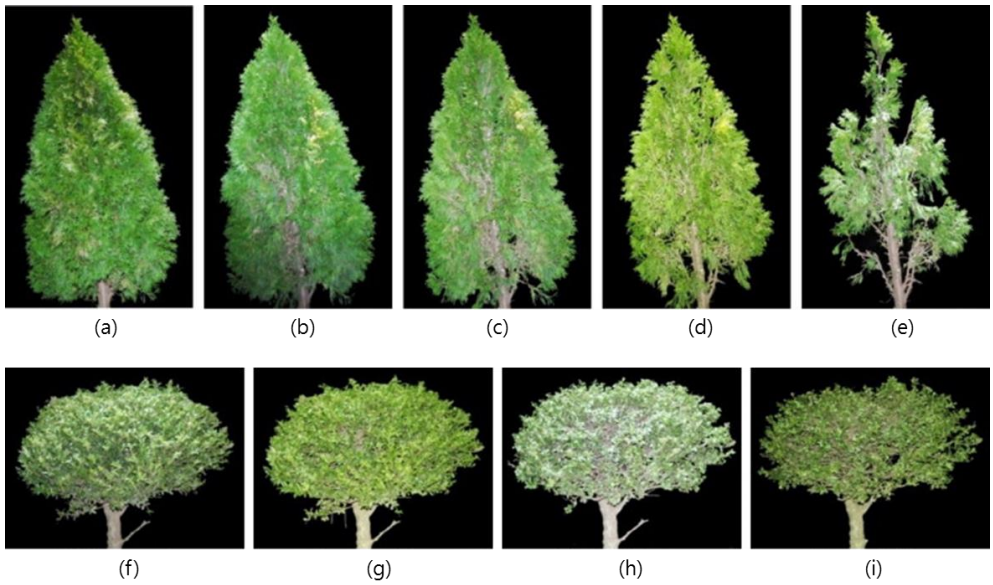

Figure 9 Variation of shape of the Emerald Cedar (a ~ e) and Japanese Holly (f ~ i) according to pruning. (a) initial shape of the Emerald Cedar, (b) 1st pruning of the Emerald Cedar, (c) 2nd pruning of the Emerald Cedar, (d) 3rd pruning of the Emerald Cedar, (e) 4th pruning of the Emerald Cedar, (f) initial shape of the Japanese Holly, (g) 1st pruning of the Japanese Holly, (h) 2nd pruning of the Japanese Holly, (i) 3rd pruning of the Japanese Holly (Cao et al., 2012)

Chapter 3. Development of a micro-scale CFD model to predict wind environment on mountain terrain using a commercial CFD package

3.1. Introduction

The aim of this chapter was to develop a 3D aerodynamic CFD model using commercial CFD package in order to qualitatively and quantitatively predict the wind environment in a mountain area considering topographical conditions and the air resistance of the tree canopy. The primary steps in this study were 1) development of the 3D CFD simulation model, 2) development of the method for applying aerodynamic porosity resistance of tree on 3D CFD simulation model, and 3) validation of the designed CFD model.

3.2. Materials and methods

3.2.1. The study area

The study site was the Gwangneung arboretum (37°45′08.0″N, 127°09′57.5″E) which is located in Pocheon-city, Gyeonggi-province, Republic of Korea. The area of the Gwangneung arboretum is approximately 1100 ha, and the 2800 kinds of plants are divided into coniferous, deciduous, blooming, and foreign botanical garden. The elevation range of the study area, Gwangneung arboretum, was 75 m to 535 m above sea level and the valley runs in an east-west direction. In the arboretum, two KoFlux (Korea Flux) towers, Gwangneung Conifer Korea (GCK) tower and Gwangneung Deciduous Korea (GDK) tower, have been operated in order to observe wind environment, carbon dioxide, photosynthesis since 2006 and 2002, respectively

(Fig. 10).

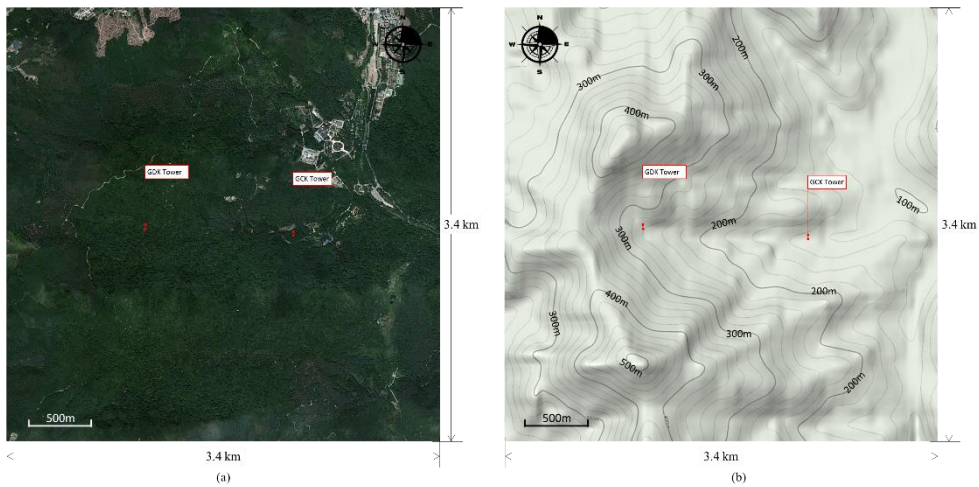

Figure 10 (a) Satellite image of the study area and (b) the contour image of the study area.

The elevation of the GCK tower (37°44′54.7″N, 127°09′46.6″E) was 128 m and its height was 40 m. Three-dimensional sonic anemometers (CSAT3, Campbell Scientific Inc., USA) were installed at 4, 9, 18, 29, 34, and 40 m heights to measure the wind speed and direction with height. Open-path infrared gas analysers (Li-7500, Li-Cor, USA) were installed at 0.1, 1, 4, 9, 18, 29, 34, and 40 m heights to measure the air temperature and concentrations of water vapor and carbon dioxide. The data were sampled at 10 Hz and averaged every 30 minute. The elevation of the GDK flux tower (37°45′N, 127°09′E) was 260 m and its height was 40 m. A three-dimensional sonic anemometer and an open-path infrared gas analyser were installed at 40 m on the GDK tower differently than the GCK tower. The data were also sampled at 10 Hz and averaged every 30 minute.

Primarily coniferous trees (Abies holophylla) and deciduous trees (Quercus serrata) were distributed around the GCK tower and the GCK tower, respectively.

The height of the coniferous and deciduous trees located near the towers were measured using a laser distance measurement sensor by the tangent method (SD-120C, Sincon Co. Ltd., Republic of Korea) (Fig. 11). The heights of 13 coniferous trees and 11 deciduous trees were measured, and the average heights were 30.2 m and 17.0 m, respectively (Table 6).

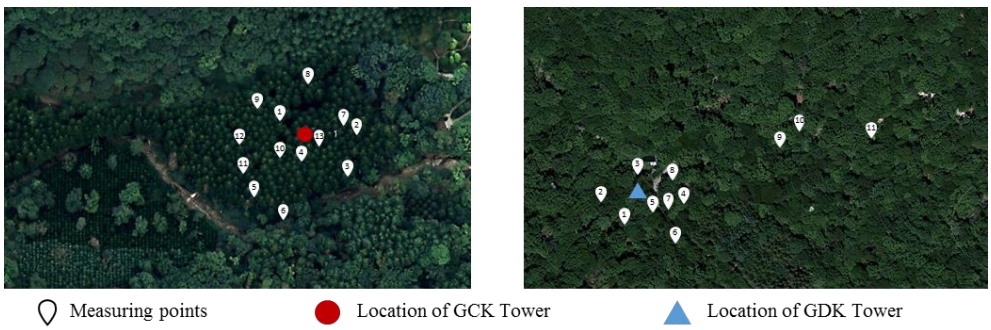

Figure 11 Points at which tree heights were measured near the GCK (left) and GDK (right) towers

Table 6 Characteristics of tree of the study area

	Coniferous tree	Deciduous tree
Representative tree type	*Abies holophylla*	*Quercus serrata*
Number of measured tree	13	11
Average height (m)	30.2	17.0
Standard deviation of height (m)	2.0	3.9
Average height of trunk (m)	13.4	-
Standard deviation of height of trunk (m)	4.2	-
Leaf area index (LAI) (dimensionless)	4 ~ 8	1 ~ 6

3.2.2. Computational fluid dynamics (CFD)

A CFD is a numerical method for predicting the behavior of an airflow by

solving energy equation and conservation equations for mass and momentum. Figure 12 shows a simulation procedure of a 3D CFD modelling.

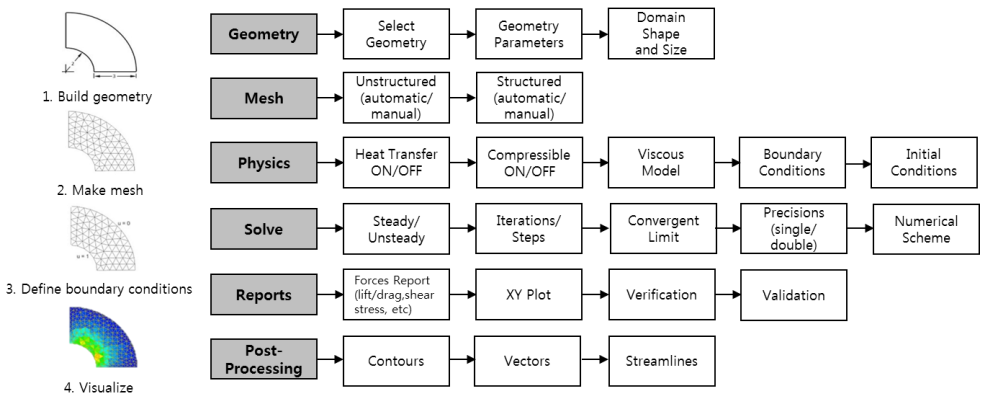

Figure 12 Simulation procedure of a 3D CFD modelling

In addition, The governing equations are as follow:

$$\frac{\partial \rho}{\partial t} + \nabla \cdot (\rho \vec{v}) = S_m \quad (1)$$

$$\frac{\partial}{\partial t}(\rho \vec{v}) + \nabla \cdot (\rho \vec{v} \vec{v}) = -\nabla p + \nabla \cdot (\bar{\bar{\tau}}) + \rho \vec{g} + \vec{F} \quad (2)$$

$$\frac{\partial}{\partial t}(\rho E) + \nabla \cdot \left(\vec{v}(\rho E + p)\right) = \nabla \cdot \left(k_{eff} \nabla T - \sum h \vec{J} + \left(\bar{\bar{\tau}}_{eff} \cdot \vec{v}\right)\right) + S_h \quad (3)$$

where S_m is the source term of the mass (kg m^{-3} s^{-1}), p is the static pressure (Pa), $\bar{\bar{\tau}}$ is the stress tensor (Pa), $\rho \vec{g}$ is the gravitational body force (kg m^{-2} s^{-2}), $\vec{F}$ is the external body force (N), E is the total energy (J), k_{eff} is the effective conductivity (W m^{-1} K^{-1}), h is the sensible enthalpy (J mol^{-1}), $\vec{J}$ is the diffusion flux of species (kg m^{-2} s^{-1}), and S_h is the heat source (W m^{-2}) (Fluent, 2013).

The commercial CFD software Fluent (ver. 15, ANSYS Inc., CA, USA) was used in this study, and it provides various turbulence models such as the RANS

model (e.g., Spalart-Allmaras model, k-ε models, k-ω models, Reynold stress model (RSM), etc.) and the LES model to calculate the turbulent motion according to the researcher's purpose. The k-ε turbulence models and k-ω turbulence RANS models were used in this study, because of the previously mentioned limitations.

The RANS equations are:

$$\frac{\partial \rho}{\partial t} + \frac{\partial}{\partial x_i}(\rho u_i) = 0 \quad (4)$$

$$\frac{\partial}{\partial t}(\rho u_i) + \frac{\partial}{\partial x_j}(\rho u_i u_j) = -\frac{\partial p}{\partial x_i} + \frac{\partial}{\partial x_j}\left[\mu\left(\frac{\partial u_i}{\partial x_j} + \frac{\partial u_j}{\partial x_i} - \frac{2}{3}\delta_{ij}\frac{\partial u_l}{\partial x_l}\right)\right] + \frac{\partial}{\partial x_j}\left(-\rho\overline{u_i' u_j'}\right) \quad (5)$$

where t is the time (s), u is the mean velocity component (m s^{-1}), u' is the fluctuating velocity component (m s^{-1}), μ is the dynamic viscosity (kg m^{-1} s^{-1}).

3.2.3. Porosity of the trees

The tree effect is important to simulate the airflow in a complex terrain, because it acts as an obstacle. When the wind passes through the canopy, wind energy was transformed into turbulent energy or wind direction was changed. The speed of the wind passing through the tree is decreasing in this situation. There are two methods to realize the decreasing wind speed decreasing; the design of the exact physical shape of tree in a numerical CFD model and design of porous media for tree. In this study, the tree effect was realized using porous media based on the land use classification of the study area, and the process was adopted in the main process of CFD simulation by UDF (User Defined Function) code.

The pressure drop due to the porous media in CFD simulation was calculated by a source term in the momentum equation. The source term was modelled as a quadratic equation of the velocity magnitude (equation 6).

$$S_{\Phi} = -\left(\frac{\mu}{\alpha} v_i + C_2 \frac{1}{2} \rho |v| v_i\right) \quad (6)$$

where v is the wind velocity (m s^{-1}), α is the permeability (m^2), μ is the absolute viscosity coefficient (kg s^{-1} m^{-1}), ρ is the air density (kg m^{-3}), and C_2 is the inertial resistance coefficient (m^{-1}).

In a laminar flow through a porous media, the pressure drop is typically proportional to the velocity and the constant C_2 can be assumed to be zero. Therefore, the porous media model reduces to Darcy's Law:

$$\nabla p = -\frac{\mu}{\alpha} \vec{v} \quad (7)$$

Otherwise, the Darcy term can be ignored when the flow velocity is very fast or the Reynolds number (Re) is larger than 5,000. Therefore, the porous media model reduces to the Forchheimer term (Fluent, 2013; Hong, 2008):

$$\nabla p = -C_2 \frac{1}{2} \rho |v| v_i \quad (8)$$

In this study, the porous resistance of tree was realized using the inertial resistance coefficient with assumption of Reynolds number in canopy was larger than 5,000.

To calculate the inertial resistance coefficient of the coniferous trees located near the GCK tower, the raw data of corresponding author who participate in research of Bitog et al. (2012) were used. The inertial resistance coefficient was deduced using the experimental results of the pressure difference between the windward and leeward according to the wind speed. The inertial resistance coefficient was determined with the pressure difference, the air density, and the wind velocity using equation (8) and the result is shown in figure 13. The average inertial resistance was approximately 0.268, 0.539, and 0.885 for one, two, and three trees, respectively. In this study, the inertial resistance coefficient of one coniferous tree was used as the input value for the coniferous tree section in the CFD simulation considering the *in situ* tree density.

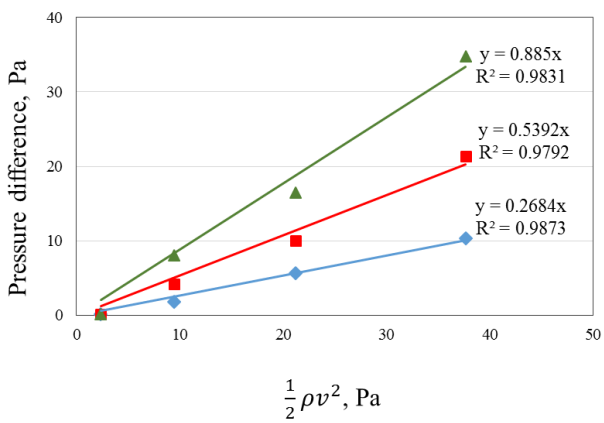

Figure 13 Calculated inertial resistance coefficient according to the conifer tree density using raw data from Bitog et al. (2012)

To determine the value of inertial resistance coefficient of the deciduous tree, various advanced studies were reviewed. However, in the majority of the advanced studied, only the drag coefficient (C_D) was determined in a field experiment or in a wind tunnel test, not the value of inertial resistance coefficient. Therefore, the

relationship between the value of inertial resistance coefficient and the drag coefficient was clarified.

The pressure drop due to the trees could be expressed using the leaf area density (L_{ad}), the drag coefficient, and the wind velocity (Wilson, 1985). Additionally, the leaf area density could be calculated using the leaf area index (LAI) and the tree height (h) (Loughner et al., 2012)

$$\nabla p = -L_{ad} \times \rho \times C_D \times v^2 \tag{9}$$

$$C_2 = 2 \times L_{ad} \times C_D \tag{10}$$

$$L_{ad} = \frac{LAI}{h} \tag{11}$$

$$C_2 = 2 \times \frac{LAI}{h} \times C_D \tag{12}$$

The inertial resistance coefficient was described by the relationship between the drag coefficient and the leaf area density using equation (8) and (9). Then the value of inertial resistance coefficient can be calculated using the drag coefficient, the leaf area index, and the height of tree canopy. However specific physical characteristics of experimental tree such as the leaf area density, the leaf area index, and the tree height were not provided in investigated various previous studies. Therefore, the inertial resistance coefficient of deciduous tree was calculated using investigated drag coefficients (0.176 – 0.748) from various papers and the calculated leaf area density (0.353) of deciduous trees located in the Gwangneung arboretum, and the height of tree(Kane & Smiley, 2006; Koizumi, Motoyama, Sawata, Sasaki, & Hirai, 2010; Roodbaraky, Baker, Dawson, & Wright, 1994; Vollsinger, Mitchell, Byrne, Novak, & Rudnicki, 2005). The averaged inertial resistance coefficient was 0.462,

and it was used as the input value of the deciduous tree section of the CFD simulation.

3.2.4. Modelling procedure

The three-dimensional geometry was designed using a digital contour map provided by the National Geographical Information Institute (NGII) in Republic of Korea, and the coniferous and deciduous tree section were classified using a forest type map provided by the Korea Forest Service (KFS). The classified land use data were subsequently digitized, and the UDF module was developed to set the air resistance of the coniferous and deciduous trees using the digitized data. The CFD model was validated by a comparison with the simulated and measured wind environment data. Figure 14 shows a brief flow chart of the experimental procedure for this study.

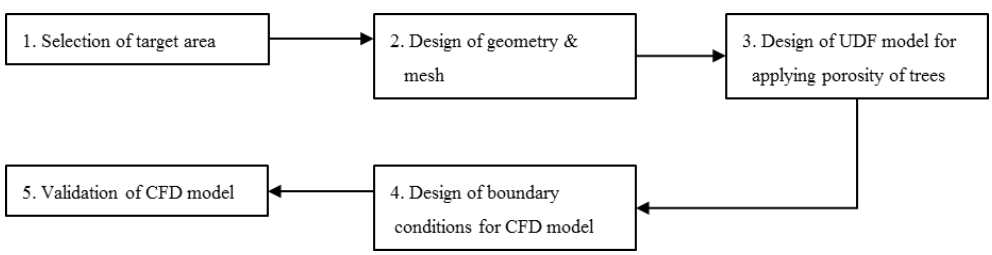

Figure 14 Research process for this study of the development of a micro-scale 3D CFD model

3.2.4.1. Topographical modelling

The 3D solid surface model and mesh were designed using a numerical digital map of the study area with various pre-processing softwares packages such as ArcMap 10(ver. 10, ESRI Inc., USA), AutoCAD(ver. 2014, Autodesk Inc., USA), SketchUp(ver. 7, Google, USA), Rhinoceros(ver 5, McNeel North America, USA),

DesignModeler(ver. 15, ANSYS Inc., USA).

The error of the numerical contour map provided from National Geographic Information Institute in Republic of Korea was confirmed and then modified using AutoCAD software. Then, the 3D complex topography CFD model was designed using the study area contour lines following further study (Hong et al., 2011a). Firstly, a Triangulated Irregular Network (TIN) structure was created using the SketchUp software on the imported the contour map. Second, a solid object was created using the Rhinoceros software on the created TIN structure. Finally, the 3D complex topography CFD model was designed using DesignModeler mesh design tool.

Considering the amount of mesh and the mountain terrain range, only regions up to 3.4 km diameter were used for wind environmental prediction modelling. The ground surface was meshed with a 15 m triangular horizontal grid size. The cell height was designed with various heights according to the distance from the ground surface. The first 30 layers were concentrated up to 30 m in height with the same cell height to predict the airflow in the low atmosphere, especially near the ground, where the airflow based on porosity of the trees was the primary concern. A total of 21 layers were added up to 100 m in height. The cell height of the first layer height of the 21 layers was designed with a 1.1 m height and the cell height was increased by a 1.1 ratio to a height of 100 m. next, a tetrahedral grid was used to design an upper volume with a 100 m maximum face size, resulting in a total of 2.0 km in height. The total amount of mesh was approximately 8,439,864. The Skewness was generally used to evaluate quality of meshes. The maximum skewness, generally used to evaluate the mesh quality, was 0.87 indicating a reasonable mesh quality.

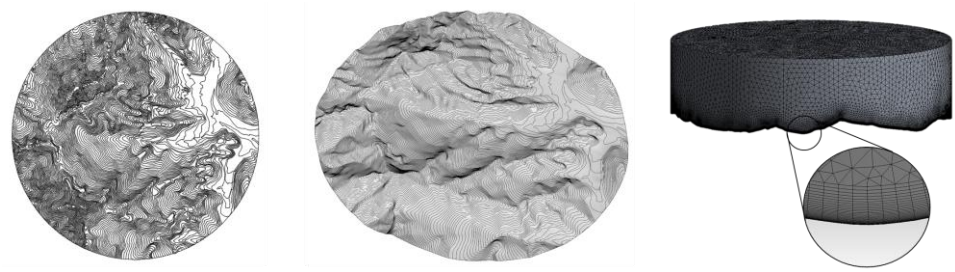

Figure 15 Design procedure for the 3D complex topography CFD model

3.2.4.2. Tree porosity modelling

Changing the wind flow according to the tree porosity should be considered for a wind environment simulation over complex terrain. There are two methods to design the porosity. The first method is the direct design of the tree shape in a CFD model. It directly implements the tree porosity by acting as an obstacle to prevent wind flow. However, a huge amount of mesh is required to design tree shapes in a CFD model over a large region, and it is difficult to design a good quality mesh due to the complex tree shapes. The other method is the implementation of the tree porosity as a porous medium, which has a porosity coefficient. The pressure drop was occurred when the airflow passes through a porous medium according to the porosity coefficient. In this study, the tree porosity was implemented using second method, because it can generate a good quality meshes economically. Many methods are possible for simulating a pressure drop by the tree porosity in CFD, but this paper suggests the following two methods as shown in figure 16.

Method 1: Porosity modelling by separated geometry volume based on forest type classification

Method 2: Porosity modelling by UDF code based on digitized forest type classification

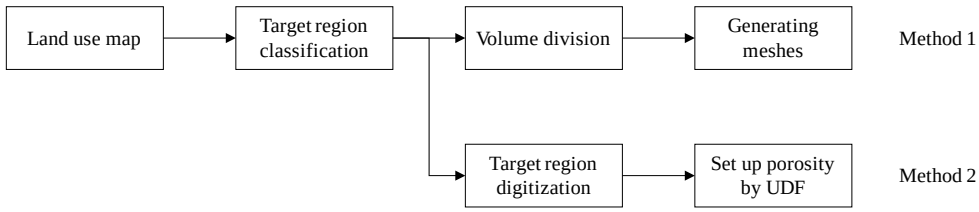

Figure 16 Two methods for simulating a pressure drop by tree porosity

3.2.4.2.1. Porosity modelling using separated geometry volume based on forest type classification

A 3D CFD model was designed using the forest type map provided by Korea Forest Service which was designated as the type of trees, the kind of trees, the diameter of trees, the age of tree, and the density of trees. Volume of the canopy region were designed to be separated from the entire domain in order to implement the porous resistance in the canopy region of trees.

The target region forest was classified according to the kind of trees and we used data which was reclassified as conifer forest, deciduous forest, mixed forest, and unstocked area according to tree type for simulation of the difference in the air resistance between each tree type. The trunk and canopy of conifer forest were designed as 13.4 m from the bottom and 13.4 m to 30.2 m, respectively. In addition, the deciduous and mixed forest canopy were designed as 17.0 m from the bottom and 23.6 m from the bottom, respectively. The height of the mixed forest canopy was calculated using both the height of the coniferous and the deciduous trees.

During the geometric design process, the DesignModeler software repeatedly crashed while dividing the 3.4 km target region surface by surface classification according to the tree. This problem was assumed to be caused by too many points, lines, and faces. To overcome this limitation, the 3D surface model and reclassified

surface were simplified as shown in figure 17. The 3D CFD model can be designed using the simplified land use classification, however it could distort the actual phenomenon because it acts as an additional assumption.

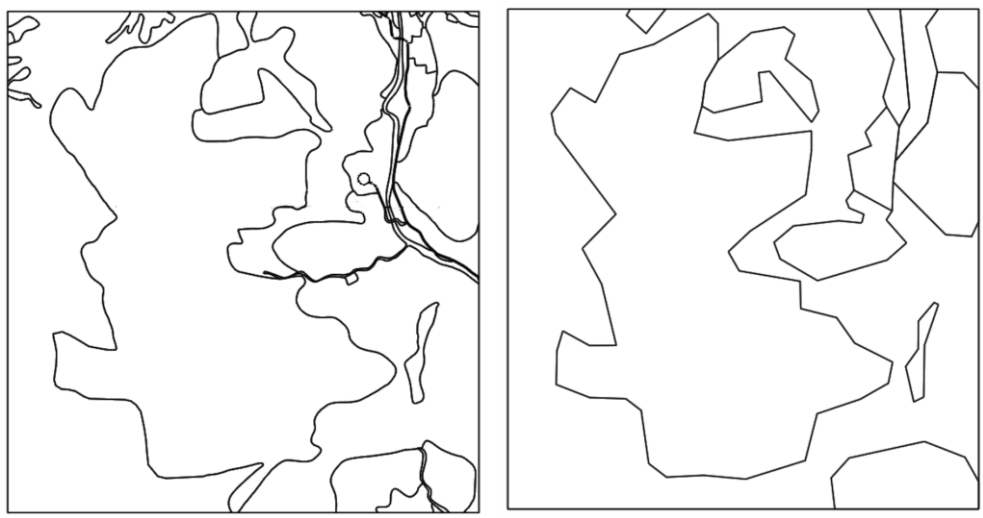

Figure 17 Land use classification of study area (left) and simplified land use classification (right)

In the meshing process, if a divided volume was separately designed, the porosity coefficient can be simply set up at the cell zones of the target region on Fluent and the pressure drop through the porous medium can be simulated. However, for complicated geometry modelling as occurs in this study, excessive computer capacity is required for the mesh design process due to the large number of point, line, and face informations. We used an i7 3.40 GHz quad core CPU and 32.0 GB RAM computer to design a 3D complex terrain model 3.4 km diameter, however we failed to design a good quality meshes due to computer corruption. In addition, the quality of the mesh was poor and it could not be used for the simulation, when the 3D topography model was designed by adjusting the total amount of mesh.

3.2.4.2.2. Porosity modelling using a UDF code based on a digitized forest type classification

The surface classification data were converted to raster data with 5 m ×5 m grid size and the coordinates of farthest southeast cell, grid size, number of columns and rows were added in order to set porosity with the developed UDF code. The porosity coefficients for coniferous, deciduous, and mixed trees were set up in each cell by the UDF code using converted ASCII surface classification data and the measured trunk and canopy as shown in figure 18 (d).

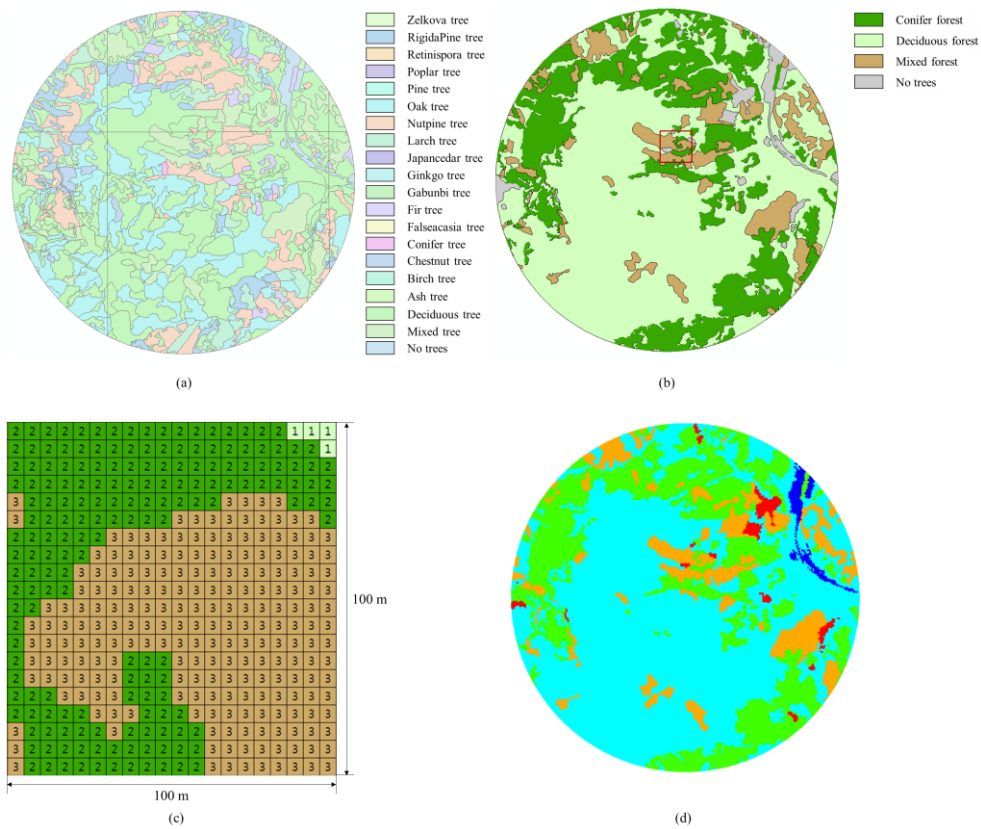

Figure 18 (a) Forest type map of the target region provided by the Korea Forest Service (KFS), (b) surface classification of the target region according to tree type, (c) digitized surface classification data converted to 5 m grid size

(each black has 5 m ×5 m gr id size) with red box area of (b) enlarged, (d) image applied forest type in the 3D CFD model using the UDF.

The implementation process for tree porosity by the UDF code is shown as figure 19. Firstly, the height from the ground of each cell was calculated using the 'cell wall distance' UDF code, which was saved to the User Defined Memory (UDM) of each cell. Then, the digitized land use classification database was also saved to the UDM of each cell. Finally, the porosity coefficient of the trees was implemented by a cross analysis of the height of the cell and digitized land use classification data in each cell using the UDF. Appendix I gives the specific informations of the UDF code.

The digitized land use classification database was constructed as follows; 1) Import the SHP forest type maps provided by the Korea Forest Service (KFS) and extract a target region in ArcMap 10, 2) Categorize forest type based on the research objective, 3) Convert the reclassified vector data to raster data; the raster data could be converted as a specific grid size that fits the researcher's purpose, and 4) Convert the raster data to ASCII data.

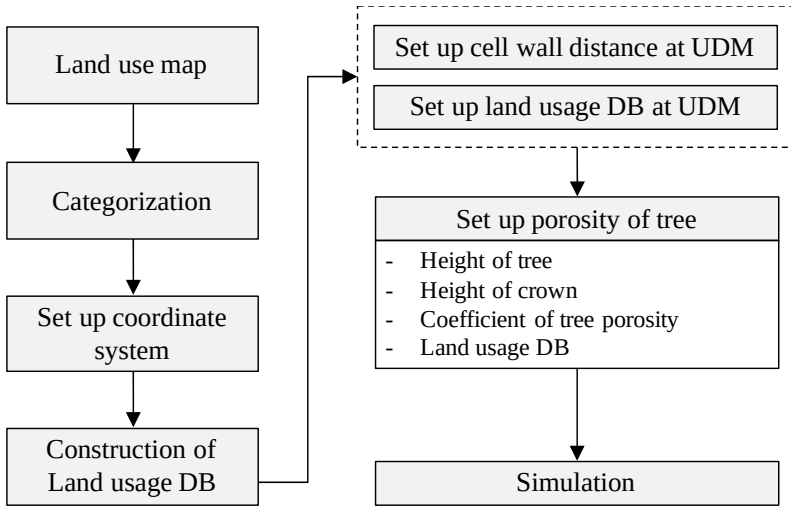

Figure 19 Flow chart for the procedure for the implementation of the tree porosity to CFD model.

As mentioned earlier, each porosity modelling method has its unique strengths and weaknesses, and should be chosen in terms of the research objective, the size of research area, the computational cost, etc. it this study, we used the second method for porosity modelling.

3.2.4.3. Methodology for validation of the CFD model

There is no single turbulence model universally accepted as being superior for all problems. The turbulence model should be selected depending on considerations such as the physics of the flow, the level of accuracy required, the available computational resources, and the amount of time available for the simulation (Fluent, 2013). RANS turbulence models are typically used to economically simulate complex turbulent flows. In this study, five RANS turbulence models which are standard k-ε, RNG k-ε, realizable k-ε, standard k-ω, and SST k-ω were used to simulate airflow in complex mountain terrain, and a suitable turbulence model was

determined by comparison with measured field data.

The simulated CFD results should be validated to verify the reliability of the CFD model by comparing the results with the wind speed and wind direction data measured from the GCK and GDK towers. Of the various evaluation methods, the coefficient of determination is generally used to verify the similarity between the simulated CFD results and the measured field data. It has a strength related to an evaluation of tendency, but it has a limitation related to the evaluation of the difference between the simulated result and the observed data. Therefore, Root Mean Square Error (RMSE) was used to validate the CFD model.

Additionally, a confidence interval estimation method was used for validation. It was a technique for the verification of the statistical homogeneity between the statistics and a parameter. The technique was based on the central limit theorem (CLT), i.e., the sum of independent random variables with the number of the same distribution function is close to a normal distribution (Ross, 1987). If the probability distribution of samples follow a normal distribution, a confidence interval can be estimated using the standard normal random variable (Z) (Hwang, 2010). Therefore, the confidence interval of the wind environment data observed in the field is derived using the standard normal random variable assuming that the natural phenomenon follows the normal distribution.

3.3. Results and discussions

3.3.1. Wind environment analysis of the study area

The prevailing wind speed and direction of GCK and GDK towers were analysed using data measured at 40m height of each towers from January to December in 2015. The prevailing wind direction at the GCK tower was from the west at 34.6 percent and the prevailing wind speed had a range of 0.5 ~ 1.5 m s^{-1} at 52.6 percent as shown in figure 20. In addition, the prevailing wind direction at GDK tower was also from the west at 27.7 percent and the prevailing wind speed was in range of 0.5 ~ 1.5 m s^{-1} at 56.1 percent. The maximum and minimum wind speeds of the GCK tower were 2.95 m s^{-1} and 0.19 m s^{-1} under west wind condition, respectively. In addition, the maximum and minimum wind speeds of the GDK tower were 2.53 m s^{-1} and 0.14 m s^{-1} under west wind condition, respectively.

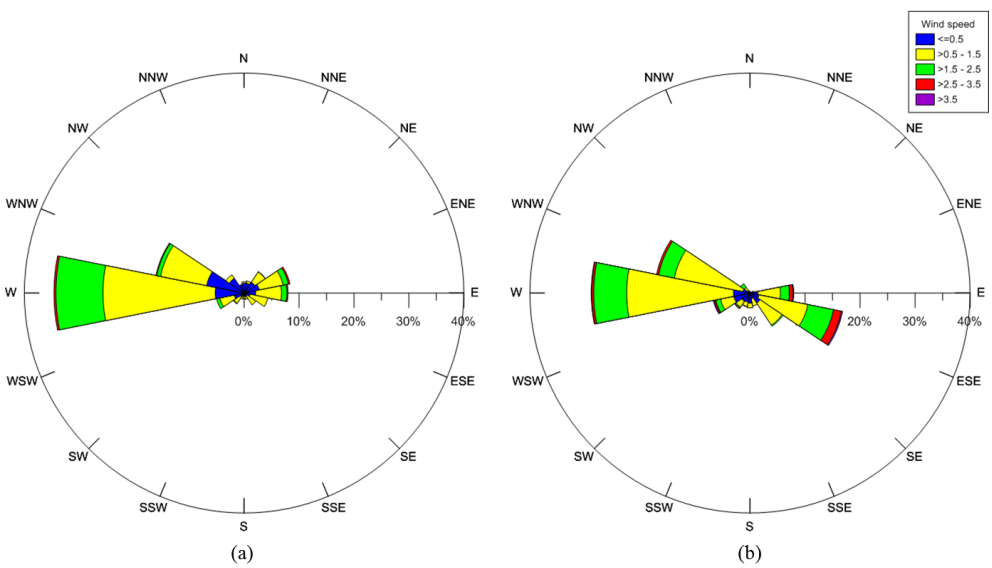

Figure 20 Wind environments of (a) GCK tower and (b) GDK tower in 2015.

The measured wind speed data according to the altitude were normalized based on the measured wind speed data at the point of 40 m of tower GCK tower in order to compare vertical tendency of computed wind speed data according to the altitude (Fig. 21). Theoretically, the wind speed tend to increase logarithmically as altitude increases from the ground. However, the measured wind speed data at elevation of 10 m – 30 m in the GCK tower showed a decreasing tendency. It was due to the aerodynamic porous resistance of the canopy region of the trees, which were distributed near the GCK tower. The wind speed of the canopy region in the west wind condition was observed lower than the wind speed in the east wind condition. This is probably due to the more dense distribution of the coniferous trees on the west side of the GCK tower, as shown in figure 22.

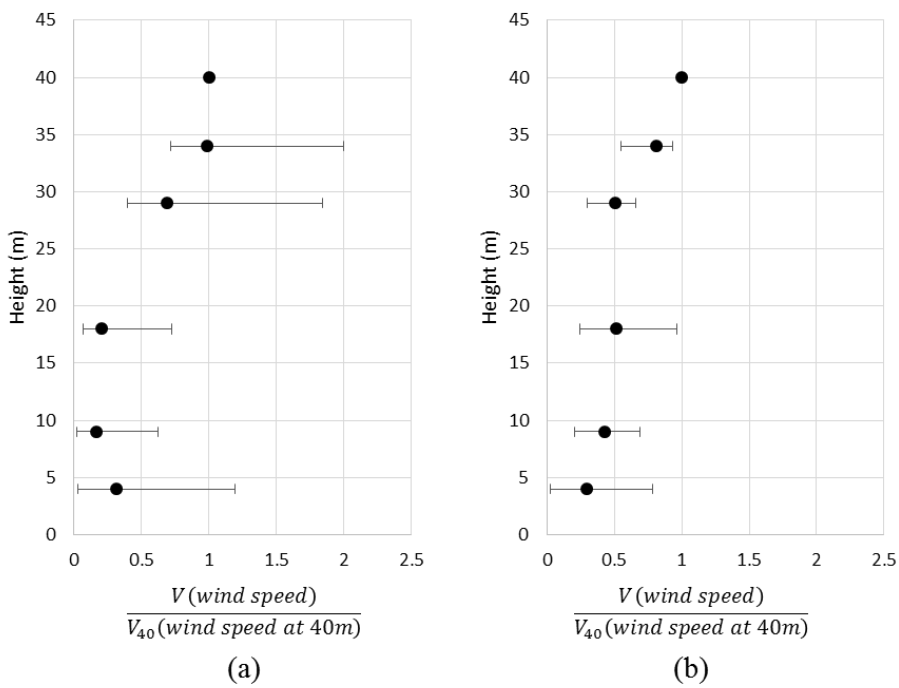

Figure 21 (a) Normalized wind speed distribution at GCK tower according to the height of the anemometers in a west wind condition, (b) normalized wind

speed distribution at GCK tower according to the height of the anemometers in an east wind condition.

(a) (b)

Figure 22 (a) Picture looking west direction from the GCK tower, (b) picture looking east direction from the GCK tower.

3.3.2. Validation of the CFD simulation model

3.3.2.1. Horizontal wind verification

The simulated data and the 95% confidence interval of the observed wind speed and the direction of GCK and GDK towers were compared to validate the accuracy of the CFD simulation model and determine appropriate turbulence model. Firstly, the 95% confidence interval of the wind speed and direction were analyzed using measured data at 40 m of GCK and GDK towers in an east wind condition. The confidence interval for the wind speed was 1.23 m $s^{-1} \leq WS_{GCK} \leq$ 1.77 m s^{-1} from GCK, and 1.51 m $s^{-1} \leq WS_{GDK} \leq$ 2.22 m s^{-1} from GDK. The confidence interval of the wind direction was 76.7° $\leq WD_{GCK} \leq$ 89.4° from GCK, and 93.0° $\leq WD_{GDK} \leq$ 98.4° from GDK. Next, the simulated wind speed and direction at 40 m from the GCK and GDK tower locations were deduced using CFD simulation model with five turbulence models, which were the standard k-ε, RNG k-ε, realizable k-ε, standard

k-ω, and SST k-ω turbulence models. Table 7 and 8 show the results.

A comparison of the measured and simulated results from GCK tower indicated that the simulated data using the Standard k-ε and Realizable k-ε turbulence models were included within the 95% confidence intervals for both the wind speed and direction. However, both the wind speed and direction simulated using the RNG k-ε and Standard k-ω turbulence model did not conform within the 95% confidence interval. The comparison of the measured and simulated data indicated that only the simulated wind speed and direction data satisfied the 95% confidence interval if the standard k-ε turbulence model was used to simulate the wind environment.

Table 7 The measured data from the GCK and GDK towers when wind boundary condition was an east wind considering 95% confidence interval (C.I.).

		Mean value	Standard deviation	Lower limit of C.I.	Upper limit of C.I.	Length of C.I.
GCK	Wind speed (m s^{-1})	1.50	0.53	1.23	1.77	0.54
	Wind direction (°)	83.1	12.29	76.7	89.4	12.7
GDK	Wind speed (m s^{-1})	1.86	0.69	1.51	2.22	0.71
	Wind direction (°)	95.7	5.27	93.0	98.4	5.4

Table 8 The simulated results of the CFD model according to various turbulence models when the wind boundary condition was an east wind.

		Mean value	Standard deviation	Lower limit of C.I.	Upper limit of C.I.	Length of C.I.
GCK	Wind speed (m s^{-1})	1.72	1.97	1.60	1.14	1.63
	Wind direction (°)	82.5	76.4	79.1	94.4	67.3

GDK	Wind speed (m s^{-1})	1.65	1.38	1.61	1.16	1.36
	Wind direction (°)	93.2	86.3	92.8	87.8	93.2

Additionally, the 95% confidence interval of the wind speed and direction measured at 40 m height of the GCK and GDK towers were also analyzed in a west wind condition. As a result, the confidence interval of the wind speed was 0.54 m $s^{-1} \leq WS_{GCK} \leq 1.90$ m s^{-1} from GCK, and 0.37 m $s^{-1} \leq WS_{GDK} \leq 1.25$ m s^{-1} from GDK. Additionally, the confidence interval of the wind direction was $263.3° \leq WD_{GCK} \leq 286.4°$ from GCK, and $321.7° \leq WD_{GDK} \leq 348.4°$ from GDK.

A comparison of the observed and simulated results from the GCK tower indicated that the simulated data using the Standard k-ε and Standard k- ω turbulence model were within the 95% confidence interval for both the wind speed and direction. However, the Realizable k-ε and SST k-ω turbulence models showed similar result only for wind direction. In addition, the simulated data from the GDK tower using the Standard k-ε and SST k- ω turbulence models were included within the 95% confidence intervals for both wind speed and direction.

Table 9 The measured data from the GCK and GDK towers when wind boundary condition was an west wind considering 95% confidence interval (C.I.).

		Average	Standard deviation	Lower limit of C.I.	Upper limit of C.I.	Length of C.I.
GCK	Wind speed (m s^{-1})	1.22	0.83	0.54	1.90	1.36
	Wind direction (°)	274.9	14.13	263.3	286.4	13.1
GDK	Wind speed (m s^{-1})	0.81	0.54	0.37	1.25	0.88
	Wind direction (°)	335.1	16.40	321.7	348.4	26.7

Table 10 The simulated results of the CFD model according to various turbulence models when the wind boundary condition was an west wind.

		Standard k-ε	RNG k-ε	Realizable k-ε	Standard k-ω	SST k-ω
GCK	Wind speed ($m\ s^{-1}$)	1.86	2.06	2.00	1.86	2.10
	Wind direction (°)	264.8	260.5	266.2	266.1	267.7
GDK	Wind speed ($m\ s^{-1}$)	0.68	0.69	0.73	0.67	0.63
	Wind direction (°)	346.7	358.8	351.5	348.8	347.6

3.3.2.2. Vertical wind verification

The vertical wind speed distribution of the measured data and simulated results from the GCK tower were also compared to validate the CFD model. The measured and simulated wind speed data according to height were normalized by the wind speed at 40m height in order to analyse the tendency of the wind speed change according to the altitude change.

In five turbulence model conditions, the wind speed reduction according to the porous resistance of the canopy was well simulated. There was a slight difference in the turbulence model condition, but it was confirmed that the slow wind speed was maintained until 30 m where the leaves of the coniferous tree were distributed, and then the wind speed was increased. The RMSE and R^2 value were calculated to compare the observed wind speed data and the simulated wind speed data at six points in height, and we used the calculated values to determine the appropriate turbulence model to simulate the wind environment in the mountain complex terrain.

In west wind condition, the R^2 values between the measured data and the simulated results under the conditions of standard k-ε, RNG k-ε, realizable k-ε, standard k-ω, and SST k-ω turbulence model were 0.926, 0.926, 0.934, 0.927, and 0.931, respectively, and it was judged that the wind speed tendency according to the height were well simulated. The RMSE values between the measured data and the simulated results under five turbulence models were 0.111, 0.132, 0.114, 0.112, and 0.142 m s^{-1}, respectively. According to the calculated RMSE values, the error between the simulated results and the observed results was judged to be low when the standard k-ε, realizable k-ε, and standard k-ω turbulence model conditions were used. In east wind condition, the R^2 values between the measured data and the simulated results under five turbulence models were 0.987, 0.931, 0.974, 0.966, and 0.971, respectively, and the RMSE values were 0.104, 0.168, 0.103, 0.121, and 0.140 m s^{-1}, respectively.

Comprehensively, when we used standard k-ε turbulence model in order to simulate the wind environment simulation in mountain complex terrain, the wind environment distribution was simulated similarly. Therefore, the Standard k-ε turbulence model was determined as a appropriate turbulence model in order to simulate the airflow over mountain complex terrain.

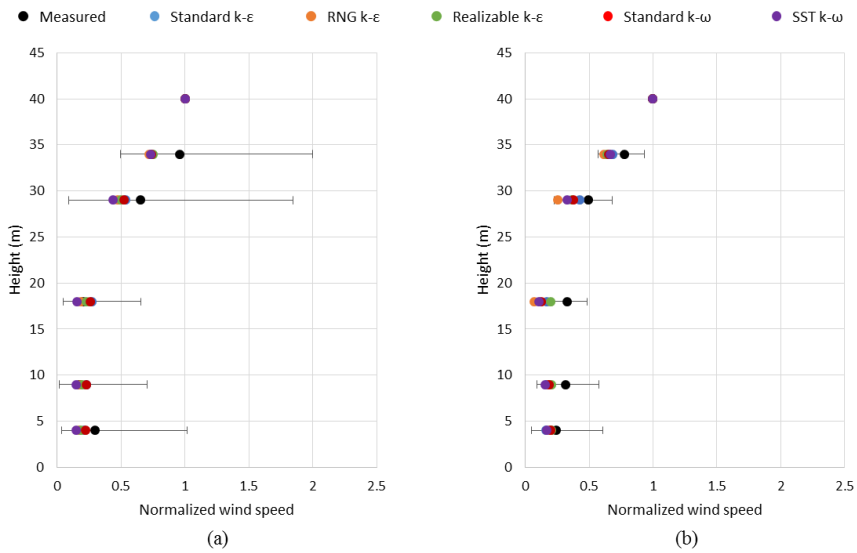

Figure 23 (a) Comparison of the measured wind speed and the simulated wind speed according to the height of anemometers in a west wind condition, (b) Comparison of the measured wind speed and the simulated wind speed according to the height of anemometers in an east wind condition.

3.4. Conclusions

This chapter presented two methodologies for forested complex mountain terrain modelling to estimate the wind environment using Commercial CFD technology. The porosity modelling method using separated geometry volume based on forest type classification was limited to develop complex mountain terrain model due to the excessive point, line, and surface information. Therefore, in this study, the porosity modelling method using a UDF code based on a digitized forest type classification was suggested to develop 3D CFD model for complex mountain terrain, and the suggested method had advantages that the 3D CFD model for forested mountain terrain can be designed more easily because the method did not require separately designed cell zone.

The k-ω turbulence models are generally recommended for cases where the flow separates under adverse pressure gradients from smooth surface such as airfoils. Threrfore, the results simulated with k-ε turbulence models were better than the results simulated with k-ω turbulence models, because airflow was simulated from nonsmooth surface such as mountain region. A reasonable accuracy was confirmed when the developed 3D CFD model was simulated using the standard k-ε turbulence model. To improve the accuracy of simulation result, field experiments should be conducted to derive the inertial resistance coefficient of the target tree in future study.

Chapter 4. Development of a micro-scale CFD model to predict wind environment in mountain terrain using an open-source CFD package

4.1. Introduction

The aim of this chapter was to develop a 3D aerodynamic open-source CFD model to qualitatively and quantitatively predict the wind environment in a mountain area considering topographical conditions and the air resistance of the tree canopy. Both commercial CFD and open-source CFD simulate fluid flow using the Navier-Stokes equations but it have difference characteristics (Table 11).

Table 11 summary of commercial CFD and open-source CFD

	ANSYS (Commercial CFD)	OpenFOAM (Open-source CFD)
License	Commercial	Free
Operating system	Windows	Linux
Interface	GUI (Graphical User Interface)	TUI (Text User Interface)
Flexibility	Non-modifiable of computational algorism	Modifiable of C++ solver code
Expandability	Adding functions using C language program	Modifying and developing source codes using C++
Pre-processor	Design Modeler	None
Post-processor	CFD-post	ParaFoam

Open-source CFD software is free simulation software that is provided under a software license that permits users to study, change, and improve the source code of

the open-source CFD software. The primary steps in this study were 1) development of the 3D open-source CFD simulation model, 2) development of the method for applying aerodynamic porosity resistance of tree to the open-source CFD model, 3) evaluation of the porosity coefficient of target trees by field experiment, and 4) validation of the designed the open-source CFD model.

4.2. Materials and methods

4.2.1. The study area

The study site was the Gwangneung arboretum (37°45′08.0″N, 127°09′57.5″E) located in Pocheon-city, Gyeonggi-province, Republic of Korea, which is the same as the study area of Chapter 3. The forest type map provided by the Korea Forest Service distinguishes 44 kinds of trees distributed in mountain areas. There are 13 species of trees such as Chestnut, Fir, Ginkgo, Larch, mixed forest, Nutpine, Oak, coniferous, deciduous, Pine, Retinispora, Rigidapine and Zelkova, as shown in figure 24 (a). However, since it is impractical to apply the porosity coefficient of each tree type to the CFD model, the trees distributed in the study area were classified into three groups: coniferous forest, deciduous forest and mixed forest, as shown in figure 24 (b).

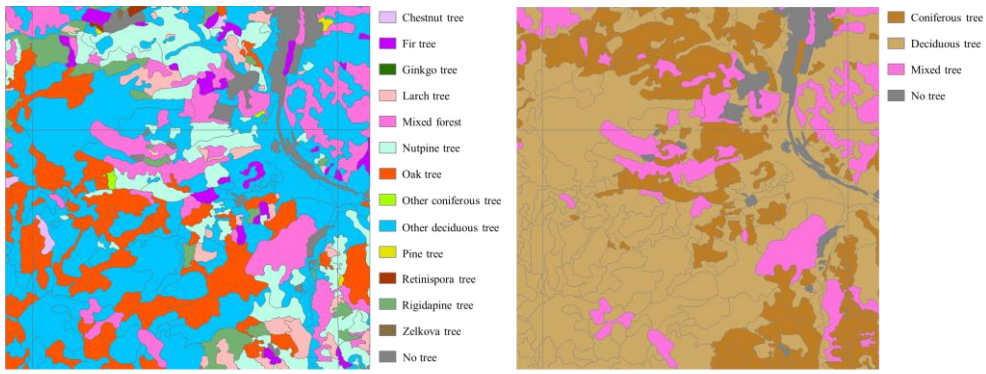

Figure 24 (a) Forest type map of the target region provided by the Korea Forest Service (KFS), (b) forest type map of the study area reclassified as coniferous forest, deciduous forest, and mixed forest.

4.2.2. Experimental trees for evaluating porosity coefficient

Field experiments were conducted to evaluate porosity coefficients of coniferous trees (*Abies holophylla*) and deciduous trees (*Quercus serrata*) which are primarily distributed around the study area, however, the field experiments were limited due to the excessive height and density of these trees. Therefore, the field experiments were carried out using a coniferous tree located in National Institute of Forest Science (37°46′01.8″N, 127°10′45.7″E) and a deciduous tree located in National Institute of Forest Science (37°46′01.8″N, 127°10′45.7″E).

The height and the trunk height of the coniferous tree were 5.5 m and 2.7 m, respectively, and the width of the canopy was 3.0 m (Fig. 25 (a)). The height and the trunk height of the deciduous tree were 7.0 m and 1.0 m, respectively, and the width of canopy was 6.0 m (Fig. 25 (b)).

(a) (b)

Figure 25 (a) Picture of coniferous tree (*Abies holophylla*) which was used to field experiment (37°46′01.8″N, 127°10′45.7″E), (b) Picture of deciduous tree (*Quercus serrata*) which was used to field experiment(37°46′01.8″N, 127°10′45.7″E).

4.2.3. Open-source CFD

3D CFD model was developed in order to predict wind environment in mountain region considering mountain topography using OpenFOAM (Open source Field Operation And Manipulation), which is widely used in fluid flow analysis among various open-source CFD software packages such as OpenFOAM, SU2, and REEF3D. OpenFOAM was originally developed by Henry Weller under the name FOAM from the late 1980s at Imperial College, London to develop a more powerful and flexible general simulation platform. In 2004, Henry Weller, Chris Greenshields and Mattijs Janssens found OpenCFD Ltd to develop and release freely OpenFOAM. OpenFOAM has the advantage of following the GNU-GPL (GNU is Not Unix - General Public License) licensing policy, so that the source code can be modified and redistributed without license fees. In addition, there is no restriction on the

commercial and non-commercial use of the software by individuals and entities because the GNU-GPL license applies to any secondary works. Since OpenFOAM was designed to run on the Linux operating system, researchers who do not have experience with Linux can experience difficulties in using it. Although there is a way to run OpenFOAM on a Windows operating system, it has a disadvantage in that operation speed is slow, and so it is advantageous to operate on Linux operating system where possible. OpenFOAM was developed based on C++ programing language, one of the popular programming languages, therefore researchers using the software need knowledge of the programming language. The simulation solver's code can be modified or completely replaced according to the purpose of the researcher. However, if researchers lack understanding of computational fluid dynamics and C++ programming language, they may have difficulty in modifying and developing code. In addition, it is necessary to write the code using a predetermined format for the initial conditions, boundary conditions and various constants in order to simulate using OpenFOAM, so that the programming ability is required to the researchers.

A simulation procedure of a 3D open-source CFD modelling and a case structure of The OpenFOAM can generally be presented as shown in figure 26 and 27. Each case should be saved as a directory, and it must contain at least the three directories: system, constant and 0. Material properties, turbulence properties and mesh information were located in ‘constant’ directory. Solution controls, discretization schemes, mesh design controls and time step controls were located in ‘system’ directory. And boundary condition and initial condition for simulation were located in ‘0’ directory. All of the files consisting the OpenFOAM structure were written in text based on C++ programing language, and appendix II gives specific

information of the files. As the case is solved, new time data are written in their own directories.

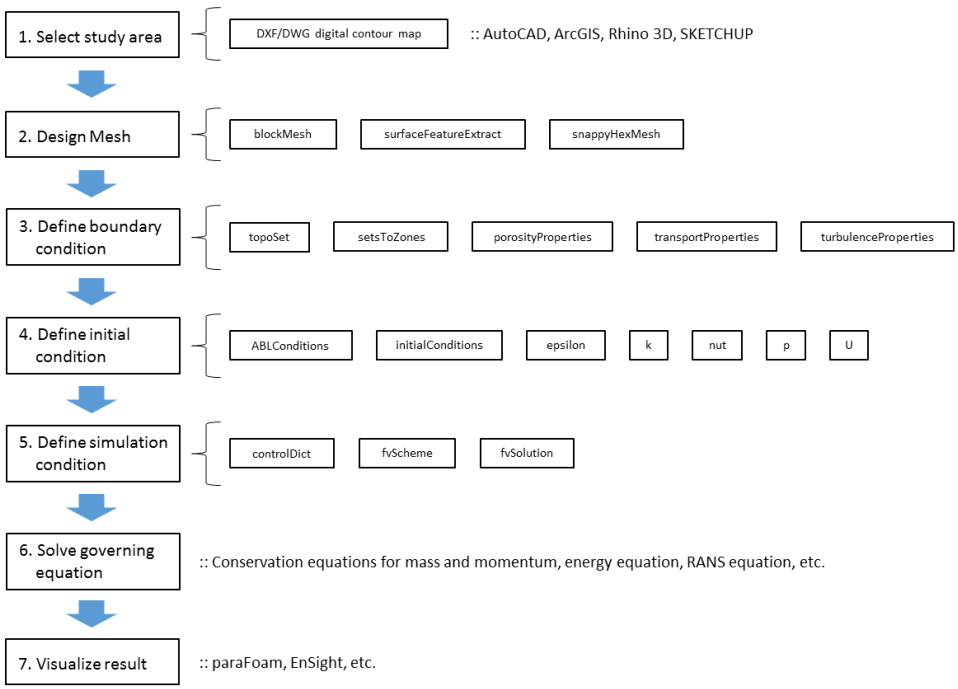

Figure 26 Simulation procedure of a 3D open-source CFD modelling

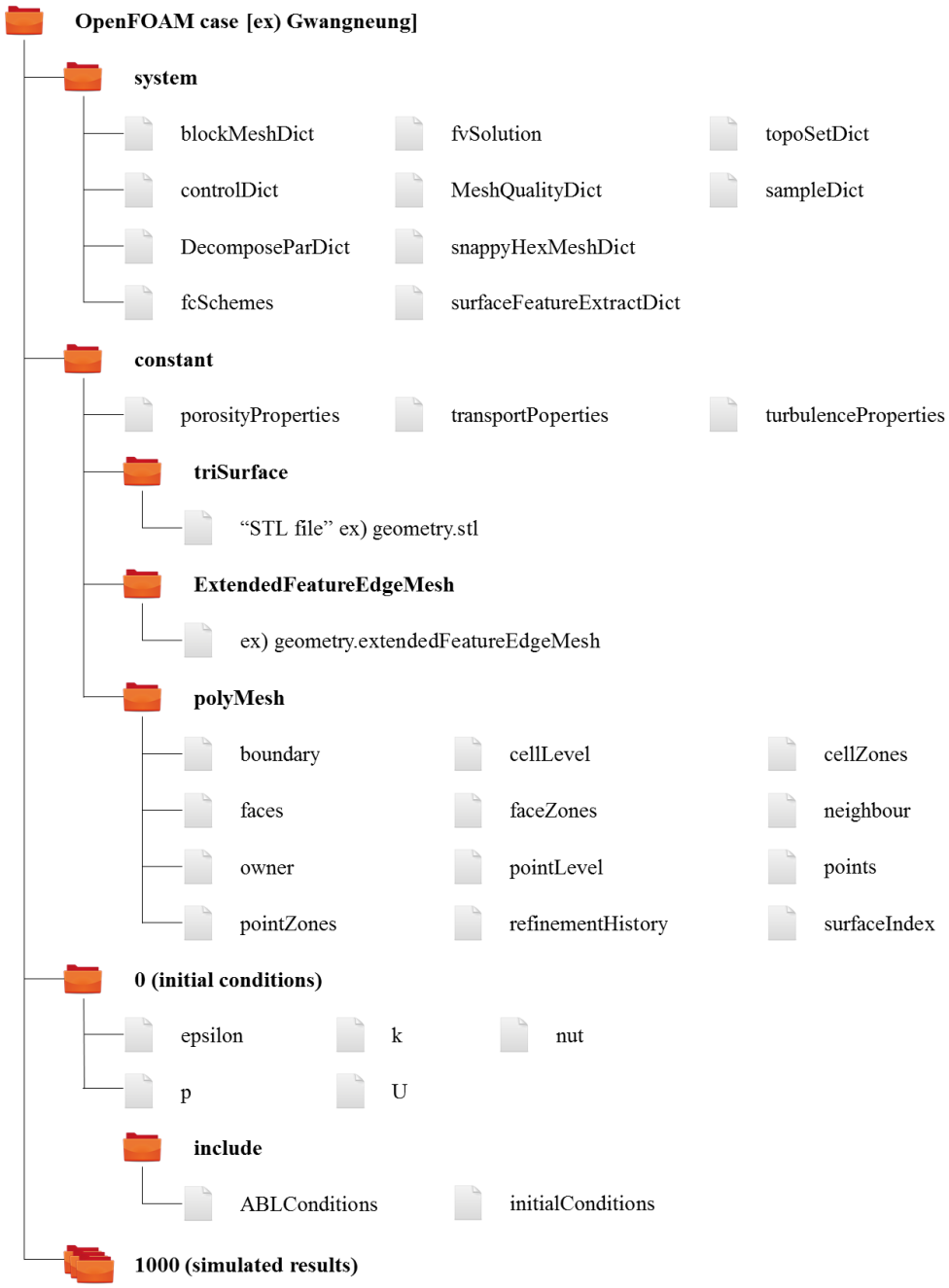

Figure 27 Simulation case structure of the OpenFOAM

4.2.4. Experimental procedure

The three-dimensional geometry was designed using a digital contour map

provided by the National Geographical Information Institute (NGII) of the Republic of Korea, and the coniferous, deciduous, and mixed forest sections were classified using a forest type map provided by the Korea Forest Service (KFS) in order to investigate changes in the airflow caused by trees. The air-resistance of the coniferous and deciduous trees was evaluated by field experiments, and the measured air-resistances applied to the separated forest sections. Finally, the 3D open-source CFD model was validated by a comparison with simulated and measured wind environment data.

4.2.4.1. Evaluating the inertial resistance coefficient of trees

Field experiments were conducted from August 10 to August 11 2016 to determine the inertial resistance coefficient of the coniferous tree, and the maximum wind speed was 3.66 m s^{-1} during the experiment. In addition, field experiments were conducted from September 5 to September 6 2016 to determine the inertial resistance coefficient of the deciduous tree, and the maximum wind speed was 5.35 m s^{-1} during the experiment. The wind speed reduction caused when the airflow passing through the tree was measured by installing hot-wire anemometers in eight directions at 0.5 m and 1.0 m from the target tree as shown figure 28. A 3D ultra-sonic anemometer (DeltaOHM, Italia) was installed near the experimental tree to determine the wind speeds of the windward and leeward sides among the measured wind speed in eight directions. The wind speed reduction which occurred as the airflow passed through the target tree was calculated using the measured wind speeds of windward and leeward sides determined using the wind direction data measured by the 3D ultra-sonic anemometer.

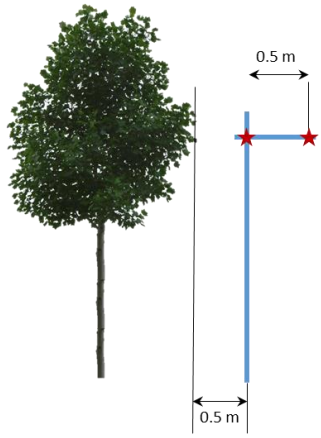

(a)

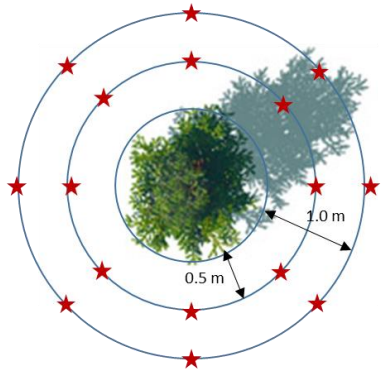

(b)

(c)

(d)

Figure 28 (a) Experimental schematic side view, (b) experimental schematic top view, (c) experimental pictures for evaluating air-resistance of the

coniferous tree and (d) the deciduous tree

The inertial resistance coefficient can be derived directly from the measurement of the pressure reduction that occurs when the airflow passes through the tree. Because the wind tunnel experiment was conducted in a closed space, it is possible to measure the pressure reduction directly caused by the experimental tree. However, it is more challenging to derive the inertial resistance coefficient using field measurements since pressure effects are not only caused by the tree itself, but also by the diffusion of airflow to the surrounding. Therefore, in this study, the wind speed reduction caused when the airflow passing through the experimental tree was measured in the field experiment, and then the inertial resistance coefficient was reversely estimated using CFD simulations and measured wind speed reduction by field experiments.

The domain lengths of windward and leeward sides and the domain height of the 3D CFD model were designed as shown in figure 29 following designs described in other studies (Bournet and Boulard, 2010; Bournet et al., 2007; Franke et al., 2004; Hefny and Ooka, 2008; Tominaga et al., 2008). The inertial resistance coefficient of the canopy was set at 0.1 m^{-1} intervals from 0 m^{-1} to 1.0 m^{-1}, and the wind speed was set at 0.5 m s^{-1} intervals from 0.5 m s^{-1} to 3.0 m s^{-1}. Through the CFD simulation, the wind speed reduction tendency according to the inertial resistance coefficient of the canopy was analyzed, and the internal resistance coefficient of the target tree was deduced by comparing with these results with the wind speed reduction measured in the field experiment.

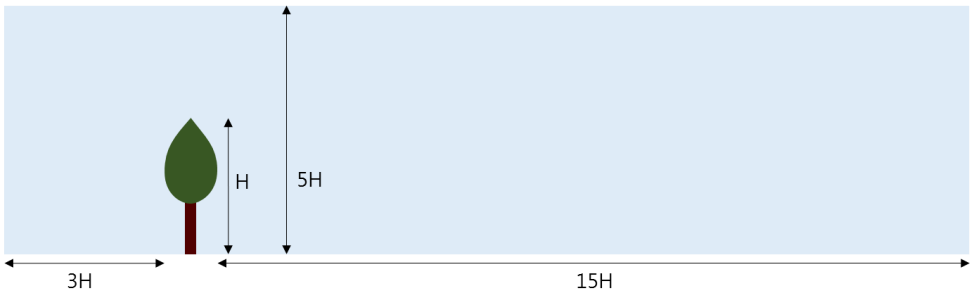

Figure 29 CFD simulation domain for deriving inertial resistance coefficient of experimental trees, where H is the tree height

4.2.4.2. Design of 3D open-source CFD model

The ‘solid object’ was designed using the contour lines of the target area provided by the National Geographic Information Institute in Republic of Korea in order to develop a 3D open-source CFD model for mountain terrain following the modelling procedure described in Chapter 3 and other study (Hong et al., 2011a). The designed 3D terrain 'solid object' was converted to the 'STL' format, and the 3D complex terrain CFD model was developed using OpenFOAM and the converted ‘STL’ format 3D surface data by following precedure; 1) Design a primary grid with a domain size that includes the study area of the ‘solid object’ in ‘STL’ format data using the ‘blockMesh’ function as shown in figure 30,

```
17 vertices
18 (
19     (-3300 -3300 0)
20     (5700 -3300 0)
21     (5700 5700 0)
22     (-3300 5700 0)
23     (-3300 -3300 1500)
24     (5700 -3300 1500)
25     (5700 5700 1500)
26     (-3300 5700 1500)
27 );
28
29 blocks
30 (
31     hex (0 1 2 3 4 5 6 7) (90 90 15) simpleGrading (1 1 1)
32 );
```

Figure 30 OpenFOAM code for design a primary grid

2) Extract feature lines from ‘solid object’ in ‘STL’ format data using ‘surfaceFeatureExtract’ function as shown in figure 31, and

```
34 contour|.stl
35 {
36     extractionMethod    extractFromSurface;
37
38     extractFromSurfaceCoeffs
39     {
40         // Mark edges whose adjacent surface normals are at an angle less
41         // than includedAngle as features
42         // - 0  : selects no edges
43         // - 180: selects all edges
44         includedAngle   180;
45     }
46
47     // Write options
48     writeFeatureEdgeMesh    yes;
49 }
```

Figure 31 OpenFOAM code to extract feature lines

3) Design 3D complex terrain CFD model through the castellation step and Snapping step using ‘snappyHexMesh’ function. In the castellation process, the mesh of the domain was refined according to the level set in the ‘snappyHexMeshDict’ code and the mesh located at outer region of interested domain was removed. Then, the shape of the castellated mesh created in the castellation process was smoothly redesigned according to the feature line through the snap process. In this process, the vertex coordinates of the ‘Castellated Mesh’ were shifted repeatedly under the mesh quality condition defined in the code by the researcher, and the 3D complex terrain model with a smooth surface, as like as 'Snapped Mesh' in figure 32, was developed.

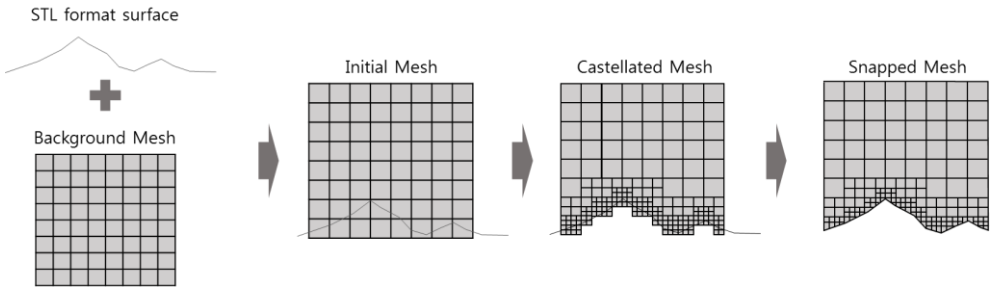

Figure 32 design procedure of 3D complex terrain CFD model using OpenFOAM CFD package

In order to evaluate the effect of the size of the mesh on the simulation results and to determine the appropriate size of the mesh for economic simulation time, three models with different mesh sizes are designed as shown in figure 33.

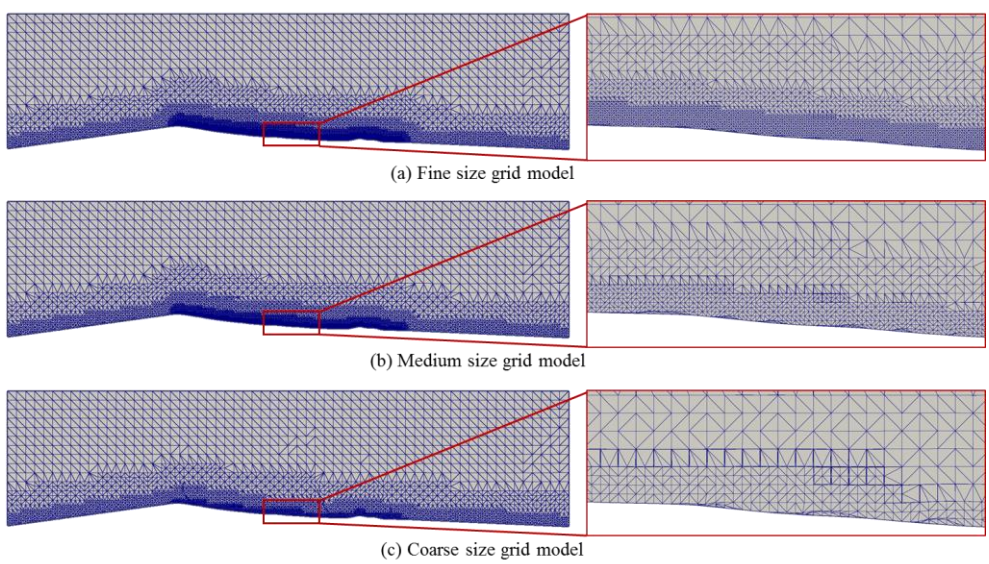

Figure 33 3D complex terrain CFD models for grid independence test (mesh size near the interested experimental ground surface: (a) 3.12 m, (b) 6.25 m, and (c) 12.5 m))

It is important to realize that the air-resistance of trees can have a large influence on the airflow near the ground surface, and hence on the simulation of the wind

environment in mountain terrain. Various researchers have designed the canopy area of the tree as a porous medium and simulated the change of the airflow according to the inertial resistance coefficient. However, this is not always practical since designing each tree canopy area separately for each cell zone requires an excessive number of meshes. In Chapter 3, a method for designing a 3D model including the forest regions distributed in the mountain area was proposed using a commercial CFD simulation program (ANSYS). However, the method proposed in Chapter 3 requires complicated processes such as the analysis of the forest area using the forest type map, UDF code development for height calculation from the ground of each cell and application of an inertial resistance coefficient to the canopy area.

On the other hand, if you use the OpenFOAM simulation software, you can apply the inertial resistance coefficient of the tree to the target area relatively easily by using the 'topoSetDict' function. The inertial resistance coefficients of the experimental trees were applied to the 3D CFD open-source model as follow; 1) Separate forest regions according to the type of tree using the forest type map provided by the KFS and then extract an each forest regions, 2) Divide the ground surface using the separated forest regions and the designed 3D terrain ‘solid object’, 3) Design 3D volume of each canopy region using the divided ground surface and height data of each forest canopy and then extract the designed 3D volumes, 4) Generate a mesh “Set” in the name of each forest 3D volume in the “constant/polyMesh” folder comparing the coordinates of the designed 3D volume and the designed 3D CFD open-source model using the ‘topoSet’ function as shown in figure 34,

```
actions
(
    {
        name    ConiferBox;
        type    cellSet;
        action  new;
        source  surfaceToCell;
        sourceInfo
        {
            file "ConiferBox0921.stl";
            outsidePoints       ((1000 1000 1000)) ;
            includeCut          false;
            includeInside       true;
            includeOutside      false;
            nearDistance        -1;
            curvature           0.9;
        }
    }
    {
        name    DeciduousBox;
        type    cellSet;
        action  new;
        source  surfaceToCell;
        sourceInfo
        {
            file "DeciduousBox0921.stl";
            outsidePoints       ((1000 1000 1000)) ;
            includeCut          false;
            includeInside       true;
            includeOutside      false;
            nearDistance        -1;
            curvature           0.9;
        }
    }
    {
        name    MixedBox;
        type    cellSet;
        action  new;
        source  surfaceToCell;
        sourceInfo
        {
            file "MixedBox0921.stl";
            outsidePoints       ((1000 1000 1000)) ;
            includeCut          false;
            includeInside       true;
            includeOutside      false;
            nearDistance        -1;
            curvature           0.9;
        }
    }
```

Figure 34 OpenFOAM code of 'topoSetDict' function to set the forest region

5) Generate cellZones using the generated mesh "Set" with 'setsToZones' function of OpenFOAM and 6) Write 'porosityProperties' code in the "constant" folder and apply the inertial resistance coefficient in the canopy region of forest.

4.2.4.3. Methodology for validation of the open-source CFD model

A grid independence test and a turbulence model test were conducted in order to verify the reliability of the simulated results using the developed 3D open-source

CFD model. Generally, it is known that model accuracy increases as the resolution of the mesh constituting the model increases, but over a certain resolution the gains from increasing mesh resolution become negligible, while processing time can become uneconomic. Therefore, determining an appropriate size of mesh for economic simulation is essential in designing a 3D CFD model. In addition, turbulence should also be considered when simulating airflow. Many researchers used various turbulence models to simulate turbulent flow because direct computation of turbulent flow requires excessive computational processing. It is necessary to determine the suitable turbulence model for the exact research purpose, since each may simplify calculation of the turbulent flow in varying hypothesis.

Therefore, in this study, a gird independence test was conducted for three mesh sizes (3.12m, 6.25m, and 12.5m), and the turbulence model test was also conducted for four turbulence model (Standard k-ε, RNG k-ε, Realizable k-ε, SST k-ω) which are widely used in airflow simulation. The simulated CFD results were validated by comparing the results with vertical distribution wind speed data measured from the GCK tower. In order to evaluate the influence on the wind environment of the conifer canopy distributed near the GCK tower, vertical distribution of the wind speed was analysed using the measured data from a total of six points from the 40 m point, which is installed 10 m higher than the height of coniferous trees distributed around the GCK tower, to the 4 m point which is installed nearest to the ground. The measured wind speed data of the six points were normalized using wind speed data from the 40 m point which was not affected by the coniferous trees distributed around the GCK tower. Wind environment data were excluded from the analysis when the wind speed of 40 m point was less than 0.5 m s^{-1} because wind speeds less than 0.5 m s^{-1} are classified as no-wind (calm wind)

according to the wind environment data analysis method of the Korea Meteorological Administration. In the same way, the vertical wind environment data simulated by the 3D open-source CFD model were normalized by using wind speed data from the 40 m point and the 3D open-source CFD model was validated by comparison with field data by RMSE.

Table 12 Input data of the 3D open-source CFD model

Contents	Values	
Velocity of reference height	1.5 m s^{-1}	
Reference height	40 m	
Turbulence kinetic energy (k)	0.03375 m^2 s^{-2}	
Turbulence dissipation (ε)	0.000213 m^2 s^{-3}	
Boundary type of inlets	U	atmBoundaryLayerInletVelocity
	k	atmBoundaryLayerInletK
	epsilon	atmBoundaryLayerInletEpsilon
Grid size (Total number of meshes)	3.12 m (7.95 M.), 6.25 m (1.84 M.), 12.5 m (0.72 M.)	
Wind direction	East wind, west wind	
Turbulence model	Standard k-ε, RNG k-ε, Realizable k-ε, Standard k-ω	

4.3. Results and discussions

4.3.1. Inertial resistance coefficient of experimental trees

As a first step to derive the inertial resistance coefficient of the test tree, wind speed data of the windward and leeward sides was measured from the field experiments, and used to derive wind speed reduction caused by airflow passing through trees. In the second step, s single tree located in open space was designed as a CFD model, and the wind speed reduction caused by the inertial resistance coefficient of the canopy was analysed. Finally, the inertial resistance coefficients of the experimental trees were estimated using the wind speed reduction derived from the field experiments and the relationship between the inertial resistance coefficient and the wind speed reduction derived from the CFD simulation.

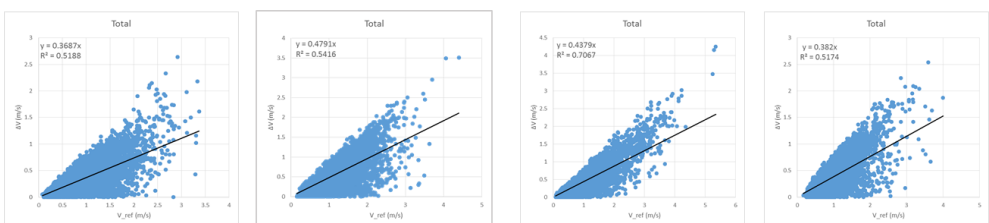

(a) (b) (c) (d)

Figure 35 Measured wind speed reduction according to wind speed of windward by field experiment during August 10 to September 6 (a : Coniferous tree 1, b : coniferous tree 2, c : deciduous tree 1, d : deciduous tree 2)

The wind speed reduction ratio (α) defined as the ratio of the wind speed reduction to the wind speed of on the windward side was derived from wind speed of the windward and leeward sides as measured from the field experiments. The wind speed reduction ratios (α) of the experimental coniferous trees were calculated as

0.368 to 0.495, and the wind speed reduction ratios (α) of experimental deciduous trees were calculated as 0.382 to 0.438.

Table 13 Wind speed reduction derived from the CFD simulation according to inertial resistance coefficient and wind speed of the windward side (wind speed of windward side – wind speed of leeward side)

		Inertial resistance coefficient (C_i)					
		0.1	0.15	0.2	0.25	0.3	0.4
Wind speed of windward ($m\ s^{-1}$)	0.5	0.04	0.06	0.08	0.09	0.11	0.13
	1.0	0.08	0.12	0.16	0.19	0.22	0.27
	1.5	0.13	0.18	0.23	0.28	0.32	0.40
	2.0	0.17	0.24	0.31	0.37	0.43	0.54
	3.0	0.25	0.36	0.47	0.56	0.65	0.80
		Inertial resistance coefficient (C_i)					
		0.5	0.6	0.7	0.8	0.9	1.0
Wind speed of windward ($m\ s^{-1}$)	0.5	0.16	0.18	0.19	0.21	0.22	0.23
	1.0	0.31	0.35	0.38	0.41	0.44	0.46
	1.5	0.47	0.53	0.58	0.62	0.66	0.69
	2.0	0.62	0.70	0.77	0.82	0.87	0.91
	3.0	0.94	1.05	1.15	1.24	1.31	1.37

The wind speed reduction showed a tendency to increase as the wind speed of the windward side increased. Likewise, the wind speed reduction caused by passing through the tree was increased as the inertial resistance coefficient was increased. It was confirmed that the wind speed reduction increased linearly with increasing wind speed on the windward side for each inertial resistance coefficient. In addition, the relationship between the wind speed reduction ratio (α) and the inertial resistance coefficient was derived as shown in figure 36.

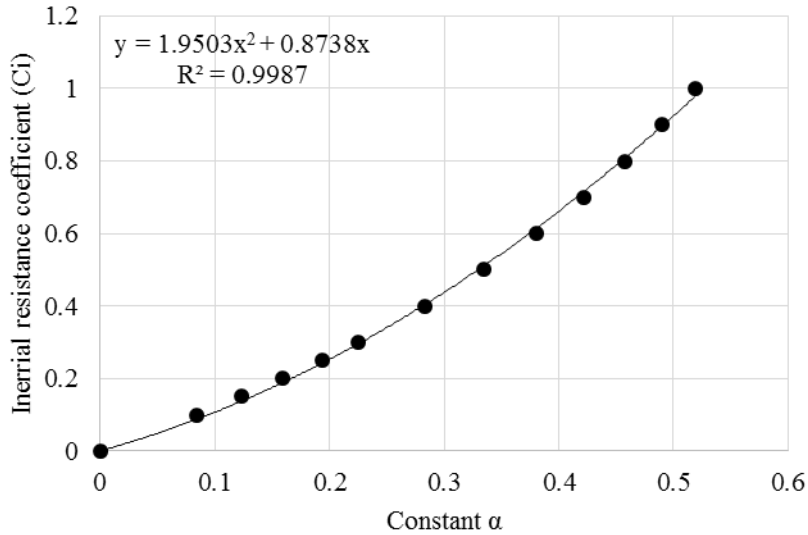

Figure 36 Relationship between the wind speed reduction ration (α) and inertial resistance coefficient (C_i) of tree

The average inertial resistance coefficients of the experimental coniferous trees and deciduous trees were 0.712 and 0.768, respectively. The inertial resistance coefficients of the coniferous tree and deciduous tree derived from the field experiments were applied to the developed the 3D open-source CFD model to simulate the change of airflow by coniferous trees and deciduous trees distributed in the study area.

Table 14 Inertial resistance coefficient of coniferous tree and deciduous tree

	Ratio of wind speed reduction to windward wind speed		Coefficient of inertial resistance (C_i)		
	1st Exp.	2nd Exp.	1st Exp.	2nd Exp.	Average
Coniferous tree 1	0.368	0.419	0.586	0.709	0.768
Coniferous tree 2	0.479	0.495	0.866	0.912	
Deciduous tree 1	0.437	0.438	0.756	0.757	0.712
Deciduous tree 2	0.382	0.422	0.618	0.718	

4.3.2. Validation of the open-source CFD model

In this study, the smallest mesh size was designed as 3.12 m, considering the total number of meshes of the entire domain. In this case, the total number of meshes of the designed CFD model was about 7.95 million. The total number of meshes of the CFD model were about 1.87 million and 0.72 million meshes, while the size of the mesh was doubled to 6.25 m and doubled again to 12.5 m, respectively.

The RMSEs of the wind speed of the 3D open-source CFD models with mesh sizes of 3.12 m, 6.25 m, and 12.5 m were calculated as 0.12, 0.11 and 0.20, respectively, under westerly wind conditions. The RMSE values of the models with mesh sizes of 3.12m and 6.25m were similar, but the RMSE value was about twice as large when the mesh size of the CFD model was 12.5 m. Based on these results, it was concluded that the model designed with a mesh size of 6.25m effectively simulated the wind environment in the study area. Turbulence model test was conducted on various turbulence models using the CFD model with a mesh size of 6.25 m which was determined as a proper mesh size. The RMSE values of the wind

speed of the Standard k-ε turbulence model and the RNG k-ε turbulence model were calculated as 0.108 and 0.104, respectively, lower than the RMSE values of the Realizable k-ε turbulence model and the Standard k-ω turbulence model.

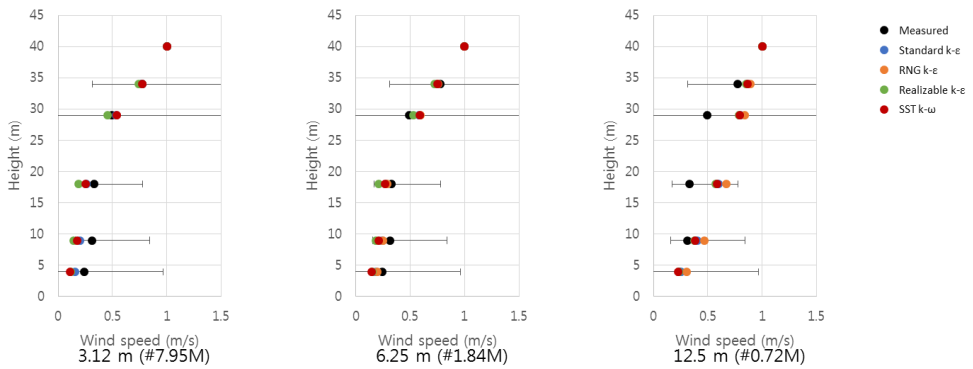

Figure 37 Results of grid independence test of the 3D open-source CFD model under the west wind condition

Table 15 RMSE of turbulence model test of the 3D open-source CFD model under the west wind condition

Size of mesh (Total number of meshes)	Turbulence model	RMSE	
		Normalized wind speed (dimensionless)	Wind direction (degree)
3.12 m (7.95 Million)	Standard k-ε	0.110	9.22
	RNG k-ε	0.097	13.26
	Realizable k-ε	0.140	7.30
	SST k-ω	0.117	17.39
6.25 m (1.87 Million)	Standard k-ε	0.108	11.53
	RNG k-ε	0.104	9.98
	Realizable k-ε	0.123	8.88
	SST k-ω	0.112	21.99
12.5 m (0.72 Million)	Standard k-ε	0.199	18.45
	RNG k-ε	0.239	17.11
	Realizable k-ε	0.185	18.69
	SST k-ω	0.192	28.86

In Easterly wind conditions, the RMSEs of the wind speed of the 3D open-source CFD model with mesh sizes of 3.12 m, 6.25 m, and 12.5 m were calculated as 0.055, 0.046 and 0.209, respectively. Similar results to the results of the grid independence test under the westerly wind condition were obtained when the mesh size of the open-source CFD model was 3 m and 6 m, and it was confirmed that the error increased when the mesh size of the open-source CFD model was increased to 12 m. The RMSE values between the measured data and the simulated results under the Standard k-ε turbulence model, the RNG k-ε turbulence model, the Realizable k-ε turbulence model, and the Standard k- ω turbulence model were 0.044, 0.048, 0.045 and 0.045, respectively.

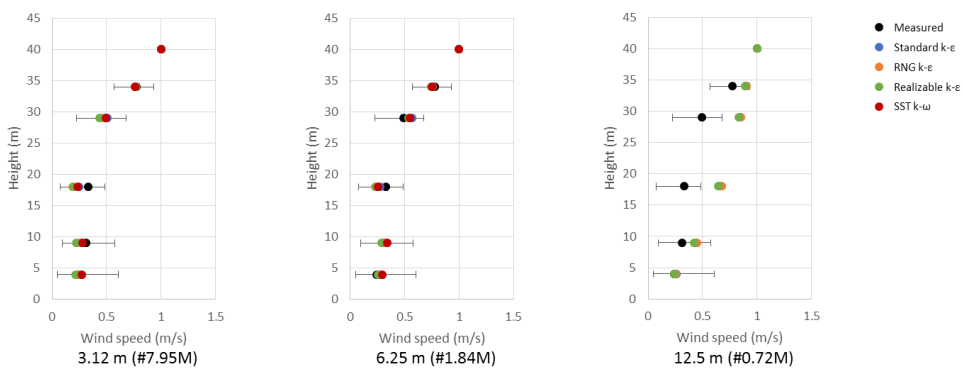

Figure 38 Results of grid independence test of the 3D open-source CFD model under easterly wind conditions

Table 16 RMSE of turbulence model test of the 3D open-source CFD model under easterly wind conditions

Size of mesh (Total number of meshes)	Turbulence model	RMSE	
		Normalized wind speed (dimensionless)	Wind direction (degree)
3.12 m (7.95 Million)	Standard k-ε	0.040	35.32
	RNG k-ε	0.065	36.14
	Realizable k-ε	0.071	38.05
	SST k-ω	0.044	36.58
6.25 m (1.87 Million)	Standard k-ε	0.044	33.24
	RNG k-ε	0.048	33.69
	Realizable k-ε	0.045	36.35
	SST k-ω	0.045	35.28
12.5 m (0.72 Million)	Standard k-ε	0.212	34.13
	RNG k-ε	0.217	34.29
	Realizable k-ε	0.199	35.64
	SST k-ω	0.209	35.58

Consistently, when the wind environment of mountain study area was simulated using the 3D open-source CFD model designed with a mesh size of 3.12 m or 6.25 m, the simulated wind environment distribution was similarly to the measured field data. Therefore, the optimal mesh size of the CFD model was determined to be 6.25 m for economic simulation. In addition, it was confirmed that the wind environment in the study area was properly simulated when the Standard k-ε turbulence model or the RNG k-ε turbulence model were used as turbulence model of the CFD model. Based on the results of turbulence model test, the Standard k-ε turbulence model was decided that it was appropriate for simulating the airflow over mountain complex terrain.

4.4. Conclusions

This chapter presented a methodology for simulating the wind enfironment in forested complex mountain terrain using open-source CFD package. The forest areas were classified according to the forest type using the forest map provided by the Korea Forest Service, and the canopy region of each forest type was defined by using the forest area classification and the height of the trees. Then, I proposed a method for applying the aerodynamic porosity coefficient of the trees to the 3D open-source CFD model by comparing the coordinates of the defined canopy region of forest with the coordinates of the developed CFD model.

The proposed 3D modelling method of forested mountain terrain considering air-resistance of forest conopy presented in this chapter has the merits that the modelling procedure is relatively simple, the quality of the mesh is relatively easy to improve and the distortion of the forest region boundary occurred in process of designing the CFD model is relatively small, since there is no need to design the canopy region of forest separately.

Chapter 5. Recommendation of installation method for meteorological observation system in mountain region based on open-source CFD simulations

5.1. Introduction

Wind conditions in mountain areas are different from those in flat areas due to differing topographical characteristics and the influence of the air resistance of trees which are distributed in mountain terrain. Therefore, a different installation method for weather station in the mountain terrain is required. The aim of this chapter is to recommend the proper installation method for weather station in mountain region through the analysis of wind environment according to the type of trees present, their height and air-resistance, the size of clear-cut around weather station and the reference velocity. In addition, the conversion factor for estimating the reference velocity is derived using the observed wind environment at the station when the weather station was not installed according to the proposed installation method.

5.2. Materials and methods

5.2.1. Design of open-source CFD model for suggesting the appropriate installation method

In designing process of a 3D open-source CFD model to analyze the internal wind environment in clear-cut according to various environmental conditions, the size of the entire domain was designed as 800 m x 800 m considering the largest size condition of clear-cut (400 m). The mesh near the ground surface where the trees are distributed was designed with a high resolution and the size of the mesh increased

gradually with increasing height in order to create a computationally economic mesh. The 25 layers were concentrated up to 50 m in height with the same cell height to predict the airflow in the low atmosphere, especially near the ground, where the airflow as affected by the air resistance of the trees was the primary concern. The cell height of the first 10 layers was 1.0 m, layers up to from 10 m to 33 m were 2.1 m height and layers from 33 m to 50 m were 4.2 m height, and so on. In this way, the height of the mesh was gradually increased to 2.0 km, and the entire domain of the 3D open-source CFD model was designed with a total of 8,377,500 meshes. The mesh was redesigned when the quality of the designed mesh exceeded the threshold values of the mesh quality in the process of designing the 3D open-source CFD model using OpenFOAM software. The threshold values and the finally designed mesh quality of 3D open-source CFD model are shown in the table 17.

Table 17 Threshold values of the mesh quality and finally designed mesh quality of 3D open-source CFD model.

Quality index	Threshold value	Mesh quality
Non-orthogonality	65	24.3491
Skewness of boundary mesh	20	0.333344
Skewness of internal mesh	4	
Aspect ratio	-	1.0417

The 3D open-source CFD model was designed in order to analyze the airflow inside the clear-cut as shown in figure 39, and the airflow was analyzed according to the size of clear-cut, the height of the trees, and the type of trees. The slope of the

ground was excluded from the simulation conditions because it is recommended to install stations on flat areas as far as possible from international standards. The shape of the clear-cut was designed as a circle, under the assumption that the distance from the station to the forest edge is the same in every direction and that the trees are uniformly distributed. In addition, the coniferous model cases were designed as shown in figure 39 (c), assuming that leaves are presented only in the top 50% since coniferous trees are generally divided into an upper part, where the majority of leaves are distributed and a lower part, where there are few leaves.

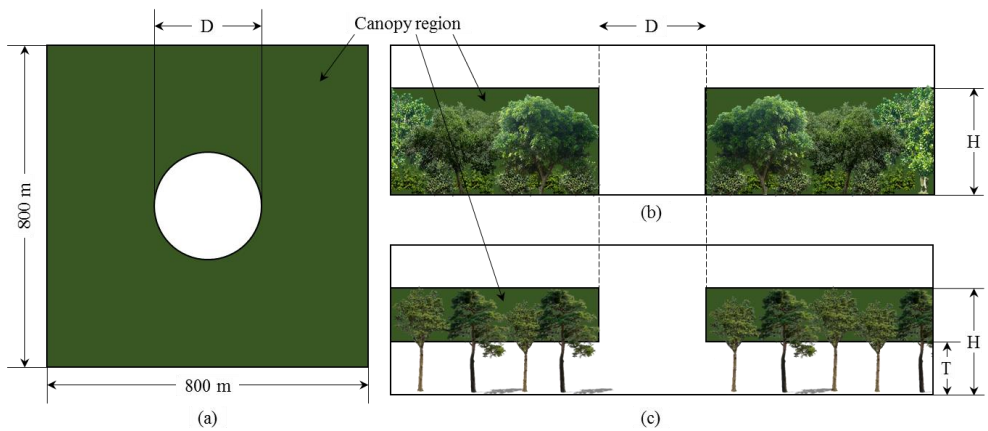

Figure 39 Schematic diagram of the 3D open-source CFD model; (a) top view of the model, (b) side view of the deciduous case, and (c) side view of the coniferous case.

5.2.2. CFD simulation cases for evaluating the appropriate installation method

The experimental cases were simulated to investigate the vertical distribution of wind speed according to the type of tree, the height of the trees, the air resistance of the trees, the size of the clear-cut, the air-resistance of the trees and the reference

velocity (Table 18). The boundary condition of wind speed was designed by using the prevailing wind speeds (0.5 – 1.5 m s^{-1}) and the maximum wind speeds (5.5 – 6.5 m s^{-1}) in the study region. The 3D open-source CFD model was simulated using the standard k-ε turbulence model which is the appropriate turbulence model as derived in chapters 3 and 4. In addition, we designed simulation cases with no clear-cut as control simulation cases in order to compare with the airflow inside clear-cut due to the influence of the trees.

Table 18 Experimental cases for the 3D open-source CFD simulation

Contents	Values
Velocity of reference height	1.0, 3.0, 6.0 m s^{-1}
Dimension of clear-cut (D)	0, 10, 20, 30, 50, 100, 200, 300, 400 m
Type of tree	Coniferous tree, deciduous tree
Height of tree (H)	10, 15, 20, 25, 30 m
Trunk height of coniferous tree (T)	5, 7.5, 10, 12.5, 15 m
Inertial resistance coefficient of tree	0.3, 0.5, 0.7, 0.9 m^{-1}
Turbulence model	Standard k-ε

The 3D open-source CFD simulation model was computed under steady state conditions and the vertical distribution of wind speed was analyzed by using the simulated wind speed from the bottom of the center of the clear-cut to the reference height. Here, the reference height is the height required to install an anemometer to observe the wind environment in mountain areas, as proposed by international standards, and it is 10 m higher than the height of trees distributed around the clear-cut.

5.3. Results and discussions

Meteorological observation systems in mountain region for observing the wind environment are basically recommended to be installed at a height of 10m in an open area and at a distance of more than 10 times the average height of the trees from the edge of the forest when installing the observation system in the forest. If no clear-cut is available at all, the proper height of the observation system would be 10 m above the average treetop level. However, clear-cut of proper size can be difficult to find, and tall observation system can be expensive and may not be as safe as 10m observation system. Therefore, to avoid these issues, the appropriate height for observing the wind environment was chosen for sites specifically according to the size of clear-cut and the average height of the trees distributed around the observation system, as suggested for stations in Canada by Lawson & Armitage (2008) and reproduced in table 19.

Table 19 Recommended height of the anemometer for observing wind environment located in small clear-cut (Lawson and Armitage, 2008).

		Average height of the trees (H, m)				
		10 m	**15 m**	**20 m**	**25 m**	**30 m**
Diameter of clear-cut (D, m)	**10 m**	20	25	30	35	40
	20 m	18.4	23.8	30	35	40
	30 m	16.7	22.6	28.1	33.2	38.7
	50 m	13.2	19.9	25.1	30.9	36.7
	100 m	10	12.1	16.5	22.2	28.2
	200 m	10	10	10	11.4	14.1
	300 m	10	10	10	10	10
	400 m	10	10	10	10	10

However, the types of trees and the air resistance characteristics of trees distributed in forest regions were not considered in the above Canadian standard. Therefore, in this chapter, an installation method for wind environment observation systems for mountain terrain was proposed considering not only the size of clear-cut and the height of the trees, but also the type of the trees, the air resistance of the trees, and wind speed. In the case of the control case without clear-cut, the wind speed at the reference height was simulated and the simulated wind speed was defined as the reference wind speed in order to analyze the wind environment of the simulation cases. The reference heights of the simulation cases with tree heights of 10 m, 15 m, 20 m, 25 m and 30 m were 20 m, 25 m, 30 m, 35 m and 40 m, respectively, while the reference wind speeds were about 0.6 m s^{-1} (Table 20). The reference wind speed tended to increase as the height of the trees increased and to decrease as the inertial resistance coefficient of the trees increased. The reference wind speeds of the coniferous tree case and the deciduous tree case were similar to each other when the inertial resistance coefficients of each case were same. This is because the main difference between the coniferous tree case and the deciduous tree case in the 3D open-source CFD simulation model was presence or absence of leaves on the tree column, as shown in figure 39.

Table 20 Simulated reference wind speed (m s^{-1}) at the reference height (H + 10 m) according to the type of tree and the inertial resistance coefficient (Ci) of tree

			Height of tree (H, m)				
			10 m	**15 m**	**20 m**	**25 m**	**30 m**
C_i	**Deciduous tree**	**0.3 m^{-1}**	0.62	0.61	0.64	0.67	0.66
		0.5 m^{-1}	0.59	0.59	0.62	0.65	0.63
		0.7 m^{-1}	0.58	0.57	0.60	0.63	0.61
		0.9 m^{-1}	0.57	0.56	0.59	0.63	0.61
	Coniferous tree	**0.3 m^{-1}**	0.63	0.62	0.64	0.67	0.65
		0.5 m^{-1}	0.60	0.58	0.60	0.63	0.60
		0.7 m^{-1}	0.58	0.56	0.58	0.61	0.58
		0.9 m^{-1}	0.57	0.55	0.57	0.60	0.57

5.3.1. Wind environment in clear-cut according to type of tree

The wind environment in the clear-cut was analyzed for the cases in which the inertial resistance coefficient of the coniferous and deciduous trees was 0.3 m^{-1}, as an example. The simulated wind speed at the recommended height of each simulation case was compared with the reference wind speed under the control case, where there was no clear-cut.

Table 21 Simulated wind speeds at the recommended height by the CFS (Table 19) where the inertial resistance coefficient of the deciduous tree canopy was 0.3 m^{-1} (wind speed difference from wind speed at reference height in control condition)

		Height of tree (H, m)				
		10 m	**15 m**	**20 m**	**25 m**	**30 m**
Diameter of clear-cut (D, m)	**10 m**	0.63 (0.00)	0.62 (0.00)	0.64 (0.00)	0.67 (0.00)	0.65 (0.00)
	20 m	0.59 (0.04)	0.59 (0.03)	0.65 (-0.01)	0.68 (-0.01)	0.65 (0.00)
	30 m	0.56 (0.07)	0.57 (0.05)	0.61 (0.03)	0.65 (0.02)	0.63 (0.02)
	50 m	0.50 (0.13)	0.54 (0.08)	0.57 (0.07)	0.62 (0.05)	0.62 (0.03)
	100 m	0.50 (0.13)	0.46 (0.16)	0.48 (0.16)	0.56 (0.11)	0.59 (0.06)
	200 m	0.58 (0.05)	0.52 (0.10)	0.47 (0.17)	0.49 (0.18)	0.51 (0.14)
	300 m	0.64 (-0.01)	0.59 (0.03)	0.55 (0.09)	0.54 (0.13)	0.51 (0.14)
	400 m	0.67 (-0.04)	0.63 (-0.01)	0.60 (0.04)	0.59 (0.08)	0.56 (0.09)

Using deciduous tree, the simulated wind speeds at the recommended height by the CFS tended to increase as the height of the tree increases. In the cases where the

size of clear-cut was 10 m or the size of clear-cut was 20 m and the height of the trees were 20 m, 25 m and 30 m, there were no difference from the reference wind speed because the recommended height of each case and the reference height of the control case were same. In addition, it was confirmed that the difference between the reference wind speed and the simulated wind speed at the recommended height tended to increase as the size of the clear-cut increases or the height of the trees decreases. The smallest difference and biggest difference were 0.00 m s^{-1} and 0.16 m s^{-1}, respectively. The smallest difference was found when the size of the clear-cut was 400 m and the height of the tree was 25 m.

Table 22 Simulated wind speeds at the recommended height by the CFS (Table 19) where the inertial resistance coefficient of the coniferous tree canopy was 0.3 m^{-1} (wind speed difference from wind speed at reference height in control condition)

		Height of tree (H, m)				
		10 m	**15 m**	**20 m**	**25 m**	**30 m**
Diameter of clear-cut (D, m)	**10 m**	0.63 (-0.01)	0.62 (-0.01)	0.64 (0.00)	0.67 (0.00)	0.66 (0.00)
	20 m	0.58 (0.04)	0.59 (0.02)	0.65 (-0.01)	0.68 (-0.01)	0.66 (0.01)
	30 m	0.55 (0.07)	0.57 (0.04)	0.61 (0.03)	0.64 (0.03)	0.64 (0.02)
	50 m	0.49 (0.13)	0.53 (0.08)	0.56 (0.08)	0.61 (0.06)	0.62 (0.04)
	100 m	0.49 (0.13)	0.44 (0.17)	0.46 (0.18)	0.50 (0.17)	0.51 (0.15)
	200 m	0.58 (0.04)	0.55 (0.06)	0.47 (0.17)	0.44 (0.23)	0.41 (0.25)
	300 m	0.63 (-0.01)	0.59 (0.02)	0.56 (0.08)	0.52 (0.15)	0.47 (0.19)
	400 m	0.67 (-0.05)	0.64 (-0.03)	0.62 (0.02)	0.59 (0.08)	0.55 (0.11)

As for the results of the analysis for the deciduous tree conditions, when using coniferous trees the simulated wind speed at the recommended height decreased as the clear-cut size increased, and the simulated wind speed increased as the height of the tree increased. However, the difference between the simulated wind speed at the recommended height and the reference wind speed was found to be smaller than for the result of the analysis for the deciduous tree conditions. The smallest difference and biggest difference were 0.00 m s^{-1} and 0.25 m s^{-1}, respectively. The smallest difference was simulated when the size of the clear-cut was 400 m and the height of the tree was 25 m, and the biggest difference was simulated when the size of the clear-cut was 200 m and the height of the tree was 25 m. The simulated wind speeds of the coniferous tree case and the deciduous tree case were similar to each other because the main difference between the coniferous tree case and the deciduous tree case in the 3D open-source CFD simulation model was the presence or absence of leaves on the tree column as shown in figure 39.

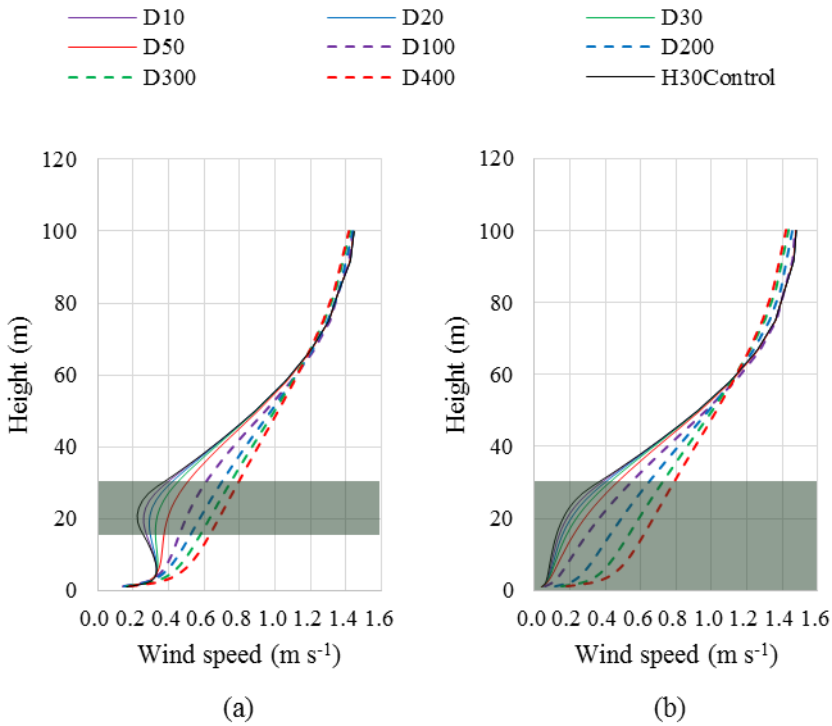

Figure 40 Vertical distribution of wind speed when the height of tree was 30 m according to type of tree; (a) Coniferous tree, (b) Deciduous tree (shaded green region was the canopy of the tree region)

In the simulation case of a tree height of 30 m, the vertical distribution of the wind speed is analyzed as an example (Fig. 40). In the coniferous tree and deciduous tree conditions, it was found that the wind speed increased with increasing altitude. In the case of coniferous trees, it was confirmed that relatively high wind speeds are formed in the bottom column, where there are few leaves, and wind speed was decreased in the canopy region as shown in figure 40 (a). In the case of deciduous trees, it was confirmed that the wind speed rapidly decreased in the canopy region and increased logarithmically with height above the top of the tree as shown in figure 40 (b).

The average wind speed foamed in the clear-cut center where coniferous trees

were distributed was about 82.8% higher than for the case where deciduous trees were distributed. The average wind speed under coniferous conditions was 100.2% faster than the average wind speed under deciduous conditions when the diameter of the clear-cut was 10 m. In addition, the average wind speeds under coniferous conditions were 93.0%, 88.4%, 78.2% and 54.3% faster than the average wind speed under deciduous conditions when the diameter of the clear-cut was 20 m, 30 m, 50 m, and 100 m, respectively.

The wind speed at 22.5 m height, where leaves are distributed in both coniferous and deciduous trees, was analyzed under conditions of 30 m height of trees in order to compare the effects of different types of trees. The wind speed at 7.5 m, where leaves are only distributed in deciduous trees, was analyzed. The difference in simulated wind speed at 22.5 m height between the coniferous tree case and the deciduous tree case was about 22.1%, and the difference in wind speed at 7.5 m height was about 187.4%. In addition, when clear-cut size were 10 m, 20 m, 30 m, 50 m and 100m, the wind speed difference at 7.5m height was 244.6%, 217.6%, 197.6%, 166.7% and 110.5%, respectively.

5.3.2. Wind environment in clear-cut according to the inertial resistance coefficient of the canopy

The simulated wind speed at the recommended height was found to increase as the height of the tree increased. And the simulated wind speeds gradually decreased as the size of the clear-cut increased up to a certain point, above this point the simulated wind speeds were reduced with increasing clear-cut size, since the effect of the trees on the airflow at center of the clear-cut was reduced due to the constant monitoring height of 10 m. For example, the simulated wind speed at the proposed

height decreased to 0.48 m s^{-1} when the clear-cut size was 100 m and then increased to 0.7 m s^{-1} as the clear-cut size was increased to 400 m using an inertial resistance coefficient and the height of coniferous tree of 0.5 m^{-1} and 10 m, respectively. The simulated wind velocity at the center of the clear-cut increased as the diameter of the clear-cut increased, so that the wind speed at the height of 10 m also increased, as shown in figure 41.

The average wind speed at the recommended monitoring height by the CFS was 0.58 m s^{-1} using an inertial resistance coefficient of 0.3 m^{-1}. As the inertial resistance coefficient was increased to 0.5 m^{-1}, 0.7 m^{-1}, and 0.9 m^{-1}, the average wind speed at the recommended height decreased to 0.55 m s^{-1} (5.3%), 0.53 m s^{-1} (8.3%) and 0.52 m s^{-1} (11.0%), respectively.

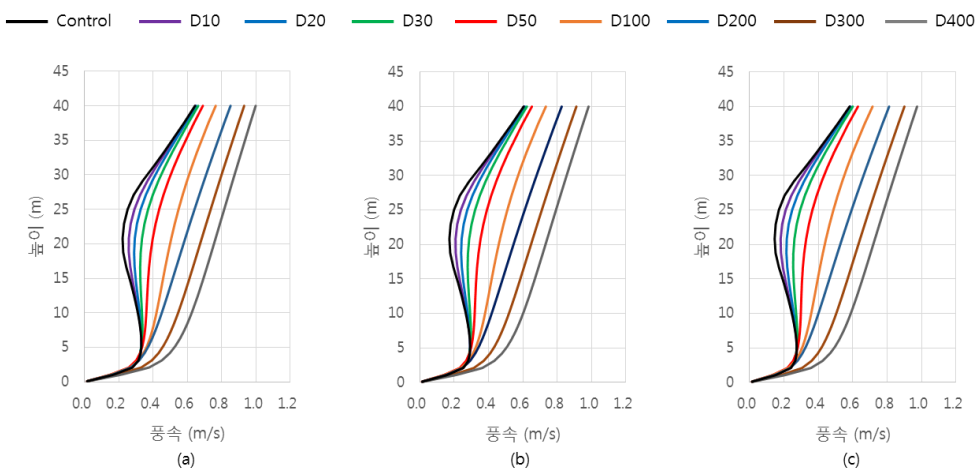

Figure 41 Vertical distribution of wind speed when the height of the coniferous tree was 30 m using an inertial resistance coefficient of (a) 0.3 m^{-1}, (b) 0.5 m^{-1}, and (c) 0.7 m^{-1}

Table 23 Simulated wind speeds at the recommended monitoring height by the CFS (Table 19) using an inertial resistance coefficient for a coniferous canopy of 0.5 m^{-1} (wind speed difference from wind speed at reference height in control conditions)

		Height of tree (H, m)				
		10 m	**15 m**	**20 m**	**25 m**	**30 m**
Diameter of clear-cut (D, m)	**10 m**	0.60 (0.00)	0.59 (0.00)	0.61 (0.00)	0.63 (0.00)	0.61 (0.00)
	20 m	0.56 (0.04)	0.56 (0.03)	0.61 (-0.01)	0.64 (-0.01)	0.61 (-0.01)
	30 m	0.53 (0.07)	0.54 (0.04)	0.57 (0.03)	0.61 (0.03)	0.59 (0.01)
	50 m	0.47 (0.13)	0.51 (0.08)	0.53 (0.07)	0.58 (0.05)	0.58 (0.02)
	100 m	0.48 (0.12)	0.43 (0.16)	0.44 (0.16)	0.52 (0.11)	0.55 (0.06)
	200 m	0.57 (0.03)	0.50 (0.09)	0.45 (0.16)	0.45 (0.18)	0.47 (0.14)
	300 m	0.63 (-0.03)	0.57 (0.01)	0.53 (0.08)	0.51 (0.13)	0.48 (0.12)
	400 m	0.67 (-0.06)	0.62 (-0.04)	0.59 (0.02)	0.57 (0.07)	0.54 (0.07)

Table 24 Simulated wind speeds at the recommended monitoring height by the CFS (Table 19) using an inertial resistance coefficient for a coniferous canopy of 0.7 m^{-1} (wind speed difference from wind speed at reference height in control conditions)

		Height of tree (H, m)				
		10 m	**15 m**	**20 m**	**25 m**	**30 m**
Diameter of clear-cut (D, m)	**10 m**	0.58 (0.00)	0.57 (0.00)	0.59 (0.00)	0.61 (0.00)	0.58 (0.00)
	20 m	0.54 (0.04)	0.54 (0.03)	0.59 (-0.01)	0.62 (-0.01)	0.59 (-0.01)
	30 m	0.51 (0.07)	0.52 (0.04)	0.55 (0.03)	0.58 (0.03)	0.57 (0.01)
	50 m	0.45 (0.13)	0.49 (0.08)	0.51 (0.07)	0.56 (0.05)	0.56 (0.02)
	100 m	0.46 (0.12)	0.41 (0.16)	0.42 (0.16)	0.50 (0.11)	0.53 (0.06)
	200 m	0.56 (0.02)	0.48 (0.08)	0.43 (0.15)	0.43 (0.18)	0.45 (0.13)
	300 m	0.62 (-0.04)	0.56 (0.00)	0.52 (0.07)	0.49 (0.12)	0.46 (0.12)
	400 m	0.66 (-0.08)	0.62 (-0.05)	0.58 (0.06)	0.55 (0.06)	0.53 (0.06)

Table 25 Simulated wind speeds at the recommended monitoring height by the CFS (Table 19) using an inertial resistance coefficient for a coniferous canopy of 0.9 m^{-1} (wind speed difference from wind speed at reference height in control conditions)

		Height of tree (H, m)				
		10 m	**15 m**	**20 m**	**25 m**	**30 m**
Diameter of clear-cut (D, m)	**10 m**	0.57 (0.00)	0.55 (0.00)	0.57 (0.00)	0.60 (0.00)	0.57 (0.00)
	20 m	0.53 (0.04)	0.52 (0.03)	0.58 (-0.01)	0.60 (-0.01)	0.57 (-0.01)
	30 m	0.50 (0.07)	0.51 (0.05)	0.54 (0.03)	0.57 (0.03)	0.55 (0.02)
	50 m	0.44 (0.13)	0.47 (0.08)	0.50 (0.07)	0.55 (0.05)	0.54 (0.02)
	100 m	0.45 (0.12)	0.39 (0.16)	0.41 (0.16)	0.48 (0.11)	0.51 (0.05)
	200 m	0.55 (0.02)	0.48 (0.07)	0.42 (0.15)	0.42 (0.18)	0.38 (0.18)
	300 m	0.62 (-0.05)	0.56 (-0.01)	0.51 (0.06)	0.48 (0.11)	0.40 (0.17)
	400 m	0.66 (-0.09)	0.62 (-0.06)	0.58 (-0.01)	0.55 (0.05)	0.47 (0.10)

Similar to the simulation cases for coniferous trees, when using deciduous trees the wind speed at the recommended height increased as the height of the tree was increased. Wind speeds gradually decreased as the size of the clear-cut increased, but again this trend was reversed above a certain clear-cut size because the effect of the tree on the airflow at center of clear-cut was reduced. For example, the simulated wind speed at the proposed height decreased to 0.46 m s^{-1} when the clear-cut size was 50 m and then increased to 0.68 m s^{-1} as the clear-cut size was increased to 400 m using an inertial resistance coefficient and the height of deciduous tree of 0.5 m^{-1} and 10 m, respectively.

The average wind speed at the recommended monitoring height by CFS was 0.57 m s^{-1} using an inertial resistance coefficient of 0.3 m^{-1}. As the inertial resistance coefficient increased to 0.5 m^{-1}, 0.7 m^{-1} and 0.9 m^{-1}, the average wind speed at the recommended height decreased to 0.55 m s^{-1} (3.9%), 0.54 m s^{-1} (6.0%) and 0.53 m s^{-1} (7.8%), respectively.

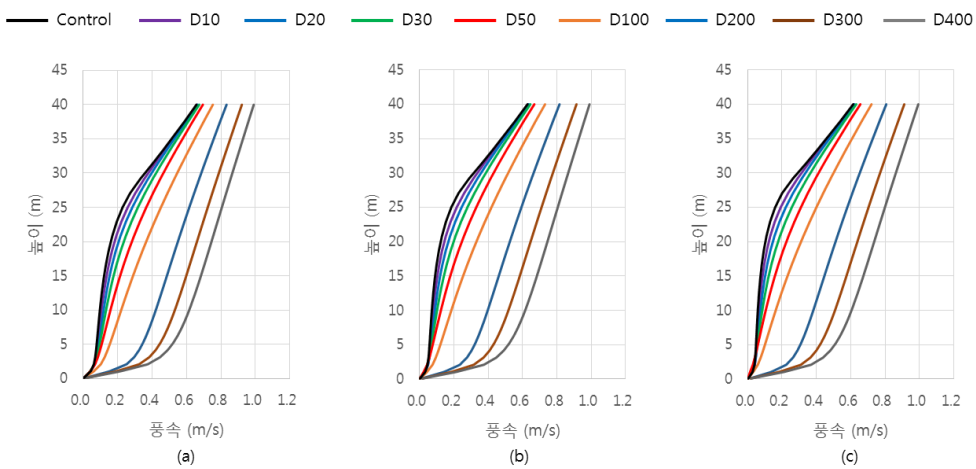

Figure 42 Vertical distribution of wind speed when the height of the deciduous tree was 30 m using an inertial resistance coefficient of (a) 0.3 m^{-1}, (b) 0.5 m^{-1}, and (c) 0.7 m^{-1}

Table 26 Simulated wind speeds at the recommended monitoring height by the CFS (Table 19) using an inertial resistance coefficient for a deciduous canopy of 0.5 m^{-1} (wind speed difference from wind speed at reference height in control conditions)

		Height of tree (H, m)				
		10 m	**15 m**	**20 m**	**25 m**	**30 m**
Diameter of clear-cut (D, m)	**10 m**	0.60 (0.00)	0.59 (0.00)	0.62 (0.00)	0.65 (0.00)	0.63 (0.00)
	20 m	0.56 (0.04)	0.56 (0.03)	0.62 (-0.01)	0.65 (-0.01)	0.64 (-0.01)
	30 m	0.52 (0.08)	0.54 (0.05)	0.58 (0.04)	0.61 (0.03)	0.61 (0.02)

	50 m	0.46 (0.14)	0.50 (0.09)	0.53 (0.08)	0.58 (0.07)	0.59 (0.04)
	100 m	0.47 (0.13)	0.42 (0.17)	0.43 (0.18)	0.47 (0.18)	0.48 (0.15)
	200 m	0.57 (0.03)	0.50 (0.08)	0.46 (0.16)	0.43 (0.22)	0.38 (0.24)
	300 m	0.63 (-0.03)	0.58 (0.00)	0.55 (0.07)	0.51 (0.17)	0.45 (0.18)
	400 m	0.67 (-0.07)	0.64 (-0.05)	0.61 (0.00)	0.59 (0.06)	0.54 (0.09)

Table 27 Simulated wind speeds at the recommended monitoring height by the CFS (Table 19) using an inertial resistance coefficient for a deciduous canopy of 0.7 m^{-1} (wind speed difference from wind speed at reference height in control conditions)

		Height of tree (H, m)				
		10 m	**15 m**	**20 m**	**25 m**	**30 m**
Diameter of clear-cut (D, m)	**10 m**	0.58 (0.00)	0.57 (0.00)	0.60 (0.00)	0.64 (0.00)	0.62 (0.00)
	20 m	0.54 (0.04)	0.54 (0.03)	0.61 (-0.01)	0.64 (-0.01)	0.62 (-0.01)
	30 m	0.50 (0.08)	0.52 (0.05)	0.56 (0.04)	0.60 (0.04)	0.60 (0.02)
	50 m	0.44 (0.14)	0.48 (0.09)	0.51 (0.09)	0.56 (0.07)	0.57 (0.04)
	100 m	0.46 (0.12)	0.41 (0.17)	0.42 (0.18)	0.45 (0.18)	0.46 (0.15)
	200 m	0.56 (0.02)	0.50 (0.07)	0.45 (0.15)	0.41 (0.22)	0.37 (0.25)
	300 m	0.62 (-0.04)	0.58 (-0.01)	0.55 (0.06)	0.51 (0.13)	0.44 (0.17)
	400 m	0.66 (-0.09)	0.64 (-0.06)	0.61 (-0.01)	0.58 (0.05)	0.54 (0.08)

Table 28 Simulated wind speeds at the recommended monitoring height by the CFS (Table 19) using an inertial resistance coefficient for a deciduous canopy of 0.9 m^{-1} (wind speed difference from wind speed at reference height in control conditions)

		Height of tree (H, m)				
		10 m	**15 m**	**20 m**	**25 m**	**30 m**
Diameter of clear-cut (D, m)	**10 m**	0.57 (0.00)	0.56 (0.00)	0.59 (0.00)	0.63 (0.00)	0.61 (0.00)
	20 m	0.53 (0.04)	0.53 (0.03)	0.60 (-0.01)	0.63 (-0.01)	0.61 (-0.01)
	30 m	0.49 (0.08)	0.51 (0.05)	0.55 (0.04)	0.59 (0.04)	0.59 (0.02)
	50 m	0.43 (0.14)	0.47 (0.09)	0.50 (0.09)	0.56 (0.07)	0.56 (0.04)
	100 m	0.45 (0.12)	0.40 (0.16)	0.41 (0.19)	0.44 (0.18)	0.45 (0.16)
	200 m	0.56 (0.01)	0.49 (0.07)	0.44 (0.15)	0.41 (0.22)	0.34 (0.27)
	300 m	0.62 (-0.08)	0.58 (-0.02)	0.54 (0.05)	0.50 (0.12)	0.41 (0.20)
	400 m	0.66 (-0.09)	0.63 (-0.07)	0.61 (-0.02)	0.58 (0.04)	0.50 (0.11)

5.3.3. Proper height for wind environment monitoring

In order to observe the wind environment in mountain region where coniferous and deciduous trees are distributed, the appropriate observation height was derived according to the height of the tree and the size of the clear-cut, and the appropriate clear-cut size was also derived. The appropriate height of observation was defined as the height at which the simulated wind speed matched the reference wind speed, and the appropriate size of clear-cut was defined as the size of simulated clear-cut at which the reference wind speed match the simulated wind speed at 10 m height.

The appropriate heights for wind environment monitoring according to the size of clear-cut and the height of tree are shown in figures 43 – 50. The appropriate observation height under the deciduous tree case was higher than that of the coniferous tree case. The average difference of appropriate observation height between the coniferous tree case and the deciduous tree case was about 0.5 m, and the maximum difference was 3.0 m.

The appropriate size of clear-cut were 287.1 m, 366.7 m, 465.0 m, 562.5 m, and 609.1 m when the heights of coniferous tree distributed around the clear-cut with an inertial resistance coefficient of 0.3 m^{-1} were 10 m, 15 m, 20 m, 25 m and 30 m, respectively. In addition, the appropriate sizes of clear-cut were 275.0 m, 343.3, 437.2 m, 521.6 m, and 548.3 m when the height of deciduous tree with an inertial resistance coefficient of 0.3 m^{-1} were 10 m, 15 m, 20 m, 25 m and 30 m, respectively.

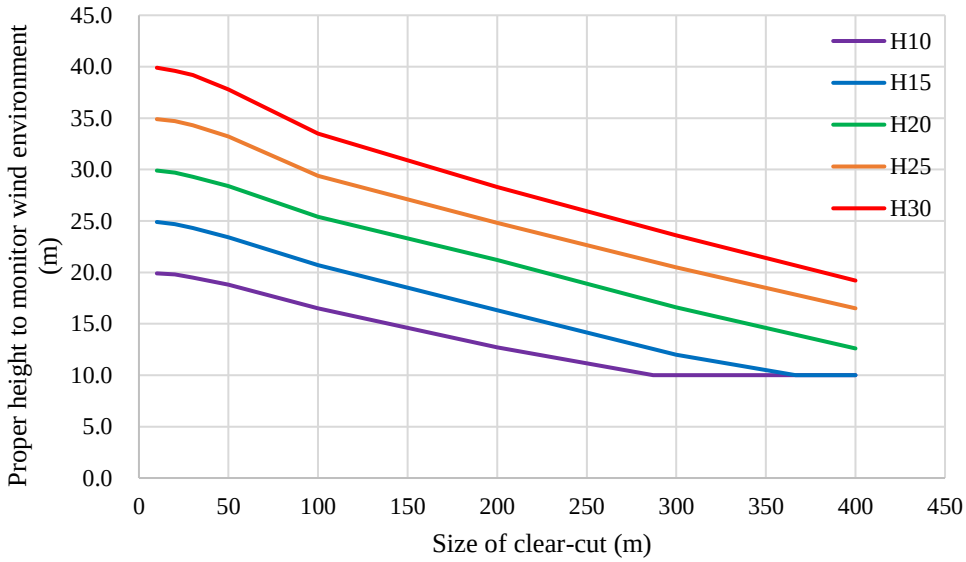

Figure 43 Appropriate height for wind environment monitoring when the inertial resistance coefficient of the coniferous tree was 0.3 m^{-1}.

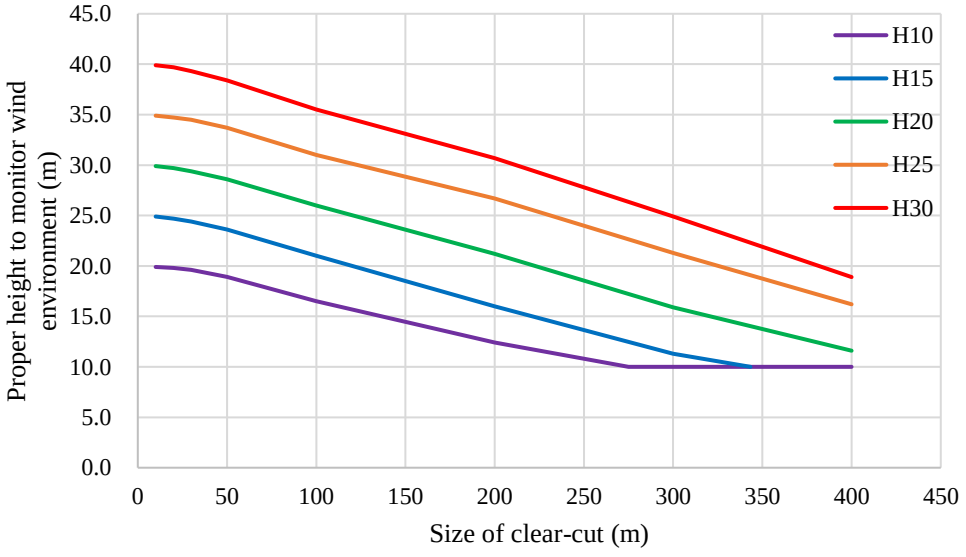

Figure 44 Appropriate height for wind environment monitoring when the inertial resistance coefficient of the deciduous tree was 0.3 m^{-1}.

Table 29 appropriate heights for wind environment monitoring when the inertial resistance coefficient of the coniferous trees was 0.3 m^{-1}

		Height of tree (H, m)				
		10 m	**15 m**	**20 m**	**25 m**	**30 m**
Diameter of clear-cut (D, m)	**10 m**	19.9	24.9	29.9	34.9	39.9
	20 m	19.8	24.7	29.7	34.7	39.6
	30 m	19.5	24.3	29.3	34.3	39.2
	50 m	18.8	23.4	28.4	33.2	37.8
	100 m	16.5	20.7	25.4	29.4	33.5
	200 m	12.7	16.3	21.2	24.8	28.3
	300 m	10.0	12.0	16.6	20.5	23.6
	400 m	10.0	10.0	12.6	16.5	19.2

Table 30 appropriate heights for wind environment monitoring when the inertial resistance coefficient of the deciduous trees was 0.3 m^{-1}

		Height of tree (H, m)				
		10 m	**15 m**	**20 m**	**25 m**	**30 m**
Diameter of clear-cut (D, m)	**10 m**	19.9	24.9	29.9	34.9	39.9
	20 m	19.8	24.7	29.7	34.7	39.7
	30 m	19.6	24.4	29.4	34.5	39.3
	50 m	18.9	23.6	28.6	33.7	38.4
	100 m	16.5	21.0	26.0	31.0	35.5
	200 m	12.4	16.0	21.2	26.7	30.7
	300 m	10.0	11.3	15.9	21.3	24.9
	400 m	10.0	10.0	11.6	16.2	18.9

The appropriate sizes of clear-cut were 254.5 m, 323.3 m, 422.7 m, 508.7 m, and 554.2 m when the heights of coniferous tree distributed around the clear-cut with the inertial resistance coefficient of 0.5 m^{-1} were 10 m, 15 m, 20 m, 25 m and 30 m, respectively. The appropriate size of clear-cut were 245.5 m, 303.4 m, 402.3 m, 480.0 m, and 506.1 m when the heights of deciduous tree with an inertial resistance coefficient of 0.5 m^{-1} were 10 m, 15 m, 20 m, 25 m and 30 m, respectively. The appropriate sizes of clear-cut were 238.2 m, 300.0 m, 402.2 m, 487.5 m, and 533.3 m when the height of coniferous trees with the inertial resistance coefficient of 0.7 m^{-1} were 10 m, 15 m, 20 m, 25 m and 30 m, respectively. The appropriate size of clear-cut were 229.4 m, 278.6 m, 384.4 m, 461.4 m, and 485.7 m when the height of deciduous trees with the inertial resistance coefficient of 0.7 m^{-1} were 10 m, 15 m, 20 m, 25 m and 30 m, respectively. In addition, the appropriate sizes of clear-cut were 226.5 m, 290.2 m, 389.1 m, 472.0 m, and 553.8 m when the height of coniferous trees with the inertial resistance coefficient of 0.9 m^{-1} were 10 m, 15 m, 20 m, 25 m and 30 m, respectively. The appropriate size of clear-cut were 220.0 m, 259.3 m, 373.3 m, 449.2 m, and 524.6 m when the height of deciduous trees with the inertial resistance coefficient of 0.9 m^{-1} were 10 m, 15 m, 20 m, 25 m and 30 m, respectively.

As the inertial resistance coefficient of coniferous tree increased to 0.5 m^{-1}, 0.7 m^{-1} and 0.9 m^{-1}, the average recommended clear-cut size was decreased 45.4 m (9.9%), 65.8 m (14.4%) and 71.7 m (15.7%), respectively. In addition, as the inertial resistance coefficient of deciduous tree increased to 0.5 m^{-1}, 0.7 m^{-1} and 0.9 m^{-1}, the average recommended clear-cut size was decreased 37.6 m (8.9%), 57.2 m (13.5%) and 59.8 m (14.1%), respectively.

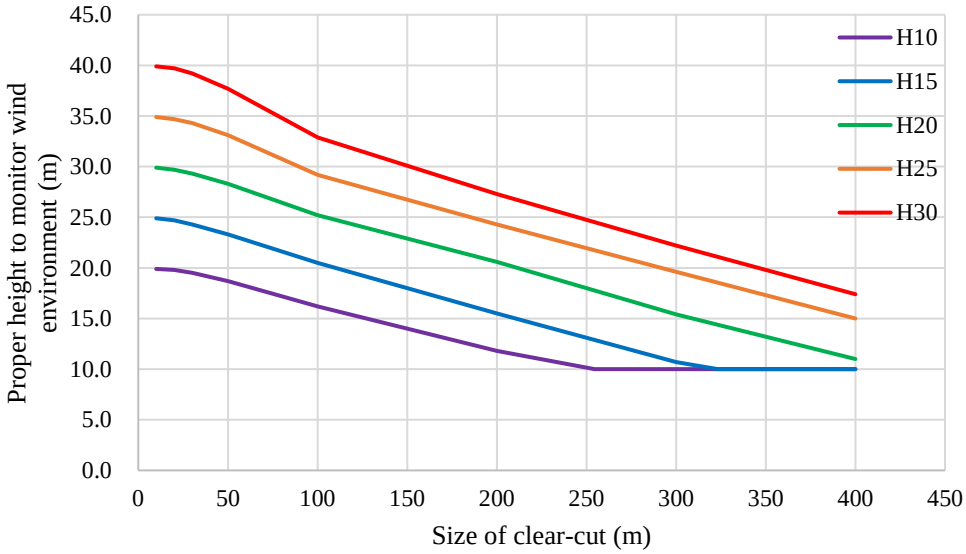

Figure 45 Appropriate height for wind environment monitoring when the inertial resistance coefficient of the coniferous tree was 0.5 m^{-1}.

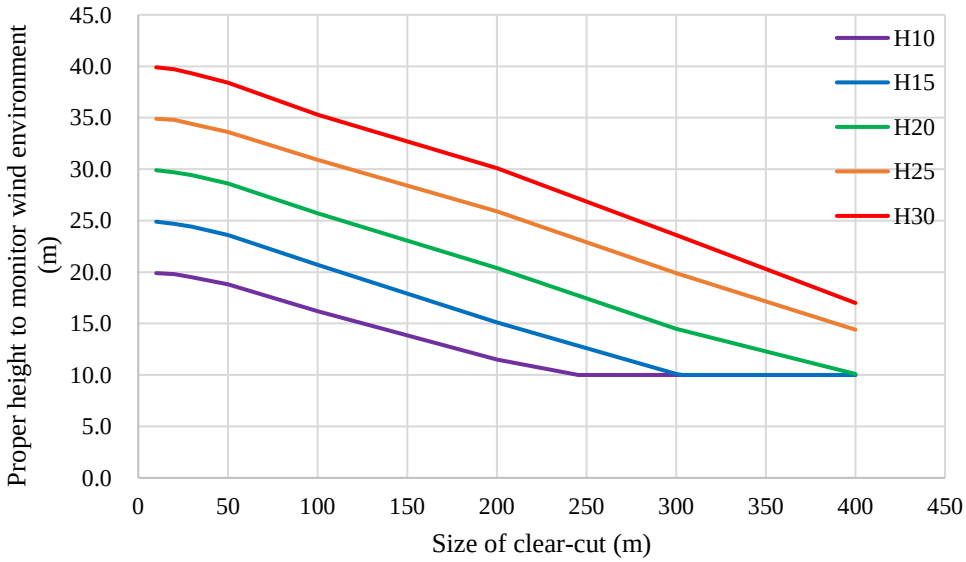

Figure 46 Appropriate height for wind environment monitoring when the inertial resistance coefficient of the deciduous tree was 0.5 m^{-1}.

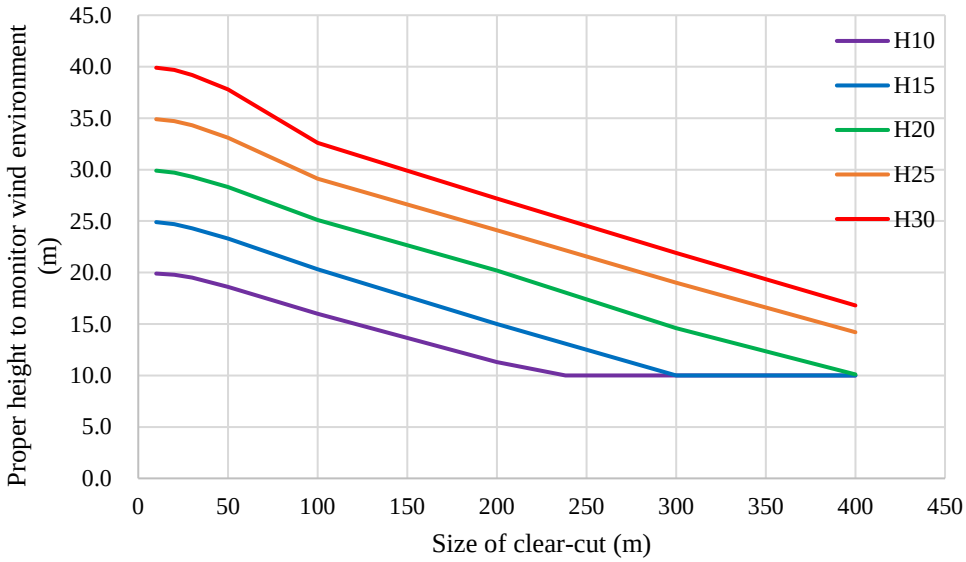

Figure 47 Appropriate height for wind environment monitoring when the inertial resistance coefficient of the coniferous tree was 0.7 m^{-1}.

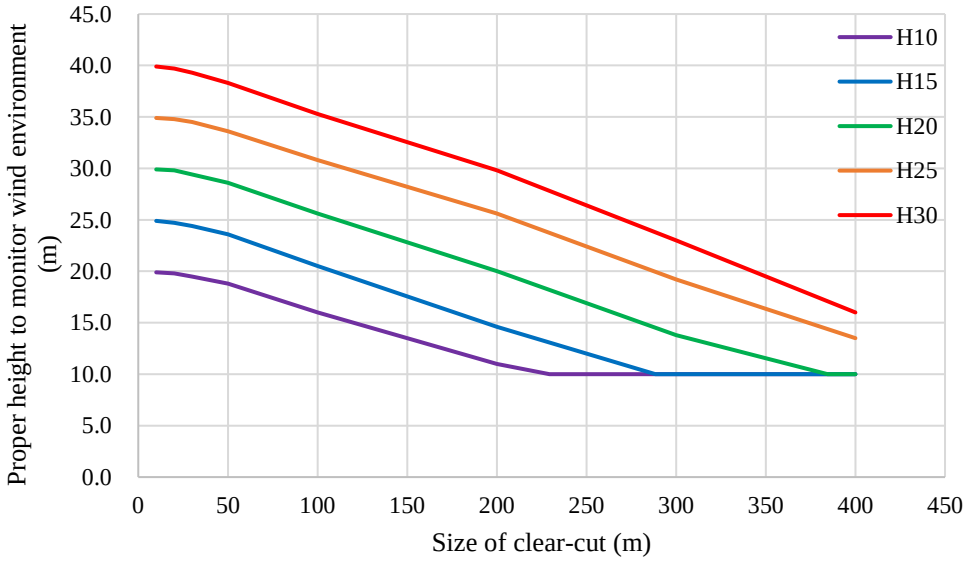

Figure 48 Appropriate height for wind environment monitoring when the inertial resistance coefficient of the deciduous tree was 0.7 m^{-1}.

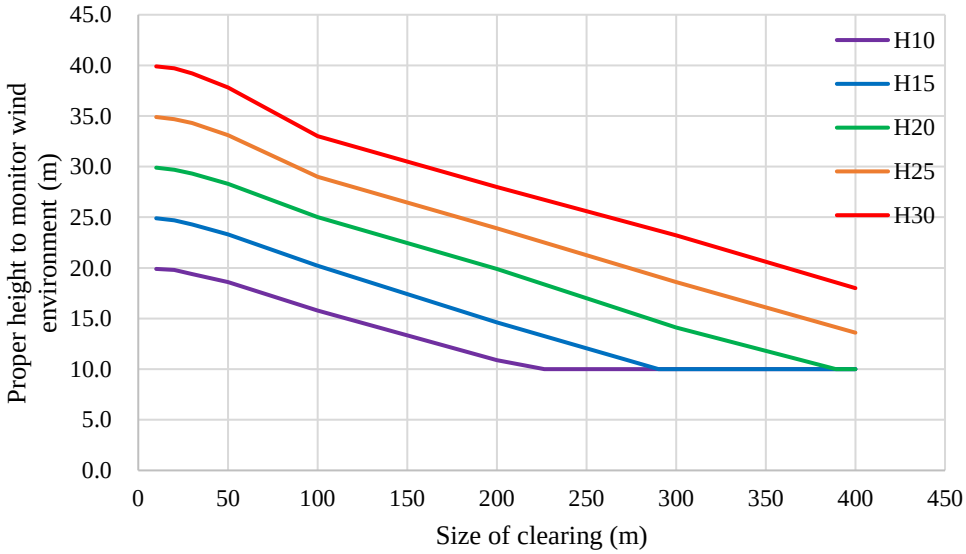

Figure 49 Appropriate height for wind environment monitoring when the inertial resistance coefficient of the coniferous tree was 0.9 m^{-1}.

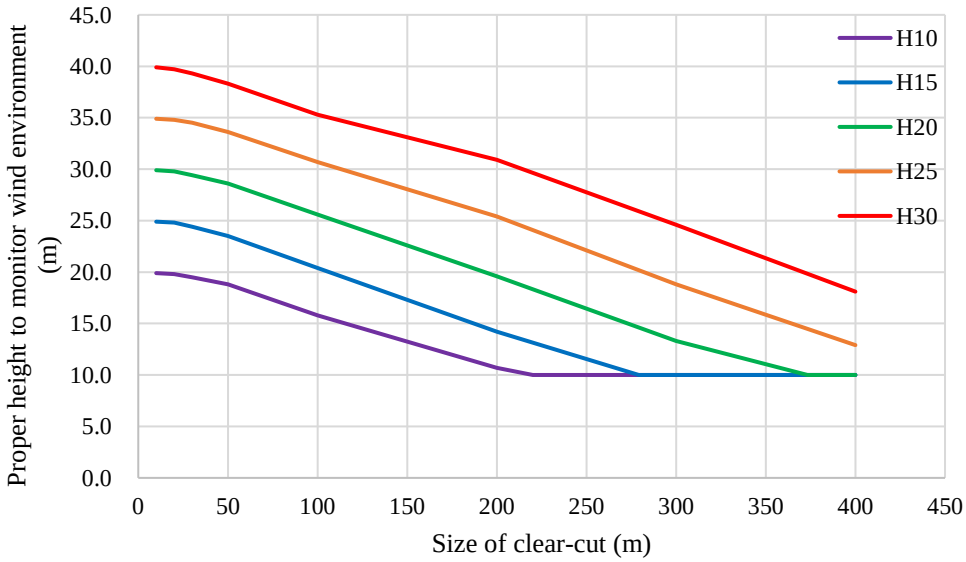

Figure 50 Appropriate height for wind environment monitoring when the inertial resistance coefficient of the deciduous tree was 0.9 m^{-1}.

5.3.4. Conversion factor for the reference wind speed

The mountainous weather stations of Republic of Korea have been constructed at a height of 10 m from 10 m X 10 m wide clear-cut, while international standards recommended that the wind environment in mountain region should be measured at a height of 10 m higher than the surrounding trees or should be measured in a clear-cut 10 times larger than height of the surrounding trees. Therefore, the conversion factor was developed in order to estimate a wind speed which is not affected by surrounding trees using a wind speed measured from the mountainous weather stations of Republic of Korea.

In order to compare the influences of the inlet wind speed of the boundary conditions, the vertical distributions of the simulated wind speed at the center of clear-cut were compared according to the wind speed of the boundary condition (Fig. 51). The simulated wind speed at the center of clear-cut was normalized using the simulated wind speed at the tree height, and the height was also normalized using the tree height. The normalized vertical distributions had the same tendency irrespective of the wind speed at the inlet boundary, confirming that the wind speed at the inlet boundary does not affect the vertical distribution of the wind speed at the center of clear-cut. Therefore, if the environmental conditions, such as the type of trees, the inertial resistance of trees, the tree height and the size of the clear-cut, are the same, a ratio of wind speed at two different height at the center of the clear-cut is constant regardless of the wind speed at the boundary.

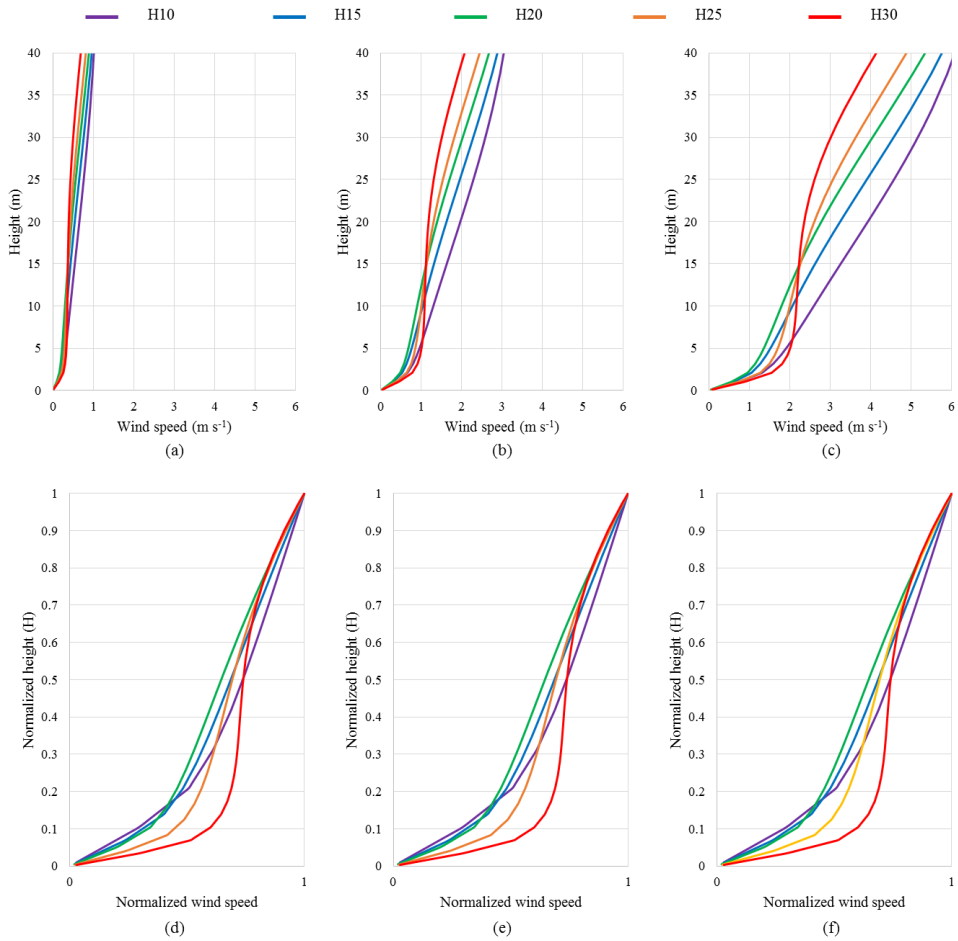

Figure 51 Vertical distribution of wind speed when the inertial resistance of coniferous tree was 0.3 m^{-1} with 50 m clear-cut; (a) wind speed at boundary condition of inlet : 1.0 m s^{-1}, (b) 3.0 m s^{-1}, and (c) 6.0 m s^{-1}, and normalized vertical wind speed when the inertial resistance of coniferous tree was 0.3 m^{-1} with 50 m clear-cut; (d) wind speed at boundary condition of inlet : 1.0 m s^{-1}, (e) 3.0 m s^{-1}, and (f) 6.0 m s^{-1}

The conversion factor (α) was the ratio of a reference wind speed which is not affected by air resistance of surrounding trees to a wind speed measured at the height of 10 m from the clear-cut center, and it can be used to estimate the reference wind speed.

$$\frac{V_{ref_i}}{V_{10_i}} = \alpha_i \ (constant) \tag{13}$$

Here, $V_{ref_i}(m\ s^{-1})$ was the reference wind speed, $V_{10_i}(m\ s^{-1})$ was the measured wind speed at 10 m height from the ground and *i* was the environmental condition according to the type of trees, the inertial resistance of trees, the tree height and the size of the clear-cut.

Table 31 Conversion factor (α) for the reference wind speed using observed wind speed at 10 m height using an inertial resistance coefficient for coniferous trees of 0.3 m^{-1}

		Height of tree (H, m)				
		10 m	**15 m**	**20 m**	**25 m**	**30 m**
Diameter of clear-cut (D, m)	**10 m**	1.82	2.54	3.04	2.50	2.05
	20 m	1.68	2.25	2.75	2.38	2.00
	30 m	1.58	2.03	2.46	2.23	1.92
	50 m	1.46	1.79	2.14	2.01	1.79
	100 m	1.26	1.47	1.70	1.67	1.54
	200 m	1.06	1.13	1.23	1.38	1.43
	300 m	1.00	1.00	1.06	1.16	1.18
	400 m	1.00	1.00	1.00	1.03	1.03

Table 32 Conversion factor (α) for the reference wind speed using observed wind speed at 10 m height using an inertial resistance coefficient for coniferous trees of 0.5 m^{-1}

		Height of tree (H, m)				
		10 m	**15 m**	**20 m**	**25 m**	**30 m**
Diameter of clear-cut (D, m)	**10 m**	1.96	2.91	3.62	2.87	2.23
	20 m	1.78	2.50	3.18	2.71	2.16
	30 m	1.65	2.20	2.77	2.49	2.06
	50 m	1.49	1.89	2.33	2.19	1.89
	100 m	1.26	1.51	1.79	1.76	1.59
	200 m	1.04	1.12	1.22	1.38	1.44
	300 m	0.93	0.96	1.03	1.15	1.17
	400 m	0.86	0.87	0.93	1.00	1.01

Table 33 Conversion factor (α) for the reference wind speed using observed wind speed at 10 m height using an inertial resistance coefficient for coniferous trees of 0.7 m^{-1}

		Height of tree (H, m)				
		10 m	**15 m**	**20 m**	**25 m**	**30 m**
Diameter of clear-cut (D, m)	**10 m**	2.06	3.20	4.08	3.15	2.34
	20 m	1.85	2.69	3.51	2.94	2.26
	30 m	1.70	2.32	3.00	2.68	2.15
	50 m	1.52	1.96	2.47	2.32	1.95
	100 m	1.26	1.53	1.85	1.82	1.62
	200 m	1.02	1.09	1.21	1.40	1.45
	300 m	1.00	1.00	1.01	1.15	1.15
	400 m	1.00	1.00	1.00	1.00	1.00

Table 34 Conversion factor (α) for the reference wind speed using observed wind speed at 10 m height using an inertial resistance coefficient for coniferous trees of 0.9 m^{-1}

		Height of tree (H, m)				
		10 m	**15 m**	**20 m**	**25 m**	**30 m**
Diameter of clear-cut (D, m)	**10 m**	2.15	3.45	4.47	3.37	2.41
	20 m	1.90	2.84	3.78	3.13	2.33
	30 m	1.74	2.42	3.18	2.82	2.20
	50 m	1.54	2.02	2.58	2.42	1.99
	100 m	1.26	1.54	1.89	1.86	1.64
	200 m	1.03	1.16	1.36	1.49	1.70
	300 m	1.00	1.00	1.12	1.24	1.41
	400 m	1.00	1.00	1.00	1.09	1.21

Table 35 Conversion factor (α) for the reference wind speed using observed wind speed at 10 m height using an inertial resistance coefficient for deciduous trees of 0.3 m^{-1}

		Height of tree (H, m)				
		10 m	**15 m**	**20 m**	**25 m**	**30 m**
Diameter of clear-cut (D, m)	**10 m**	1.90	2.88	3.92	5.04	6.17
	20 m	1.76	2.51	3.39	4.41	5.54
	30 m	1.65	2.24	2.95	3.84	4.96
	50 m	1.50	1.92	2.47	3.17	4.16
	100 m	1.27	1.52	1.86	2.31	2.98
	200 m	1.08	1.16	1.28	1.42	1.56
	300 m	1.00	1.00	1.07	1.16	1.24
	400 m	1.00	1.00	1.00	1.01	1.07

Table 36 Conversion factor (α) for the reference wind speed using observed wind speed at 10 m height using an inertial resistance coefficient for deciduous trees of 0.5 m^{-1}

		Height of tree (H, m)				
		10 m	**15 m**	**20 m**	**25 m**	**30 m**
Diameter of clear-cut (D, m)	**10 m**	2.04	3.31	4.71	6.25	7.84
	20 m	1.86	2.79	3.94	5.32	6.97
	30 m	1.72	2.43	3.34	4.53	6.16
	50 m	1.54	2.03	2.69	3.60	5.05
	100 m	1.27	1.54	1.93	2.47	3.39
	200 m	1.06	1.15	1.27	1.43	1.58
	300 m	1.00	1.00	1.05	1.14	1.22
	400 m	1.00	1.00	1.00	1.00	1.03

Table 37 Conversion factor (α) for the reference wind speed using observed wind speed at 10 m height using an inertial resistance coefficient for deciduous trees of 0.7 m^{-1}

		Height of tree (H, m)				
		10 m	**15 m**	**20 m**	**25 m**	**30 m**
Diameter of clear-cut (D, m)	**10 m**	2.14	3.64	5.37	7.29	9.32
	20 m	1.93	3.01	4.39	6.10	8.23
	30 m	1.78	2.58	3.65	5.10	7.25
	50 m	1.57	2.11	2.87	3.96	5.87
	100 m	1.27	1.55	1.98	2.60	3.78
	200 m	1.03	1.15	1.34	1.61	1.96
	300 m	1.00	1.00	1.10	1.25	1.39
	400 m	1.00	1.00	1.00	1.00	1.15

Table 38 Conversion factor (α) for the reference wind speed using observed wind speed at 10 m height using an inertial resistance coefficient for deciduous trees of 0.9 m^{-1}

		Height of tree (H, m)				
		10 m	**15 m**	**20 m**	**25 m**	**30 m**
Diameter of clear-cut (D, m)	**10 m**	2.23	3.93	5.96	8.25	10.68
	20 m	1.99	3.19	4.78	6.81	9.41
	30 m	1.82	2.69	3.91	5.62	8.29
	50 m	1.59	2.17	3.02	4.28	6.69
	100 m	1.27	1.57	2.02	2.71	4.14
	200 m	1.02	1.14	1.34	1.62	2.13
	300 m	1.00	1.00	1.09	1.24	1.48
	400 m	1.00	1.00	1.00	1.07	1.21

In addition, the wind speed regression equations for the height were derived as polynomial of degree 5 according to the environmental conditions, such as the type of trees, the inertial resistance of trees, the tree height and the size of the clear-cut in order to estimate the wind speed at any height in the center of clear-cut using the normalized distribution of wind speed and the measured wind speed.

$$V_{normalized}(z) = \frac{V_z}{V_H} = \sum_{i=1}^{5} C_i \times (H_{normalized})^i \quad (14)$$

$$H_{normalized} = \frac{H}{z} \quad (15)$$

where, $V_{normalized}$ was the normalized wind speed using the wind speed at the tree height, $V_{z,H}$ were the wind speed at the height from the ground and at the tree height, C_i were constants, $H_{normalized}$ was the normalized height using the tree height (H) and z was the height from the ground. Therefore, the wind speed at height (z) can be estimated using the polynomial regression equation and the measured wind speed.

$$V_z = \frac{V_{normalized}(z)}{V_{normalized}(z_m)} \times V_m \quad (16)$$

where, $V_z(m\ s^{-1})$ was the wind speed at height (z), $V_m(m\ s^{-1})$ was the measured wind speed at height (z_m), $V_{normalized}(z)$ was the normalized wind speed at height (z) and $V_{normalized}(z_m)$ was the normalized wind speed at height for the measured wind speed. The value of C_i and the coefficient of determination (R^2) for normalized wind speed equations were presented in the table 39 – 48 according to the type of tree, the height of tree, the inertial coefficient of tree and the size of clear-cut.

Table 39 Constants of polynomial regression equation of normalized wind speed for the height when the height of coniferous tree was 10 m

C_i	D	C_1	C_2	C_3	C_4	C_5	R^2
0.3	10 m	0.5534	-3.1939	6.7591	-6.2912	3.1635	0.9999
	20 m	0.4151	-2.4450	5.3763	-5.3776	3.0237	1.0000
	30 m	0.3966	-2.3425	5.2058	-5.3482	3.0805	0.9999
	50 m	0.4175	-2.4647	5.5004	-5.7361	3.2748	0.9999
	100 m	0.4345	-2.5841	5.8385	-6.2328	3.5355	0.9999
	200 m	0.4108	-2.4781	5.7161	-6.3096	3.6534	0.9999
	300 m	0.3761	-2.2963	5.3844	-6.0928	3.6220	0.9999
	400 m	0.3466	-2.1361	5.0740	-5.8535	3.5632	0.9999
0.5	10 m	0.5535	-3.1841	6.6699	-6.0223	2.9742	1.0000
	20 m	0.3922	-2.3098	5.0602	-4.9834	2.8338	1.0000
	30 m	0.3777	-2.2279	4.9362	-5.0198	2.9265	1.0000
	50 m	0.4109	-2.4192	5.3774	-5.5610	3.1836	0.9999
	100 m	0.4400	-2.6090	5.8706	-6.2228	3.5126	0.9999
	200 m	0.4205	-2.5299	5.8134	-6.3791	3.6674	0.9999
	300 m	0.3848	-2.3438	5.4779	-6.1679	3.6422	0.9999
	400 m	0.3535	-2.1742	5.1512	-5.9188	3.5824	0.9999
0.7	10 m	0.5505	-3.1622	6.5799	-5.8099	2.8335	1.0000
	20 m	0.3724	-2.1950	4.8005	-4.6760	2.6916	1.0000
	30 m	0.3612	-2.1304	4.7146	-4.7641	2.8118	1.0000
	50 m	0.4039	-2.3748	5.2680	-5.4213	3.1161	0.9999
	100 m	0.4421	-2.6167	5.8749	-6.2027	3.4939	0.9999
	200 m	0.4257	-2.5572	5.8640	-6.4140	3.6736	0.9999
	300 m	0.3895	-2.3694	5.5280	-6.2076	3.6525	0.9999
	400 m	0.3571	-2.1946	5.1923	-5.9533	3.5924	0.9999
0.9	10 m	2.3750	-12.9868	26.0390	-23.2052	8.7250	0.9739
	20 m	2.3750	-12.9868	26.0390	-23.2052	8.7250	0.9739
	30 m	2.3750	-12.9868	26.0390	-23.2052	8.7250	0.9739
	50 m	2.3750	-12.9868	26.0390	-23.2052	8.7250	0.9739
	100 m	2.3750	-12.9868	26.0390	-23.2052	8.7250	0.9739
	200 m	2.3750	-12.9868	26.0390	-23.2052	8.7250	0.9739
	300 m	2.3750	-12.9868	26.0390	-23.2052	8.7250	0.9739
	400 m	2.3750	-12.9868	26.0390	-23.2052	8.7250	0.9739

Table 40 Constants of polynomial regression equation of normalized wind speed for the height when the height of coniferous tree was 15 m

C_i	D	C_1	C_2	C_3	C_4	C_5	R^2
0.3	10 m	1.5162	-7.4999	13.6090	-10.6098	3.9872	0.9999
	20 m	1.2501	-6.1341	11.1575	-8.9255	3.6548	0.9999
	30 m	1.1260	-5.4726	9.9286	-8.0834	3.5039	0.9999
	50 m	1.1334	-5.4588	9.8522	-8.1149	3.5906	0.9999
	100 m	1.2750	-6.1318	11.0749	-9.2374	4.0219	0.9998
	200 m	1.3928	-6.7359	12.2804	-10.4527	4.5179	0.9998
	300 m	1.3765	-6.6985	12.3247	-10.6611	4.6602	0.9998
	400 m	1.3237	-6.4775	12.0163	-10.5377	4.6767	0.9999
0.5	10 m	1.4256	-7.1282	13.0072	-9.9918	3.6899	0.9999
	20 m	1.1256	-5.5685	10.1820	-8.0553	3.3189	0.9999
	30 m	0.9993	-4.8760	8.8716	-7.1657	3.1731	0.9999
	50 m	1.0385	-5.0006	9.0166	-7.3758	3.3237	0.9999
	100 m	1.2351	-5.9302	10.6847	-8.8600	3.8731	0.9998
	200 m	1.3994	-6.7565	12.2878	-10.4127	4.4845	0.9998
	300 m	1.3946	-6.7759	12.4388	-10.7181	4.6625	0.9998
	400 m	1.3436	-6.5656	12.1552	-10.6232	4.6916	0.9999
0.7	10 m	1.3600	-6.8666	12.6020	-9.5860	3.4933	0.9999
	20 m	1.0359	-5.1662	9.5000	-7.4586	3.0914	0.9999
	30 m	0.9075	-4.4478	8.1224	-6.5269	2.9469	0.9999
	50 m	0.9698	-4.6718	8.4251	-6.8637	3.1428	0.9999
	100 m	1.2055	-5.7835	10.4081	-8.6026	3.7752	0.9998
	200 m	1.4008	-6.7571	12.2733	-10.3760	4.4616	0.9998
	300 m	1.4033	-6.8125	12.4913	-10.7417	4.6616	0.9998
	400 m	1.3535	-6.6092	12.2233	-10.6641	4.6982	0.9998
0.9	10 m	5.9257	-26.9890	45.0722	-33.4550	10.4766	0.9736
	20 m	5.9257	-26.9890	45.0722	-33.4550	10.4766	0.9736
	30 m	5.9257	-26.9890	45.0722	-33.4550	10.4766	0.9736
	50 m	5.9257	-26.9890	45.0722	-33.4550	10.4766	0.9736
	100 m	5.9257	-26.9890	45.0722	-33.4550	10.4766	0.9736
	200 m	5.9257	-26.9890	45.0722	-33.4550	10.4766	0.9736
	300 m	5.9257	-26.9890	45.0722	-33.4550	10.4766	0.9736
	400 m	5.9257	-26.9890	45.0722	-33.4550	10.4766	0.9736

Table 41 Constants of polynomial regression equation of normalized wind speed for the height when the height of coniferous tree was 20 m

C_i	D	C_1	C_2	C_3	C_4	C_5	R^2
0.3	10 m	2.6280	-11.9528	19.9655	-14.1799	4.5474	0.9997
	20 m	2.3719	-10.5429	17.3342	-12.3299	4.1765	0.9997
	30 m	2.1235	-9.2834	15.0971	-10.8174	3.8899	0.9998
	50 m	2.0048	-8.6379	13.8939	-10.0392	3.7883	0.9998
	100 m	2.2144	-9.4736	15.1438	-11.0411	4.1674	0.9997
	200 m	2.5985	-11.1314	17.8523	-13.1875	4.8807	0.9997
	300 m	2.7328	-11.7475	18.9449	-14.1558	5.2385	0.9997
	400 m	2.7383	-11.8137	19.1568	-14.4590	5.3903	0.9997
0.5	10 m	2.3273	-10.8361	18.4409	-13.0634	4.1374	0.9998
	20 m	2.0712	-9.3418	15.5499	-10.9984	3.7270	0.9998
	30 m	1.8154	-8.0027	13.1155	-9.3414	3.4214	0.9998
	50 m	1.7299	-7.4681	12.0352	-8.6431	3.3545	0.9998
	100 m	2.0428	-8.7309	13.9332	-10.0985	3.8636	0.9998
	200 m	2.5533	-10.9240	17.4870	-12.8655	4.7618	0.9997
	300 m	2.7361	-11.7473	18.9103	-14.0817	5.1957	0.9996
	400 m	2.7608	-11.8970	19.2587	-14.4914	5.3817	0.9997
0.7	10 m	2.1272	-10.1129	17.4958	-12.3939	3.8885	0.9998
	20 m	1.8739	-8.5662	14.4232	-10.1710	3.4469	0.9998
	30 m	1.6098	-7.1562	11.8224	-8.3908	3.1218	0.9999
	50 m	1.5452	-6.6869	10.8050	-7.7298	3.0741	0.9999
	100 m	1.9271	-8.2334	13.1308	-9.4834	3.6686	0.9998
	200 m	2.5209	-10.7786	17.2379	-12.6547	4.6869	0.9997
	300 m	2.7341	-11.7314	18.8672	-14.0247	5.1678	0.9996
	400 m	2.7704	-11.9313	19.2978	-14.4981	5.3742	0.9997
0.9	10 m	10.0531	-41.1951	61.8962	-41.3341	11.6454	0.9734
	20 m	10.0531	-41.1951	61.8962	-41.3341	11.6454	0.9734
	30 m	10.0531	-41.1951	61.8962	-41.3341	11.6454	0.9734
	50 m	10.0531	-41.1951	61.8962	-41.3341	11.6454	0.9734
	100 m	10.0531	-41.1951	61.8962	-41.3341	11.6454	0.9734
	200 m	10.0531	-41.1951	61.8962	-41.3341	11.6454	0.9734
	300 m	10.0531	-41.1951	61.8962	-41.3341	11.6454	0.9734
	400 m	10.0531	-41.1951	61.8962	-41.3341	11.6454	0.9734

Table 42 Constants of polynomial regression equation of normalized wind speed for the height when the height of coniferous tree was 25 m

C_i	D	C_1	C_2	C_3	C_4	C_5	R^2
0.3	10 m	5.0305	-21.6380	34.5129	-23.7928	6.9007	0.9991
	20 m	4.9958	-20.7982	32.2206	-21.8302	6.4294	0.9991
	30 m	4.6537	-18.9810	28.8705	-19.4218	5.8965	0.9993
	50 m	4.1272	-16.5893	24.9099	-16.7707	5.3392	0.9994
	100 m	3.8108	-15.1697	22.5593	-15.2608	5.0754	0.9995
	200 m	3.9185	-15.5591	23.0601	-15.6481	5.2438	0.9995
	300 m	4.1510	-16.5089	24.5338	-16.7636	5.6036	0.9995
	400 m	4.2577	-16.9696	25.3043	-17.4106	5.8342	0.9995
0.5	10 m	4.6839	-20.5731	33.4465	-23.2107	6.6647	0.9991
	20 m	4.6893	-19.7441	30.9364	-20.9985	6.1332	0.9992
	30 m	4.3339	-17.7779	27.2147	-18.2923	5.5384	0.9993
	50 m	3.7959	-15.2790	22.9917	-15.4378	4.9444	0.9995
	100 m	3.5482	-14.1074	20.9493	-14.1079	4.7318	0.9996
	200 m	3.7670	-14.9401	22.1028	-14.9346	5.0197	0.9995
	300 m	4.0934	-16.2607	24.1213	-16.4206	5.4823	0.9995
	400 m	4.2542	-16.9355	25.2085	-17.2858	5.7747	0.9995
0.7	10 m	4.4519	-19.8864	32.8213	-22.9138	6.5371	0.9991
	20 m	4.4932	-19.0918	30.1886	-20.5388	5.9644	0.9992
	30 m	4.1307	-17.0262	26.2070	-17.6193	5.3240	0.9993
	50 m	3.5814	-14.4374	21.7740	-14.6025	4.6990	0.9995
	100 m	3.3696	-13.3917	19.8773	-13.3524	4.5105	0.9996
	200 m	3.6613	-14.5132	21.4525	-14.4609	4.8746	0.9995
	300 m	4.0493	-16.0762	23.8259	-16.1873	5.4038	0.9995
	400 m	4.2444	-16.8865	25.1129	-17.1897	5.7350	0.9995
0.9	10 m	14.2123	-54.3428	76.1891	-47.4753	12.4807	0.9732
	20 m	14.2123	-54.3428	76.1891	-47.4753	12.4807	0.9732
	30 m	14.2123	-54.3428	76.1891	-47.4753	12.4807	0.9732
	50 m	14.2123	-54.3428	76.1891	-47.4753	12.4807	0.9732
	100 m	14.2123	-54.3428	76.1891	-47.4753	12.4807	0.9732
	200 m	14.2123	-54.3428	76.1891	-47.4753	12.4807	0.9732
	300 m	14.2123	-54.3428	76.1891	-47.4753	12.4807	0.9732
	400 m	14.2123	-54.3428	76.1891	-47.4753	12.4807	0.9732

Table 43 Constants of polynomial regression equation of normalized wind speed for the height when the height of coniferous tree was 30 m

C_i	D	C_1	C_2	C_3	C_4	C_5	R^2
0.3	10 m	9.0500	-36.7420	55.8914	-37.1893	10.0083	0.9973
	20 m	9.1085	-35.9706	53.1949	-34.6421	9.3296	0.9977
	30 m	8.5973	-33.3230	48.3235	-31.0619	8.4839	0.9981
	50 m	7.4597	-28.5119	40.7513	-26.0576	7.3761	0.9987
	100 m	6.0551	-22.9107	32.4006	-20.7760	6.2452	0.9991
	200 m	5.3448	-20.1048	28.1762	-17.9934	5.5898	0.9993
	300 m	5.5727	-20.9711	29.4013	-18.8348	5.8449	0.9993
	400 m	5.7981	-21.8455	30.6873	-19.7522	6.1258	0.9993
0.5	10 m	9.0976	-37.4099	57.7172	-38.7150	10.3289	0.9970
	20 m	9.1916	-36.5708	54.5755	-35.6958	9.5201	0.9974
	30 m	8.6143	-33.5245	48.8852	-31.4766	8.5217	0.9980
	50 m	7.3241	-28.0314	40.1653	-25.6766	7.2359	0.9987
	100 m	5.7931	-21.9064	30.9772	-19.8267	5.9766	0.9992
	200 m	5.0641	-19.0319	26.6352	-16.9479	5.2924	0.9993
	300 m	5.4052	-20.3226	28.4506	-18.1652	5.6447	0.9993
	400 m	5.7196	-21.5295	30.1992	-19.3794	6.0036	0.9992
0.7	10 m	9.2091	-38.1956	59.4935	-40.1370	10.6493	0.9967
	20 m	9.3279	-37.3037	56.0189	-36.7640	9.7419	0.9973
	30 m	8.7017	-33.9625	49.7199	-32.0663	8.6275	0.9979
	50 m	7.2934	-27.9448	40.1202	-25.6551	7.2035	0.9986
	100 m	5.6453	-21.3449	30.1935	-19.3118	5.8313	0.9992
	200 m	4.8807	-18.3359	25.6456	-16.2860	5.1071	0.9994
	300 m	5.2917	-19.8875	27.8220	-17.7323	5.5185	0.9993
	400 m	5.6611	-21.3002	29.8561	-19.1291	5.9253	0.9992
0.9	10 m	18.1559	-66.1042	88.2496	-52.3622	13.1074	0.9731
	20 m	18.1559	-66.1042	88.2496	-52.3622	13.1074	0.9731
	30 m	18.1559	-66.1042	88.2496	-52.3622	13.1074	0.9731
	50 m	18.1559	-66.1042	88.2496	-52.3622	13.1074	0.9731
	100 m	18.1559	-66.1042	88.2496	-52.3622	13.1074	0.9731
	200 m	18.1559	-66.1042	88.2496	-52.3622	13.1074	0.9731
	300 m	18.1559	-66.1042	88.2496	-52.3622	13.1074	0.9731
	400 m	18.1559	-66.1042	88.2496	-52.3622	13.1074	0.9731

Table 44 Constants of polynomial regression equation of normalized wind speed for the height when the height of deciduous tree was 10 m

C_i	D	C_1	C_2	C_3	C_4	C_5	R^2
0.3	10 m	0.4180	-2.3879	4.9613	-4.4726	2.4740	1.0000
	20 m	0.3512	-2.0572	4.4795	-4.4080	2.6280	1.0000
	30 m	0.3658	-2.1501	4.7405	-4.8053	2.8419	1.0000
	50 m	0.4089	-2.4062	5.3434	-5.5230	3.1688	0.9999
	100 m	0.4376	-2.5970	5.8511	-6.2158	3.5158	0.9999
	200 m	0.4145	-2.4976	5.7517	-6.3322	3.6560	0.9999
	300 m	0.3782	-2.3074	5.4056	-6.1077	3.6247	0.9999
	400 m	0.3473	-2.1401	5.0817	-5.8583	3.5636	0.9999
0.5	10 m	0.3988	-2.2697	4.6482	-4.0016	2.2181	1.0000
	20 m	0.3173	-1.8605	4.0353	-3.8936	2.3957	1.0000
	30 m	0.3404	-2.0003	4.3994	-4.4113	2.6651	1.0000
	50 m	0.3993	-2.3454	5.1924	-5.3267	3.0724	0.9999
	100 m	0.4418	-2.6153	5.8725	-6.2017	3.4942	0.9999
	200 m	0.4227	-2.5414	5.8342	-6.3917	3.6684	0.9999
	300 m	0.3854	-2.3470	5.4836	-6.1708	3.6419	0.9999
	400 m	0.3529	-2.1711	5.1444	-5.9117	3.5794	0.9999
0.7	10 m	0.3839	-2.1808	4.4204	-3.6665	2.0375	1.0000
	20 m	0.2899	-1.7033	3.6866	-3.5018	2.2235	1.0000
	30 m	0.3197	-1.8798	4.1303	-4.1104	2.5339	1.0000
	50 m	0.3908	-2.2935	5.0692	-5.1765	3.0021	0.9999
	100 m	0.4433	-2.6210	5.8741	-6.1823	3.4773	0.9999
	200 m	0.4272	-2.5651	5.8782	-6.4224	3.6742	0.9999
	300 m	0.3894	-2.3686	5.5262	-6.2048	3.6510	0.9999
	400 m	0.3559	-2.1879	5.1785	-5.9404	3.5878	0.9999
0.9	10 m	0.3721	-2.1120	4.2463	-3.4102	1.8988	1.0000
	20 m	0.2670	-1.5727	3.3996	-3.1844	2.0859	1.0000
	30 m	0.3024	-1.7793	3.9080	-3.8658	2.4289	1.0000
	50 m	0.3835	-2.2495	4.9669	-5.0554	2.9467	0.9999
	100 m	0.4440	-2.6226	5.8701	-6.1638	3.4636	0.9999
	200 m	0.4302	-2.5805	5.9066	-6.4417	3.6774	0.9999
	300 m	0.3920	-2.3828	5.5539	-6.2268	3.6567	0.9999
	400 m	0.3579	-2.1988	5.2005	-5.9589	3.5932	0.9999

Table 45 Constants of polynomial regression equation of normalized wind speed for the height when the height of deciduous tree was 15 m

C_i	D	C_1	C_2	C_3	C_4	C_5	R^2
0.3	10 m	1.0085	-4.9484	8.7900	-6.4825	2.6345	0.9999
	20 m	0.8812	-4.3156	7.7746	-6.0325	2.6944	0.9999
	30 m	0.8726	-4.2306	7.6204	-6.0825	2.8222	0.9999
	50 m	1.0127	-4.8644	8.7317	-7.1033	3.2256	0.9999
	100 m	1.2610	-6.0534	10.9008	-9.0375	3.9317	0.9998
	200 m	1.4074	-6.8007	12.3816	-10.5140	4.5280	0.9998
	300 m	1.3856	-6.7404	12.3956	-10.7127	4.6738	0.9998
	400 m	1.3252	-6.4857	12.0330	-10.5532	4.6822	0.9999
0.5	10 m	0.8935	-4.4626	7.9904	-5.7177	2.2983	1.0000
	20 m	0.7327	-3.6425	6.6188	-5.0284	2.3209	1.0000
	30 m	0.7266	-3.5489	6.4238	-5.0618	2.4620	1.0000
	50 m	0.9116	-4.3826	7.8668	-6.3531	2.9595	0.9999
	100 m	1.2267	-5.8825	10.5757	-8.7296	3.8124	0.9998
	200 m	1.4138	-6.8232	12.4011	-10.4974	4.5082	0.9998
	300 m	1.3997	-6.8015	12.4886	-10.7645	4.6798	0.9998
	400 m	1.3394	-6.5489	12.1343	-10.6184	4.6953	0.9999
0.7	10 m	0.8137	-4.1354	7.4724	-5.2292	2.0803	1.0000
	20 m	0.6254	-3.1598	5.7998	-4.3269	2.0627	1.0000
	30 m	0.6191	-3.0495	5.5534	-4.3281	2.2065	1.0000
	50 m	0.8377	-4.0322	7.2421	-5.8177	2.7721	0.9999
	100 m	1.2012	-5.7572	10.3415	-8.5137	3.7309	0.9998
	200 m	1.4159	-6.8286	12.3991	-10.4774	4.4936	0.9998
	300 m	1.4067	-6.8317	12.5337	-10.7881	4.6815	0.9998
	400 m	1.3465	-6.5806	12.1847	-10.6503	4.7013	0.9999
0.9	10 m	0.7529	-3.8917	7.0989	-4.8801	1.9216	1.0000
	20 m	0.5413	-2.7835	5.1666	-3.7887	1.8654	1.0000
	30 m	0.5334	-2.6526	4.8647	-3.7514	2.0071	1.0000
	50 m	0.7789	-3.7540	6.7482	-5.3969	2.6258	0.9999
	100 m	1.1806	-5.6567	10.1554	-8.3447	3.6680	0.9998
	200 m	1.4162	-6.8270	12.3886	-10.4563	4.4811	0.9998
	300 m	1.4107	-6.8486	12.5580	-10.7992	4.6811	0.9998
	400 m	1.3505	-6.5986	12.2131	-10.6675	4.7041	0.9998

Table 46 Constants of polynomial regression equation of normalized wind speed for the height when the height of deciduous tree was 20 m

C_i	D	C_1	C_2	C_3	C_4	C_5	R^2
0.3	10 m	1.4286	-6.5598	10.8824	-7.2947	2.5476	0.9999
	20 m	1.3694	-6.1288	10.0391	-6.8568	2.5824	0.9999
	30 m	1.3188	-5.7784	9.3535	-6.5038	2.6157	0.9999
	50 m	1.4971	-6.4368	10.2874	-7.2868	2.9463	0.9999
	100 m	2.0307	-8.6678	13.7932	-9.9469	3.8010	0.9998
	200 m	2.6225	-11.2206	17.9612	-13.2203	4.8702	0.9996
	300 m	2.7698	-11.9000	19.1744	-14.3060	5.2749	0.9996
	400 m	2.7608	-11.9100	19.3101	-14.5709	5.4227	0.9997
0.5	10 m	1.1589	-5.5789	9.5768	-6.3465	2.1919	0.9999
	20 m	1.0819	-4.9964	8.3824	-5.6349	2.1704	1.0000
	30 m	1.0123	-4.5188	7.4274	-5.0851	2.1684	1.0000
	50 m	1.2340	-5.3297	8.5496	-5.9947	2.5467	0.9999
	100 m	1.8932	-8.0790	12.8467	-9.2207	3.5693	0.9998
	200 m	2.5965	-11.1013	17.7500	-13.0319	4.7995	0.9996
	300 m	2.7768	-11.9215	19.1885	-14.2877	5.2571	0.9996
	400 m	2.7774	-11.9742	19.3960	-14.6109	5.4245	0.9997
0.7	10 m	0.9728	-4.9209	8.7423	-5.7653	1.9718	1.0000
	20 m	0.8838	-4.2258	7.2755	-4.8312	1.9000	1.0000
	30 m	0.7963	-3.6356	6.0867	-4.1067	1.8622	1.0000
	50 m	1.0458	-4.5402	7.3155	-5.0831	2.2669	0.9999
	100 m	1.7956	-7.6633	12.1826	-8.7161	3.4102	0.9998
	200 m	2.5751	-11.0056	17.5862	-12.8927	4.7497	0.9996
	300 m	2.7771	-11.9183	19.1730	-14.2607	5.2423	0.9996
	400 m	2.7838	-11.9979	19.4256	-14.6207	5.4222	0.9997
0.9	10 m	0.8288	-4.4217	8.1333	-5.3565	1.8158	1.0000
	20 m	0.7321	-3.6413	6.4478	-4.2372	1.6998	1.0000
	30 m	0.6283	-2.9510	5.0531	-3.3565	1.6281	1.0000
	50 m	0.8969	-3.9167	6.3432	-4.3673	2.0480	1.0000
	100 m	1.7174	-7.3309	11.6537	-8.3165	3.2850	0.9998
	200 m	2.5509	-10.8996	17.4105	-12.7499	4.7008	0.9996
	300 m	2.7719	-11.8939	19.1276	-14.2169	5.2246	0.9996
	400 m	2.7835	-11.9948	19.4153	-14.6052	5.4141	0.9997

Table 47 Constants of polynomial regression equation of normalized wind speed for the height when the height of deciduous tree was 25 m

C_i	D	C_1	C_2	C_3	C_4	C_5	R^2
0.3	10 m	1.5228	-6.9721	11.4664	-7.3924	2.3780	0.9999
	20 m	1.6444	-7.0934	11.1700	-7.1227	2.4069	0.9999
	30 m	1.5869	-6.6073	10.1347	-6.4719	2.3635	0.9999
	50 m	1.7145	-6.9161	10.3402	-6.6793	2.5476	0.9999
	100 m	2.4378	-9.6696	14.2405	-9.3637	3.3648	0.9998
	200 m	3.6612	-14.4988	21.3837	-14.3518	4.8202	0.9995
	300 m	4.1658	-16.5340	24.4898	-16.6282	5.5227	0.9994
	400 m	4.3351	-17.2537	25.6700	-17.5911	5.8561	0.9994
0.5	10 m	1.0537	-5.4024	9.6181	-6.2880	2.0187	0.9999
	20 m	1.2068	-5.5297	9.1398	-5.8084	1.9947	0.9999
	30 m	1.1208	-4.8533	7.7041	-4.8540	1.8865	1.0000
	50 m	1.2534	-5.1264	7.7657	-4.9407	2.0532	0.9999
	100 m	2.1281	-8.4509	12.4523	-8.1316	3.0107	0.9998
	200 m	3.5560	-14.0771	20.7468	-13.8901	4.6784	0.9995
	300 m	4.1401	-16.4245	24.3089	-16.4767	5.4682	0.9994
	400 m	4.3401	-17.2658	25.6700	-17.5665	5.8387	0.9994
0.7	10 m	0.7266	-4.3328	8.4164	-5.6137	1.8019	0.9999
	20 m	0.9116	-4.4924	7.8301	-4.9827	1.7354	1.0000
	30 m	0.8031	-3.6667	6.0777	-3.7825	1.5712	1.0000
	50 m	0.9288	-3.8705	5.9663	-3.7318	1.7111	1.0000
	100 m	1.9084	-7.5892	11.1928	-7.2682	2.7640	0.9998
	200 m	3.4735	-13.7479	20.2531	-13.5369	4.5720	0.9995
	300 m	4.1126	-16.3111	24.1307	-16.3389	5.4227	0.9994
	400 m	4.3335	-17.2358	25.6161	-17.5161	5.8187	0.9994
0.9	10 m	0.4666	-3.4945	7.5048	-5.1281	1.6484	0.9999
	20 m	0.6845	-3.7039	6.8559	-4.3820	1.5465	1.0000
	30 m	0.5578	-2.7555	4.8393	-2.9725	1.3327	1.0000
	50 m	0.6713	-2.8760	4.5454	-2.7799	1.4421	1.0000
	100 m	1.7262	-6.8762	10.1524	-6.5568	2.5614	0.9999
	200 m	3.4031	-13.4697	19.8400	-13.2452	4.4853	0.9996
	300 m	4.0839	-16.1962	23.9562	-16.2101	5.3820	0.9994
	400 m	4.3222	-17.1895	25.5436	-17.4592	5.7994	0.9994

Table 48 Constants of polynomial regression equation of normalized wind speed for the height when the height of deciduous tree was 30 m

C_i	D	C_1	C_2	C_3	C_4	C_5	R^2
0.3	10 m	1.0726	-5.5591	10.2356	-7.0327	2.2863	0.9997
	20 m	1.5463	-6.8258	11.1368	-7.1659	2.3120	0.9998
	30 m	1.5875	-6.5839	10.1604	-6.3324	2.1718	0.9999
	50 m	1.5835	-6.2284	9.1235	-5.5711	2.0959	0.9999
	100 m	2.2312	-8.4410	11.8346	-7.2478	2.6281	0.9998
	200 m	4.1687	-15.6403	21.7779	-13.6589	4.3624	0.9995
	300 m	5.2731	-19.7937	27.6247	-17.5252	5.4335	0.9993
	400 m	5.8050	-21.8264	30.5568	-19.5429	6.0212	0.9992
0.5	10 m	0.2393	-2.8346	7.2107	-5.5000	1.8859	0.9998
	20 m	0.8463	-4.4624	8.3412	-5.5998	1.8766	0.9999
	30 m	0.8936	-4.1386	7.0505	-4.4592	1.6555	0.9999
	50 m	0.8352	-3.4922	5.4447	-3.2672	1.4811	1.0000
	100 m	1.5978	-6.0884	8.5894	-5.1665	2.0712	0.9999
	200 m	3.8781	-14.5514	20.2526	-12.6554	4.0853	0.9995
	300 m	5.1536	-19.3392	26.9732	-17.0785	5.3031	0.9993
	400 m	5.7612	-21.6544	30.2978	-19.3500	5.9590	0.9992
0.7	10 m	-0.3616	-0.8924	5.1232	-4.5094	1.6407	0.9998
	20 m	0.3661	-2.8651	6.5138	-4.6228	1.6091	0.9999
	30 m	0.4275	-2.5132	5.0234	-3.2627	1.3258	1.0000
	50 m	0.3176	-1.6066	2.9247	-1.6987	1.0633	1.0000
	100 m	1.1256	-4.3354	6.1743	-3.6219	1.6598	1.0000
	200 m	3.6549	-13.7191	19.0936	-11.8986	3.8777	0.9996
	300 m	5.0507	-18.9523	26.4271	-16.7123	5.1988	0.9993
	400 m	5.7122	-21.4684	30.0307	-19.1648	5.9038	0.9992
0.9	10 m	-0.8418	0.6519	3.4939	-3.7709	1.4670	0.9998
	20 m	-0.0008	-1.6556	5.1621	-3.9268	1.4216	0.9999
	30 m	0.0761	-1.2952	3.5229	-2.3891	1.0853	1.0000
	50 m	-0.0876	-0.1346	0.9666	-0.4862	0.7410	1.0000
	100 m	0.7518	-2.9518	4.2752	-2.4118	1.3380	1.0000
	200 m	2.8190	-10.7176	15.1712	-9.6360	3.3701	0.9998
	300 m	4.0822	-15.5404	22.0821	-14.3309	4.7169	0.9997
	400 m	4.5633	-17.3933	24.8124	-16.2984	5.3267	0.9996

5.4. Conclusions

In this chapter, to monitor the wind environment in mountain region, the appropriate sizes of the clear-cut were estimated according to the environmental conditions such as the type of trees, the inertial resistance of trees and the tree height. In addition, the appropriate heights of anemometer to monitor the wind environment in mountain region were derived according to the environmental conditions such as the type of trees, the inertial resistance of trees, the tree height and the size of the clear-cut in case that it is difficult to secure the proper size of the clear-cut.

At the beginning of the study, I found that international standards for weather station, which were established decades ago, were not provided for references, and simply suggest that the distance from the boundary of the forest should be at least 10 times the height of the surrounding trees. Since this criterion requires an excessive wide clear-cut, it is expected that the proper size of clear-cut may be reduced by the wind environment analysis using the CFD. However, since the proper sizes of clear-cut were not reduced based on the simulation results, the convention factors that can estimate the reference wind speed which is not affected by air resistance of surrounding trees were developed.

Chapter 6. Summary and concluding remarks

6.1. Summary

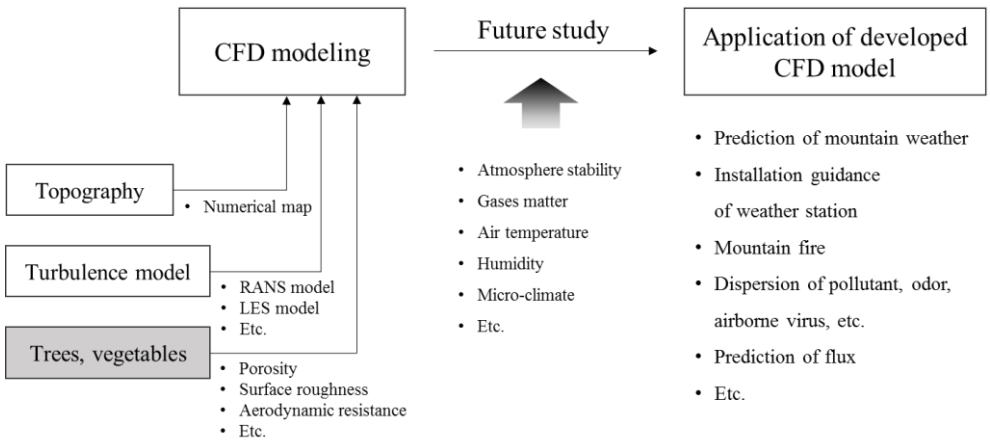

Figure 52 CFD modeling for wind environment simulation over mountainous region

In the early days of simulating external diffusion using CFD, the simulation was focused on realizing a shape of terrain. Not only the shape of the terrain but also the trees distributed on the ground are an important factor in simulating the wind environment around the ground. In this study, the design of CFD model was focused on the aerodynamic resistance of the canopy of trees, which are distributed near the ground. Based on the results, the appropriate size of the clear-cut and height for observing the wind environment in mountainous region are suggested. The CFD model is highly applicable to predicting mountain weather, predicting forest fires, predicting dispersion of airborne viruses, odor and pollutants, and further studies on gas diffusion, atmospheric stability, temperature, humidity in the mountainous region are continuously needed.

Fluxes of sensible heat, latent heat, and momentum were measured using a 3D

sonic anemometer and a gas analyzer, and the sensors were installed at the tower that is taller than nearby trees. An automatic open/close chamber system was installed on the ground to measure the respiration of soil. In addition, WMO and CFS recommended that an anemometer should be installed at a point where ambient trees do not affect the wind environment in order to measure the wind environment in mountains. Eventually, the meteorological observations in mountainous regions are conducted in various ways for various purposes. In this thesis, I focused on the wind environment in the mountain region among the various environmental factors such as wind speed, wind direction, air temperature, relative humidity, etc. which measured by weather station in mountain region. In addition, proper installation method to observe wind environment in mountain region in Republic of Korea was suggested in this thesis based on the monitoring method of the wind environment in the mountain region suggested by international standards such as WMO, CFS, etc.

Because the international standards recommended that the wind environment should be observed at points where the trees do not affect the airflow, the effect of environmental factors such as the type of the trees, the height of the trees, the coefficient of inertial resistance of trees and the size of the clear-cut on the airflow inside the clear-cut should be analyzed. Computational Fluid Dynamics (CFD) technique is an effective method for analyzing the airflow inside the clear-cut according to the various environmental factors. For this purpose, 3D CFD simulation models were developed using the widely used commercial CFD simulation package, ANSYS, and open-source CFD simulation package, OpenFOAM, which does not require license cost. Models were validated in order to analyze the wind environment in clear-cut according to the various environmental factors.

3D CFD model was designed using ANSYS and two methodologies were

suggested to apply the air resistance of the trees in mountain terrain to the CFD model. The first method was to design the model by dividing the tree canopy region in the process of designing the model. However, there are disadvantages in this approach in that it is difficult to design a qualified mesh and many points, lines and planes information constituting the 3D CFD model can cause many systematic errors when applying this method to mountain areas with a complex terrain. The second method is to design the 3D CFD model as a single area without dividing the forest canopy area and directly to apply the air resistance coefficient of the trees to the cells located in the canopy region using the UDF code developed by this study. This second method was determined to be a suitable method for mountain terrain modeling because it has the advantages of an easy process for model design and an improvement of mesh quality for CFD modeling process. In addition, CFD model was designed using OpenFOAM, to investigate the same mountain areas. When designing the 3D open-source CFD simulation model using the OpenFOAM, the mesh was designed first, then the canopy region of forest that is distributed around the mountain region area was defined, and finally the air resistance coefficient of the forest was applied. This method also designed a good quality mesh because it excludes the process of designing and dividing the tree canopy region in the process of designing the model. The simulated results using the commercial CFD software and the open-source CFD software were compared with the field experiment results. It was determined that the developed 3D CFD models appropriately simulated the wind environment in the mountain terrain with RMSE values of less than 0.1.

In this study, a proper installation methods of weather station for observing wind environment in a mountain region was suggested by analyzing the wind environment according to the type and size of trees, air resistance of tree, the size of

the clear-cut, etc. The appropriate height for monitoring the wind environment was derived when the type and size of the trees, the air resistance of tree, and the size of the clear-cut were fixed. The appropriate size of clear-cut was derived when the type and the air resistance of trees, and observation height were fixed. In addition, the wind speed conversion factor for estimating the reference wind speed using the wind speed observed at a height of 10 m in the clear-cut was derived, in case the appropriate height or the appropriate size of clear-cut cannot be satisfied.

6.2. Concluding remarks

In this thesis, considering the research budget and time constraints, the CFD model development and analysis were performed focusing on the wind environment among the various parameters to propose a proper method to observe the wind environment in mountain region. In addition, considering the above-mentioned constraints, the developed CFD model was validated by comparing the simulated and the observed wind environment data. Unsteady simulation using LES turbulence model or DNS turbulence model has the merit that it is possible to simulate turbulent kinetic energy and real-time wind environment change. However, the unsteady simulation using the LES turbulence model or the DNS turbulence model in a total of 1080 cases was not feasible due to the computer capacity limitation. Therefore, the steady simulation using the RANS turbulence model was performed to analyze the wind environment in the clear-cut according to various environmental conditions, such as the type of the trees, the height of the trees, the coefficient of inertial resistance of trees and the size of the clear-cut, and to derive the appropriate size of clear-cut and height of the monitoring. It is expected that CFD technology will be

used to analyze evaporation, respiration, and photosynthesis of vegetation, moisture evaporation, solar radiation, and so on.

In addition, a formula for estimating the wind speed at any height in the center of clear-cut was presented in the process of analyzing the wind environment inside the clear-cut. In the future, it is expected that a formula to estimate the wind environment in the forest can be proposed by analyzing the vertical wind velocity profile in the forested region. The installation method of weather station in mountain region to observe the wind environment considering the type and size of tree, air resistance of tree, and the size of clear-cut was suggested. However, the wind environment analysis was conducted only for conditions where the air resistance of trees is 0.3, 0.5, 0.7 or 0.9 m^{-1}. In order to overcome these limitations, it is necessary to develop a method that can estimate the air resistance of the target tree without measuring it through field experiments. For this purpose, it is expected that this coefficient can be easily estimated by analyzing the correlation between image analysis results and the corresponding air resistances measured in the field experiment for various species.

References

Anderson, M., Chen, Z.-Q., Kavvas, M., & Feldman, A. (2000). Coupling HEC-HMS with Atmospheric Models for the Prediction of Watershed Runoff *Building Partnerships* (pp. 1-10).

Anthes, R. A., & Warner, T. T. (1978). Development of hydrodynamic models suitable for air pollution and other mesometerological studies. *Monthly Weather Review, 106*(8), 1045-1078.

Ashie, Y., & Kono, T. (2011). Urban-scale CFD analysis in support of a climate-sensitive design for the Tokyo Bay area. *International Journal of Climatology, 31*(2), 174-188.

Baik, J.-J., Kang, Y.-S., & Kim, J.-J. (2007). Modeling reactive pollutant dispersion in an urban street canyon. *Atmospheric Environment, 41*(5), 934-949.

Bass, B., Krayenhoff, S., Martilli, A., & Stull, R. (2002). Mitigating the urban heat island with green roof infrastructure. *Urban Heat Island Summit: Toronto*.

Bergeles, G., Glekas, I., Prospathopoulos, I., & Voutsinas, S. (1996). *Statistical and physical modelling of wind resources in complex terrain: assessment of the applicability of a 3D Navier Stokes code.* Paper presented at the Proceedings of EUWEC.

Bernardet, L. R., Nance, L., Chuang, H.-Y., Loughe, A., Demirtas, M., Koch, S., & Gall, R. (2005). THE DEVELOPMENTAL TESTBED CENTER WINTER FORECASTING EXPERIMENT 7.1.

Bitog, J., Lee, I.-B., Hwang, H.-S., Shin, M.-H., Hong, S.-W., Seo, I.-H., . . . Pang, Z. (2011). A wind tunnel study on aerodynamic porosity and windbreak drag. *Forest Science and technology, 7*(1), 8-16.

Bitog, J. P., Lee, I.-B., Hwang, H.-S., Shin, M.-H., Hong, S.-W., Seo, I.-H., . . . Pang, Z. (2012). Numerical simulation study of a tree windbreak. *Biosystems engineering, 111*(1), 40-48.

Bjerknes, V. (1904). *Das Problem der Wettervorhersage: betrachtet vom Standpunkte der Mechanik und der Physik*.

Blocken, B., van der Hout, A., Dekker, J., & Weiler, O. (2015). CFD simulation of wind flow over natural complex terrain: case study with validation by field measurements for Ria de Ferrol, Galicia, Spain. *Journal of Wind Engineering and Industrial Aerodynamics, 147*, 43-57.

Bournet, P.-E., & Boulard, T. (2010). Effect of ventilator configuration on the distributed climate of greenhouses: A review of experimental and CFD studies. *Computers and Electronics in Agriculture, 74*(2), 195-217.

Bournet, P., Khaoua, S. O., & Boulard, T. (2007). Numerical prediction of the effect of vent arrangements on the ventilation and energy transfer in a multi-span glasshouse using a bi-band radiation model. *Biosystems Engineering, 98*(2), 224-234.

Bromwich, D. H., Cassano, J. J., Klein, T., Heinemann, G., Hines, K. M., Steffen, K., & Box, J. E. (2001). Mesoscale modeling of katabatic winds over Greenland with the Polar MM5. *Monthly Weather Review, 129*(9), 2290-2309.

Cabré, M. F., Solman, S., & Núñez, M. (2016). Regional climate change scenarios over southern South America for future climate (2080-2099) using the MM5

Model. Mean, interannual variability and uncertainties. *Atmósfera, 29*(1), 35-60.

Cao, J., Tamura, Y., & Yoshida, A. (2012). Wind tunnel study on aerodynamic characteristics of shrubby specimens of three tree species. *Urban forestry & urban greening, 11*(4), 465-476.

Cattin, R., Schaffner, B., & Kunz, S. (2006). *Validation of CFD wind resource modeling in highly complex terrain.* Paper presented at the 2006 European Wind Energy Association Conference.

Cescatti, A., & Marcolla, B. (2004). Drag coefficient and turbulence intensity in conifer canopies. *Agricultural and forest meteorology, 121*(3), 197-206.

Cheng, S., Chen, D., Li, J., Wang, H., & Guo, X. (2007). The assessment of emission-source contributions to air quality by using a coupled MM5-ARPS-CMAQ modeling system: a case study in the Beijing metropolitan region, China. *Environmental Modelling & Software, 22*(11), 1601-1616.

Cheng, W. Y., & Steenburgh, W. J. (2005). Evaluation of surface sensible weather forecasts by the WRF and the Eta models over the western United States. *Weather and Forecasting, 20*(5), 812-821.

Choi, H.-W., Kim, D.-Y., Kim, J.-J., Kim, K.-Y., & Woo, J.-H. (2012). Study on Dispersion Characteristics for Fire Scenarios in an Urban Area Using a CFD-WRF Coupled Model. *Atmosphere, 22*(1), 47-55.

Chow, F. K., De Wekker, S. F., & Snyder, B. J. (2012). *Mountain weather research and forecasting: recent progress and current challenges*: Springer Science & Business Media.

Coen, J. L., Cameron, M., Michalakes, J., Patton, E. G., Riggan, P. J., & Yedinak, K. M. (2013). WRF-Fire: coupled weather–wildland fire modeling with the weather research and forecasting model. *Journal of Applied Meteorology and Climatology, 52*(1), 16-38.

Cornelis, W., & Gabriels, D. (2005). Optimal windbreak design for wind-erosion control. *Journal of Arid Environments, 61*(2), 315-332.

Cui, P.-Y., Li, Z., & Tao, W.-Q. (2016). Buoyancy flows and pollutant dispersion through different scale urban areas: CFD simulations and wind-tunnel measurements. *Building and Environment, 104*, 76-91.

Dhunny, A., Lollchund, M., & Rughooputh, S. (2017). Wind energy evaluation for a highly complex terrain using Computational Fluid Dynamics (CFD). *Renewable Energy, 101*, 1-9.

Di Sabatino, S., Buccolieri, R., Pulvirenti, B., & Britter, R. (2007). Simulations of pollutant dispersion within idealised urban-type geometries with CFD and integral models. *Atmospheric Environment, 41*(37), 8316-8329.

Di Sabatino, S., Buccolieri, R., Pulvirenti, B., & Britter, R. (2008). Flow and pollutant dispersion in street canyons using FLUENT and ADMS-Urban. *Environmental Modeling & Assessment, 13*(3), 369-381.

Dudhia, J. (1993). A nonhydrostatic version of the Penn State–NCAR mesoscale model: Validation tests and simulation of an Atlantic cyclone and cold front. *Monthly Weather Review, 121*(5), 1493-1513.

Fluent, A. (2013). ANSYS fluent theory guide 15.0. *Inc, Canonsburg, PA*.

Forthofer, J. M. (2007). *Modeling wind in complex terrain for use in fire spread prediction.* Colorado State University Fort Collins.

Franke, J., Hirsch, C., Jensen, A., Krüs, H., Schatzmann, M., Westbury, P., . . . Wright, N. (2004). *Recommendations on the use of CFD in wind engineering.* Paper

presented at the Cost action C.
Gavelli, F., Bullister, E., & Kytomaa, H. (2008). Application of CFD (Fluent) to LNG spills into geometrically complex environments. *Journal of hazardous materials, 159*(1), 158-168.
Gidhagen, L., Johansson, C., Langner, J., & Olivares, G. (2004). Simulation of NO x and ultrafine particles in a street canyon in Stockholm, Sweden. *Atmospheric Environment, 38*(14), 2029-2044.
Gopalan, H., Gundling, C., Brown, K., Roget, B., Sitaraman, J., Mirocha, J. D., & Miller, W. O. (2014). A coupled mesoscale–microscale framework for wind resource estimation and farm aerodynamics. *Journal of Wind Engineering and Industrial Aerodynamics, 132*, 13-26.
Gousseau, P., Blocken, B., Stathopoulos, T., & Van Heijst, G. (2011). CFD simulation of near-field pollutant dispersion on a high-resolution grid: a case study by LES and RANS for a building group in downtown Montreal. *Atmospheric Environment, 45*(2), 428-438.
Guan, D., Zhang, Y., & Zhu, T. (2003). A wind-tunnel study of windbreak drag. *Agricultural and forest meteorology, 118*(1), 75-84.
Gultepe, I., & Milbrandt, J. (2007). Microphysical observations and mesoscale model simulation of a warm fog case during FRAM project. *Fog and Boundary Layer Clouds: Fog Visibility and Forecasting*, 1161-1178.
Hang, J., Li, Y., Sandberg, M., Buccolieri, R., & Di Sabatino, S. (2012). The influence of building height variability on pollutant dispersion and pedestrian ventilation in idealized high-rise urban areas. *Building and Environment, 56*, 346-360.
Hwang, I.-S. (2010). Comparison of confidence intervals for testing probabilities of a system. *The Journal of the Korea institute of electronic communication sciences, 5*(5), 435-443.
Hanna, S. R., Hansen, O. R., Ichard, M., & Strimaitis, D. (2009). CFD model simulation of dispersion from chlorine railcar releases in industrial and urban areas. *Atmospheric environment, 43*(2), 262-270.
Hefny, M. M., & Ooka, R. (2008). *Influence of cell geometry and mesh resolution on large eddy simulation predictions of flow around a single building.* Paper presented at the Building Simulation.
Hefny, M. M., & Ooka, R. (2009). CFD analysis of pollutant dispersion around buildings: effect of cell geometry. *Building and Environment, 44*(8), 1699-1706.
Heisler, G. M., & Dewalle, D. R. (1988). 2. Effects of windbreak structure on wind flow. *Agriculture, ecosystems & environment, 22*, 41-69.
Hodur, R. M. (1997). The Naval Research Laboratory's coupled ocean/atmosphere mesoscale prediction system (COAMPS). *Monthly Weather Review, 125*(7), 1414-1430.
Hong, S. (2008). Analytical comparison on ventilation efficiencies of naturally-ventilated multi-spant greenhouse and development of crop model using CFD technology. *MS: Seoul National University (in Korean)*.
Hong, S., Lee, I., Hwang, H., Seo, I., Bitog, J., Kwon, K., . . . Ko, H. (2011a). CFD modelling of livestock odour dispersion over complex terrain, part I: Topographical modelling. *biosystems engineering, 108*(3), 253-264.
Hong, S., Lee, I., Hwang, H., Seo, I., Bitog, J., Kwon, K., . . . Ko, H. (2011b). CFD modelling of livestock odour dispersion over complex terrain, part II:

Dispersion modelling. *Biosystems engineering, 108*(3), 265-279.
Jarraud, M. (2008). Guide to meteorological instruments and methods of observation (WMO-No. 8). *World Meteorological Organisation: Geneva, Switzerland*.
Jeong, J.-H., Song, S.-K., & Kim, Y.-K. (2014). Effects of urban canopy parameters on the simulation of wind fields in urban building environments using the WRF-CFD model. *Proceeding of Korean Meteorological Society*, 2014(10). 976-977.
Jiang, F., Liu, Q., Huang, X., Wang, T., Zhuang, B., & Xie, M. (2012). Regional modeling of secondary organic aerosol over China using WRF/Chem. *Journal of aerosol science, 43*(1), 57-73.
Jiménez, P. A., & Dudhia, J. (2012). Improving the representation of resolved and unresolved topographic effects on surface wind in the WRF model. *Journal of Applied Meteorology and Climatology, 51*(2), 300-316.
Kane, B., & Smiley, E. T. (2006). Drag coefficients and crown area estimation of red maple. *Canadian Journal of Forest Research, 36*(8), 1951-1958.
Kang, G., & Kim, J.-J. (2015). Effects of Trees on Flow and Scalar Dispersion in an Urban Street Canyon. *Atmosphere, 25*(4), 685-692.
Kaoru, I., Akira, K., & Akikazu, K. (2011). The 24-h unsteady analysis of air flow and temperature in a real city by high-speed radiation calculation method. *Building and Environment, 46*(8), 1632-1638.
Kim, E.-R., Park, R. J., Lee, D.-G., & Kim, J.-J. (2015). A Study on the Characteristics of Flow and Reactive PollutantsDispersion in Step-up Street Canyons Using a CFD Model. *Atmosphere, 25*(3), 473-482.
Kim, J.-J., & Baik, J.-J. (1999). A numerical study of thermal effects on flow and pollutant dispersion in urban street canyons. *Journal of applied meteorology, 38*(9), 1249-1261.
Kim, J.-J., & Baik, J.-J. (2001). Urban street-canyon flows with bottom heating. *Atmospheric Environment, 35*(20), 3395-3404.
Kim, J.-J., & Baik, J.-J. (2004). A numerical study of the effects of ambient wind direction on flow and dispersion in urban street canyons using the RNG k–ε turbulence model. *Atmospheric Environment, 38*(19), 3039-3048.
Kim, J.-J., & Baik, J.-J. (2005). An Investigation of Flow and Scalar Dispersion in an Urban Area Using a CFD Model *Asia-Pacific Journal of Atmospheric Sciences, 41*(5), 733-749.
Ko, M. W., Oh, C. B., Han, Y. S., & Do, K. H. (2015). Investigation of Turbulent Analysis Methods for CFD of Gas Dispersion Around a Building. *Fire Science and Engineering, 29*(5), 42-50.
Koizumi, A., Motoyama, J.-i., Sawata, K., Sasaki, Y., & Hirai, T. (2010). Evaluation of drag coefficients of poplar-tree crowns by a field test method. *Journal of wood science, 56*(3), 189-193.
Koo, H.-J., Choi, Y.-J., Kim, K.-R., & Byon, J.-Y. (2009). Simulation of Detailed Wind Flow over a Locally Heated Mountain Area Using a Computational Fluid Dynamics Model, CFD_NIMR_SNU-a fire case at Mt. Hwawang. *Korean Journal of Agricultural and Forest Meteorology, 11*(4), 192-205.
Kwak, K.-H., Baik, J.-J., Ryu, Y.-H., & Lee, S.-H. (2015). Urban air quality simulation in a high-rise building area using a CFD model coupled with mesoscale meteorological and chemistry-transport models. *Atmospheric Environment, 100*, 167-177.
Kwon, K.-s., Lee, I.-b., Zhang, G. Q., & Ha, T. (2015). Computational fluid

dynamics analysis of the thermal distribution of animal occupied zones using the jet-drop-distance concept in a mechanically ventilated broiler house. *Biosystems Engineering, 136*, 51-68.

Labovský, J., & Jelemenský, Ľ. (2013). CFD-based atmospheric dispersion modeling in real urban environments. *Chemical Papers, 67*(12), 1495-1503.

Laprise, R. (1992). The Euler equations of motion with hydrostatic pressure as an independent variable. *Monthly weather review, 120*(1), 197-207.

Lawson, B. D., & Armitage, O. (2008). Weather guide for the Canadian forest fire danger rating system.

Lee, K., Ehsani, R., & Castle, W. (2010). A laser scanning system for estimating wind velocity reduction through tree windbreaks. *Computers and electronics in agriculture, 73*(1), 1-6.

Lee, S.-J., Kim, J., Kang, M., & Bindu, M.-T. (2014). Numerical simulation of local atmospheric circulations in the valley of Gwangneung KoFlux sites. *Korean Journal of Agricultural and Forest Meteorology*, 16(3), 244-258

Lee, Y.-S., & Kim, J.-J. (2011). Effects of an apartment complex on flow and dispersion in an urban area. *Atmosphere, 21*(1), 95-108.

Li, W., Qie, X., Fu, S., Su, D., & Shen, Y. (2016). Simulation of quasi-linear mesoscale convective systems in northern China: Lightning activities and storm structure. *Advances in Atmospheric Sciences, 33*(1), 85-100.

Li, X.-X., Liu, C.-H., Leung, D. Y., & Lam, K. (2006). Recent progress in CFD modelling of wind field and pollutant transport in street canyons. *Atmospheric Environment, 40*(29), 5640-5658.

Lin, X.-J., Barrington, S., Choinière, D., & Prasher, S. (2007). Simulation of the effect of windbreaks on odour dispersion. *Biosystems engineering, 98*(3), 347-363.

Liu, B., Liu, X., Lu, C., Godbole, A., Michal, G., & Tieu, A. K. (2016). Computational fluid dynamics simulation of carbon dioxide dispersion in a complex environment. *Journal of Loss Prevention in the Process Industries, 40*, 419-432.

Liu, C.-H., & Barth, M. C. (2002). Large-eddy simulation of flow and scalar transport in a modeled street canyon. *Journal of Applied Meteorology, 41*(6), 660-673.

Loughner, C. P., Allen, D. J., Zhang, D.-L., Pickering, K. E., Dickerson, R. R., & Landry, L. (2012). Roles of urban tree canopy and buildings in urban heat island effects: Parameterization and preliminary results. *Journal of Applied Meteorology and Climatology, 51*(10), 1775-1793.

Mailhot, J., Strapp, J., MacPherson, J., Benoit, R., Belair, S., Donaldson, N., Froude, F., Benjamin, M., Zawadzki, I., & Rogers, R. (1998). The Montreal-96 Experiment on Regional Mixing and Ozone (MERMOZ): An overview and some preliminary results. *Bulletin of the American Meteorological Society, 79*(3), 433-442.

Mass, C., & Ovens, D. (2010). *WRF model physics: Problems, solutions and a new paradigm for progress.* Paper presented at the Preprints, WRF Users' Workshop, Boulder, CO, NCAR.

Mass, C., & Ovens, D. (2011). *Fixing WRF's high speed wind bias: a new subgrid scale drag parameterization and the role of detailed verification.* Paper presented at the 24th Conference on Weather and Forecasting and 20th Conference on Numerical Weather Prediction, Preprints, 91st American

Meteorological Society Annual Meeting.
Mayhead, G. (1973). Some drag coefficients for British forest trees derived from wind tunnel studies. *Agricultural Meteorology, 12*, 123-130.
Mayhead, G., Gardiner, J., & Durrant, D. (1975). A report on the physical properties of conifers in relation to plantation stability. Forestry Commission. *Research and Development Division, Edinburgh, Scotland*.
McBride, M., Reeves, A., Vanderheyden, M., Lea, C., & Zhou, X. (2001). Use of advanced techniques to model the dispersion of chlorine in complex terrain. *Process Safety and Environmental Protection, 79*(2), 89-102.
Meroney, R. N. (2012). CFD modeling of dense gas cloud dispersion over irregular terrain. *Journal of Wind Engineering and Industrial Aerodynamics, 104*, 500-508.
Miao, Y., Liu, S., Chen, B., Zhang, B., Wang, S., & Li, S. (2013). Simulating urban flow and dispersion in Beijing by coupling a CFD model with the WRF model. *Advances in atmospheric sciences, 30*(6), 1663.
Milliez, M., & Carissimo, B. (2007). Numerical simulations of pollutant dispersion in an idealized urban area, for different meteorological conditions. *Boundary-Layer Meteorology, 122*(2), 321-342.
Mughal, M. O., Lynch, M., Yu, F., McGann, B., Jeanneret, F., & Sutton, J. (2017). Wind modelling, validation and sensitivity study using Weather Research and Forecasting model in complex terrain. *Environmental Modelling & Software, 90*, 107-125.
NRFA. (2010). Guidelines for the Installation, Use and Maintenance of Remote Automated Weather Stations (RAWS) Retrieved 11, 2016, from http://www.nrfa.org.nz/Operational%20documents/RAWS%20Guidelines%20V2%20%202010.pdf
Park, S.-B., & Baik, J.-J. (2007). An investigation of flow and pollutant dispersion in three-dimensional asymmetric street canyons using a CFD model. *Journal of Korean Society for Atmospheric Environment, 23*(2), 214-224.
Pontiggia, M., Derudi, M., Alba, M., Scaioni, M., & Rota, R. (2010). Hazardous gas releases in urban areas: Assessment of consequences through CFD modelling. *Journal of Hazardous Materials, 176*(1), 589-596.
Pontiggia, M., Landucci, G., Busini, V., Derudi, M., Alba, M., Scaioni, M., . . . Rota, R. (2011). CFD model simulation of LPG dispersion in urban areas. *Atmospheric environment, 45*(24), 3913-3923.
Pospisil, J., Katolicky, J., & Jicha, M. (2004). A comparison of measurements and CFD model predictions for pollutant dispersion in cities. *Science of the total Environment, 334*, 185-195.
Raine, J., & Stevenson, D. (1977). Wind protection by model fences in a simulated atmospheric boundary layer. *Journal of Wind Engineering and Industrial Aerodynamics, 2*(2), 159-180.
Ran, N., Katul, G. G., Horn, H. S., & Thomas, S. M. (2002). Mechanisms of long-distance dispersal of seeds by wind. *Nature, 418*(6896), 409.
Raymer, W. (1962). Wind resistance of conifers.
Ren, X., & Perrie, W. (2006). Air-sea interaction of typhoon Sinlaku (2002) simulated by the Canadian MC2 model. *Advances in atmospheric sciences, 23*(4), 521-530.
Riddle, A., Carruthers, D., Sharpe, A., McHugh, C., & Stocker, J. (2004). Comparisons between FLUENT and ADMS for atmospheric dispersion

modelling. *Atmospheric environment, 38*(7), 1029-1038.
Robert, A. (1981). A stable numerical integration scheme for the primitive meteorological equations. *Atmosphere-Ocean, 19*(1), 35-46.
Robert, A. (1982). A semi-Lagrangian and semi-implicit numerical integration scheme for the primitive meteorological equations. *Journal of the Meteorological Society of Japan. Ser. II, 60*(1), 319-325.
Roodbaraky, H., Baker, C., Dawson, A., & Wright, C. (1994). Experimental observations of the aerodynamic characteristics of urban trees. *Journal of Wind Engineering and Industrial Aerodynamics, 52*, 171-184.
Ross, S. M. (1987). Introduction to Probability and Statistics for Engineers and Scientists John Wiley & Sons: Inc.
Roux, G., Liu, Y., Monache, L., Sheu, R.-S., & Warner, T. T. (2009). *Verification of high resolution WRF-RTFDDA surface forecasts over mountains and plains.* Paper presented at the Proceedings of the 10th WRF Users' Workshop.
Rudnicki, M., Mitchell, S. J., & Novak, M. D. (2004). Wind tunnel measurements of crown streamlining and drag relationships for three conifer species. *Canadian Journal of Forest Research, 34*(3), 666-676.
Salim, S. M., Buccolieri, R., Chan, A., & Di Sabatino, S. (2011). Numerical simulation of atmospheric pollutant dispersion in an urban street canyon: Comparison between RANS and LES. *Journal of Wind Engineering and Industrial Aerodynamics, 99*(2), 103-113.
Seo, I.-h., Lee, I.-b., Hong, S.-w., Noh, H.-s., & Park, J.-h. (2015). Web-based forecasting system for the airborne spread of livestock infectious disease using computational fluid dynamics. *Biosystems Engineering, 129*, 169-184.
Seo, I.-h., Lee, I.-b., Moon, O.-k., Jung, N.-s., Lee, H.-j., Hong, S.-w., Kwon, K.-s., & Bitog, J.P. (2014). Prediction of the spread of highly pathogenic avian influenza using a multifactor network: Part 1 – Development and application of computational fluid dynamics simulations of airborne dispersion. *Biosystems Engineering*, 121, 160-176
Sini, J.-F., Anquetin, S., & Mestayer, P. G. (1996). Pollutant dispersion and thermal effects in urban street canyons. *Atmospheric environment, 30*(15), 2659-2677.
Skamarock, W. C., & Klemp, J. B. (2008). A time-split nonhydrostatic atmospheric model for weather research and forecasting applications. *Journal of Computational Physics, 227*(7), 3465-3485.
Slusher, J. P., & Wallace, D. (1997). Planning tree windbreaks in Missouri.
Středová, H., Podhrázská, J., Litschmann, T., Středa, T., & Rožnovský, J. (2012). Aerodynamic parameters of windbreak based on its optical porosity. *Contributions to Geophysics and Geodesy, 42*(3), 213-226.
Takane, Y., Ohashi, Y., Kusaka, H., Shigeta, Y., & Kikegawa, Y. (2013). Effects of synoptic-scale wind under the typical summer pressure pattern on the mesoscale high-temperature events in the Osaka and Kyoto urban areas by the WRF model. *Journal of Applied Meteorology and climatology, 52*(8), 1764-1778.
Tominaga, Y., Mochida, A., Murakami, S., & Sawaki, S. (2008). Comparison of various revised k–ε models and LES applied to flow around a high-rise building model with 1: 1: 2 shape placed within the surface boundary layer. *Journal of Wind Engineering and Industrial Aerodynamics, 96*(4), 389-411.
Trusilova, K., Jung, M., Churkina, G., Karstens, U., Heimann, M., & Claussen, M.

(2008). Urbanization impacts on the climate in Europe: Numerical experiments by the PSU–NCAR Mesoscale Model (MM5). *Journal of Applied Meteorology and Climatology, 47*(5), 1442-1455.

Uchida, T., & Ohya, Y. (2003). Large-eddy simulation of turbulent airflow over complex terrain. *Journal of Wind Engineering and Industrial Aerodynamics, 91*(1), 219-229.

Vaidya, S., Mukhopadhyay, P., Trivedi, D., Sanjay, J., & Singh, S. (2004). Prediction of tropical systems over Indian region using mesoscale model. *Meteorology and Atmospheric Physics, 86*(1), 63-72.

Vollsinger, S., Mitchell, S. J., Byrne, K. E., Novak, M. D., & Rudnicki, M. (2005). Wind tunnel measurements of crown streamlining and drag relationships for several hardwood species. *Canadian Journal of Forest Research, 35*(5), 1238-1249.

Waewsak, J., Landry, M., & Gagnon, Y. (2015). Offshore wind power potential of the Gulf of Thailand. *Renewable Energy, 81*, 609-626.

Wilson, J. D. (1985). Numerical studies of flow through a windbreak. *Journal of Wind Engineering and Industrial Aerodynamics, 21*(2), 119-154.

Xie, X., Huang, Z., & Wang, J.-s. (2005). Impact of building configuration on air quality in street canyon. *Atmospheric Environment, 39*(25), 4519-4530.

Xing, J., Liu, Z., Huang, P., Feng, C., Zhou, Y., Zhang, D., & Wang, F. (2013). Experimental and numerical study of the dispersion of carbon dioxide plume. *Journal of hazardous materials, 256*, 40-48.

Xue, M., Droegemeier, K. K., & Wong, V. (2000). The Advanced Regional Prediction System (ARPS)–A multi-scale nonhydrostatic atmospheric simulation and prediction model. Part I: Model dynamics and verification. *Meteorology and atmospheric physics, 75*(3), 161-193.

Xue, M., Wang, D., Gao, J., Brewster, K., & Droegemeier, K. K. (2003). The Advanced Regional Prediction System (ARPS), storm-scale numerical weather prediction and data assimilation. *Meteorology and Atmospheric Physics, 82*(1), 139-170.

Xueling, C., & Fei, H. (2005). Numerical studies on flow fields around buildings in an urban street canyon and cross-road. *Advances in Atmospheric Sciences, 22*(2), 290-299.

Yang, H.-J., & Kim, J.-J. (2015). Assessment of Observation Environment for Surface Wind in Urban Areas Using a CFD model. *Atmosphere. Korean Meteorological Society, 25*(3), 449-459.

Zheng, Y., Miao, Y., Liu, S., Chen, B., Zheng, H., & Wang, S. (2015). Simulating flow and dispersion by using WRF-CFD coupled model in a built-up area of Shenyang, China. *Advances in Meteorology, 2015*.

Zhu, J.-j., Matsuzaki, T., & Jiang, F.-q. (2004). *Wind on tree windbreaks*: China Forestry Publishing House.

Appendix I. UDF code for porosity modelling of FLUENT

```
#include "stdio.h"
#include "udf.h"
#include "mem.h"
#include "sg.h"

#define udm_usage 1
#define udm_CW 0

typedef struct {
        real x;
        real y;
        real z;
        real usage;
}coordinates;

coordinates *input;

DEFINE_INIT(INIT_Solution, domain)
{
    #if !RP_HOST
    cell_t c;
    Thread *thread;
    FILE *fin;
    real xc[ND_ND];
    real dist, xcor, ycor, count, temp, temp2;
    int ncol, nrow, dcell, i, j, temp3;
    fin = fopen("satellite.txt", "r");
    fscanf(fin, "%d %d %f %f %d", &ncol, &nrow, &xcor, &ycor, &dcell);
    count = ncol * nrow;
    input = (coordinates*)malloc(count*sizeof(coordinates));
    for(i = 0; i<nrow; i++) {
        for(j=0; j<ncol; j++) {
            temp3 = ncol*i + j;
            input[temp3].x = xcor + dcell*j;
            input[temp3].y = ycor + (nrow-1)*dcell - dcell*i;
            fscanf(fin, "%f", &input[temp3].usage);
```

```
            }
        }
        fclose(fin);

        for(i=0; i<count; i++)
        {
//              Message("\n    input[%d].x : %5.1f     input[%d].y : %5.1f     usage : %5.1f", i, input[i].x,
i, input[i].y, input[i].usage);
            thread_loop_c (thread, domain)
            {
                begin_c_loop_int (c, thread)
                {
                    C_CENTROID(xc, c, thread);
                    temp = input[i].x + dcell;
                    if(xc[0] >= input[i].x && xc[0] < temp)
                    {
                        temp2 = input[i].y + dcell;
                        if(xc[1] >= input[i].y && xc[1] < temp2)
                        {
                            C_UDMI(c, thread, udm_usage) = input[i].usage;
                        }
                    }
                }
                end_c_loop_int (c, thread)
            }
        }

        free(input);

        thread_loop_c (thread, domain)
        {
            begin_c_loop_int (c, thread)
            {
                C_UDMI(c, thread, udm_CW) = C_WALL_DIST(c, thread);
            }
            end_c_loop_int (c, thread)
        }

        Message("\n Initialization finish");
        #endif
```

```
}

DEFINE_PROFILE(ir_porosity, thread, position)
{
    #if !RP_HOST
    real z;
    int usage;
    cell_t c;
    begin_c_loop(c, thread)
    {
        usage = C_UDMI(c, thread, udm_usage);
        switch (usage) {
            case 1 : // Broadleaf
            {
                z = C_UDMI(c, thread, udm_CW);
                    if(z<17.0)
                    {
                        C_PROFILE(c, thread, position) = 0.539;
                    }else C_PROFILE(c, thread, position) = 0.0;
            }
            break;
            case 2 : // Needleleaf
            {
                z = C_UDMI(c, thread, udm_CW);
                if(z > 13.4)
                {
                    if(z < 30.0)
                    {
                        C_PROFILE(c, thread, position) = 0.268;
                    }else C_PROFILE(c, thread, position) = 0.0;
                }else C_PROFILE(c, thread, position) = 0.0;
            }
            break;
            case 3 :
            {
                z = C_UDMI(c, thread, udm_CW);
                    if(z<23.6)
                    {
                        C_PROFILE(c, thread, position) = 0.4035;
                    }else C_PROFILE(c, thread, position) = 0.0;
```

```
                }
                break;
                case 4 :
                        C_PROFILE(c, thread, position) = 0.0;
            }
        }
        end_c_loop(c, thread)
        #endif
}
```

Appendix II. OpenFOAM codes

A. System

A.1. blockMeshDict

```
/*--------------------------------*- C++ -*----------------------------------*\
| =========                 |                                                 |
| \\      /  F ield         | OpenFOAM: The Open Source CFD Toolbox           |
|  \\    /   O peration     | Version:  4.0                                   |
|   \\  /    A nd           | Web:      www.OpenFOAM.org                      |
|    \\/     M anipulation  |                                                 |
\*---------------------------------------------------------------------------*/
FoamFile
{
    version     2.0;
    format      ascii;
    class       dictionary;
    object      blockMeshDict;
}
// * * * * * * * * * * * * * * * * * * * * * * * * * * * * * * * * * * * * //

vertices
(
    (-3300 -3300 0)
    (5700 -3300 0)
    (5700 5700 0)
    (-3300 5700 0)
    (-3300 -3300 1500)
    (5700 -3300 1500)
    (5700 5700 1500)
    (-3300 5700 1500)
);

blocks
(
    hex (0 1 2 3 4 5 6 7) (90 90 15) simpleGrading (1 1 1)
);
```

```
edges
(
);

boundary
(
    west
    {
        type patch;
        faces
        (
            (0 4 7 3)
        );
    }
    east
    {
        type patch;
        faces
        (
            (2 6 5 1)
        );
    }
    north
    {
        type patch;
        faces
        (
            (2 3 7 6)
        );
    }
    south
    {
        type patch;
        faces
        (
            (0 1 5 4)
        );
    }
    bottom
```

```
    {
        type patch;
        faces
        (
            (0 3 2 1)
        );
    }
    sky
    {
        type patch;
        faces
        (
            (4 5 6 7)
        );
    }
);

mergePatchPairs
(
);
```

A.2. controlDict

```
/*--------------------------------*- C++ -*----------------------------------*\
| =========                 |                                                 |
| \\      /  F ield         | OpenFOAM: The Open Source CFD Toolbox           |
|  \\    /   O peration     | Version:  4.0                                   |
|   \\  /    A nd           | Web:      www.OpenFOAM.org                      |
|    \\/     M anipulation  |                                                 |
\*---------------------------------------------------------------------------*/
FoamFile
{
    version     2.0;
    format      ascii;
    class       dictionary;
    location    "system";
    object      controlDict;
}
// * * * * * * * * * * * * * * * * * * * * * * * * * * * * * * * * * * * * //

application     porousSimpleFoam;
startFrom       latestTime;
startTime       0;
stopAt          endTime;
endTime         5000;
deltaT          1;
writeControl    timeStep;
writeInterval   5000;
purgeWrite      0;
writeFormat     ascii;
writePrecision  6;
writeCompression off;
timeFormat      general;
timePrecision   6;
graphFormat     raw;
runTimeModifiable true;
```

A.3. decomposeParDict

```
/*--------------------------------*- C++ -*----------------------------------*\
| =========                 |                                                 |
| \\      /  F ield         | OpenFOAM: The Open Source CFD Toolbox           |
|  \\    /   O peration     | Version:  4.0                                   |
|   \\  /    A nd           | Web:      www.OpenFOAM.org                      |
|    \\/     M anipulation  |                                                 |
\*---------------------------------------------------------------------------*/
FoamFile
{
    version     2.0;
    format      ascii;
    class       dictionary;
    location    "system";
    object      decomposeParDict;
}
// * * * * * * * * * * * * * * * * * * * * * * * * * * * * * * * * * * * * //

numberOfSubdomains 8;
method              simple;
simpleCoeffs
{
        n                   (2 2 2);
        delta               0.001;
}
```

A.4. fvSchemes

```
/*--------------------------------*- C++ -*----------------------------------*\
| =========                 |                                                 |
| \\      /  F ield         | OpenFOAM: The Open Source CFD Toolbox           |
|  \\    /   O peration     | Version:  4.0                                   |
|   \\  /    A nd           | Web:      www.OpenFOAM.org                      |
|    \\/     M anipulation  |                                                 |
\*---------------------------------------------------------------------------*/
FoamFile
{
    version     2.0;
    format      ascii;
    class       dictionary;
    location    "system";
    object      fvSchemes;
}
// * * * * * * * * * * * * * * * * * * * * * * * * * * * * * * * * * * * * //

ddtSchemes
{
    default         steadyState;
}

gradSchemes
{
    default         Gauss linear;
}

divSchemes
{
    default                         none;
    div(phi,U)                      bounded Gauss upwind;
    div((nuEff*dev2(T(grad(U)))))   Gauss linear;
    div(phi,epsilon)                bounded Gauss upwind;
    div(phi,k)                      bounded Gauss upwind;
}

laplacianSchemes
{
```

```
    default         Gauss linear corrected;
}

interpolationSchemes
{
    default         linear;
}

snGradSchemes
{
    default         corrected;
}

wallDist
{
    method          meshWave;
}
```

A.5. fvSolution

```
/*--------------------------------*- C++ -*----------------------------------*\
| =========                 |                                                 |
| \\      /  F ield         | OpenFOAM: The Open Source CFD Toolbox           |
|  \\    /   O peration     | Version:  4.0                                   |
|   \\  /    A nd           | Web:      www.OpenFOAM.org                      |
|    \\/     M anipulation  |                                                 |
\*---------------------------------------------------------------------------*/
FoamFile
{
    version     2.0;
    format      ascii;
    class       dictionary;
    location    "system";
    object      fvSolution;
}
// * * * * * * * * * * * * * * * * * * * * * * * * * * * * * * * * * * * * //

solvers
{
    p
    {
        solver                  GAMG;
        tolerance               1e-08;
        relTol                  0.05;
        smoother                GaussSeidel;
        nCellsInCoarsestLevel   20;
    }

    U
    {
        solver          smoothSolver;
        smoother        GaussSeidel;
        nSweeps         2;
        tolerance       1e-06;
        relTol          0.1;
    }

    "(k|epsilon)"
```

```
    {
        solver          smoothSolver;
        smoother        GaussSeidel;
        nSweeps         2;
        tolerance       1e-07;
        relTol          0.1;
    }

}

SIMPLE
{
    nNonOrthogonalCorrectors 0;

    residualControl
    {
        p               1e-2;
        U               1e-5;
        e               1e-3;
        "(k|epsilon|omega)" 1e-5;
    }
}

relaxationFactors
{
    fields
    {
        p               0.3;
    }
    equations
    {
        U               0.7;
        K               0.9;
        e               0.9;
    }
}
```

A.6. meshQualityDict

```
/*--------------------------------*- C++ -*----------------------------------*\
| =========                 |                                                 |
| \\      /  F ield         | OpenFOAM: The Open Source CFD Toolbox           |
|  \\    /   O peration     | Version:  4.0                                   |
|   \\  /    A nd           | Web:      www.OpenFOAM.org                      |
|    \\/     M anipulation  |                                                 |
\*---------------------------------------------------------------------------*/
FoamFile
{
    version     2.0;
    format      ascii;
    class       dictionary;
    object      meshQualityDict.cfg;
}
// * * * * * * * * * * * * * * * * * * * * * * * * * * * * * * * * * * * * //

maxNonOrtho             65;
maxBoundarySkewness     20;
maxInternalSkewness     4;
maxConcave              80;

// Minimum cell pyramid volume; case dependent
minVol                  1e-13;

//  1e-15 (small positive) to enable tracking
// -1e+30 (large negative) for best layer insertion
minTetQuality           1e-15;

// if >0 : preserve single cells with all points on the surface if the
// resulting volume after snapping (by approximation) is larger than
// minVolCollapseRatio times old volume (i.e. not collapsed to flat cell).
//  If <0 : delete always.
//minVolCollapseRatio   0.5;

minArea                 -1;
minTwist                0.02;
minDeterminant          0.001;
minFaceWeight           0.05;
```

```
minVolRatio         0.01;
minTriangleTwist    -1;
nSmoothScale        4;
errorReduction      0.75;

relaxed
{
    maxNonOrtho     75;
}
```

A.7. sampleDict

```
/*--------------------------------*- C++ -*----------------------------------*\
| =========                 |                                                 |
| \\      /  F ield         | OpenFOAM: The Open Source CFD Toolbox           |
|  \\    /   O peration     | Version:  4.0                                   |
|   \\  /    A nd           | Web:      www.OpenFOAM.org                      |
|    \\/     M anipulation  |                                                 |
\*---------------------------------------------------------------------------*/
FoamFile
{
    version     2.0;
    format      ascii;
    class       dictionary;
    location    "system";
    object      sampleDict;
}
// * * * * * * * * * * * * * * * * * * * * * * * * * * * * * * * * * * * * //

type sets;
libs ("libsampling.so");

interpolationScheme cellPoint;

setFormat       raw;

sets
(
    GCK
    {
        type        uniform;
        axis        xyz;
        start       (1417.1292 1145.5622 114.22);
        end         (1417.1292 1145.5622 154.22);
        nPoints     41;
    }
);

fields          ( U );
```

A.8. snappyHexMeshDict

```
/*--------------------------------*- C++ -*----------------------------------*\
| =========                 |                                                 |
| \\      /  F ield         | OpenFOAM: The Open Source CFD Toolbox           |
|  \\    /   O peration     | Version:  4.0                                   |
|   \\  /    A nd           | Web:      www.OpenFOAM.org                      |
|    \\/     M anipulation  |                                                 |
\*---------------------------------------------------------------------------*/
FoamFile
{
    version     2.0;
    format      ascii;
    class       dictionary;
    object      snappyHexMeshDict;
}

// * * * * * * * * * * * * * * * * * * * * * * * * * * * * * * * * * * * * //

// Which of the steps to run
castellatedMesh    true;
snap               true;
addLayers          false;


// Geometry. Definition of all surfaces. All surfaces are of class
// searchableSurface.
// Surfaces are used
// - to specify refinement for any mesh cell intersecting it
// - to specify refinement for any mesh cell inside/outside/near
// - to 'snap' the mesh boundary to the surface
geometry
{
    buffer.stl
    {
        type        triSurfaceMesh;
        name        gwangneungBuffer;
    }

    contourstl
```

```
    {
        type        triSurfaceMesh;
        name        gwangneung;
    }
};



// Settings for the castellatedMesh generation.
castellatedMeshControls
{

    // Refinement parameters
    // ~~~~~~~~~~~~~~~~~~~~~~

    // If local number of cells is >= maxLocalCells on any processor
    // switches from from refinement followed by balancing
    // (current method) to (weighted) balancing before refinement.
    maxLocalCells       10000000;

    // Overall cell limit (approximately). Refinement will stop immediately
    // upon reaching this number so a refinement level might not complete.
    // Note that this is the number of cells before removing the part which
    // is not 'visible' from the keepPoint. The final number of cells might
    // actually be a lot less.
    maxGlobalCells      20000000;

    // The surface refinement loop might spend lots of iterations
    // refining just a few cells. This setting will cause refinement
    // to stop if <= minimumRefine are selected for refinement. Note:
    // it will at least do one iteration (unless the number of cells
    // to refine is 0)
    minRefinementCells  10;

    // Number of buffer layers between different levels.
    // 1 means normal 2:1 refinement restriction, larger means slower
    // refinement.
    nCellsBetweenLevels 5;
```

```
// Explicit feature edge refinement
// ~~~~~~~~~~~~~~~~~~~~~~~~~~~~~~~~~~~~

// Specifies a level for any cell intersected by its edges.
// This is a featureEdgeMesh, read from constant/triSurface for now.
features
(
    {
        file            "buffer.eMesh";
        level           1;
    }

    {
        file            "contour.eMesh";
        level           1;
    }

);



// Surface based refinement
// ~~~~~~~~~~~~~~~~~~~~~~~~~~

// Specifies two levels for every surface. The first is the minimum level,
// every cell intersecting a surface gets refined up to the minimum level.
// The second level is the maximum level. Cells that 'see' multiple
// intersections where the intersections make an
// angle > resolveFeatureAngle get refined up to the maximum level.

refinementSurfaces
{
    gwangneungBuffer
    {
        // Surface-wise min and max refinement level
        level           (2 4);
    }

     gwangneung
```

```
        {
            level               (2 4);
        }
}

// Resolve sharp angles
resolveFeatureAngle         30;


// Region-wise refinement
// ~~~~~~~~~~~~~~~~~~~~~~~~

// Specifies refinement level for cells in relation to a surface. One of
// three modes
// - distance. 'levels' specifies per distance to the surface the
//     wanted refinement level. The distances need to be specified in
//     descending order.
// - inside. 'levels' is only one entry and only the level is used. All
//     cells inside the surface get refined up to the level. The surface
//     needs to be closed for this to be possible.
// - outside. Same but cells outside.

refinementRegions
{
        gwangneung
        {
            mode                distance;
            levels              ((40 4));
        }
}


// Mesh selection
// ~~~~~~~~~~~~~~~

// After refinement patches get added for all refinementSurfaces and
// all cells intersecting the surfaces get put into these patches. The
// section reachable from the locationInMesh is kept.
// NOTE: This point should never be on a face, always inside a cell, even
// after refinement.
```

```
    locationInMesh          (1000 1000 1000);


    // Whether any faceZones (as specified in the refinementSurfaces)
    // are only on the boundary of corresponding cellZones or also allow
    // free-standing zone faces. Not used if there are no faceZones.
    allowFreeStandingZoneFaces      true;
}



// Settings for the snapping.
snapControls
{
    //- Number of patch smoothing iterations before finding correspondence
    //  to surface
    nSmoothPatch            5;

    //- Relative distance for points to be attracted by surface feature point
    //  or edge. True distance is this factor times local
    //  maximum edge length.
    tolerance               1.0;

    //- Number of mesh displacement relaxation iterations.
    nSolveIter              30;

    //- Maximum number of snapping relaxation iterations. Should stop
    //  before upon reaching a correct mesh.
    nRelaxIter              10;

    //- Highly experimental and wip: number of feature edge snapping
    //  iterations. Leave out altogether to disable.
    //  Of limited use in this case since faceZone faces not handled.
    nFeatureSnapIter        10;
}



// Settings for the layer addition.
addLayersControls
```

```
{
    relativeSizes       true;

    // Per final patch (so not geometry!) the layer information
    layers
    {
        maxY
        {
            nSurfaceLayers  3;
        }
    }

    // Expansion factor for layer mesh
    expansionRatio      1.3;

    // Wanted thickness of final added cell layer. If multiple layers
    // is the thickness of the layer furthest away from the wall.
    // Relative to undistorted size of cell outside layer.
    // See relativeSizes parameter.
    finalLayerThickness 1;

    // Minimum thickness of cell layer. If for any reason layer
    // cannot be above minThickness do not add layer.
    // Relative to undistorted size of cell outside layer.
    minThickness        0.1;

    // If points get not extruded do nGrow layers of connected faces that are
    // also not grown. This helps convergence of the layer addition process
    // close to features.
    // Note: changed(corrected) w.r.t 17x! (didn't do anything in 17x)
    nGrow               0;

    // Advanced settings

    // When not to extrude surface. 0 is flat surface, 90 is when two faces
    // are perpendicular
    featureAngle        30;

    // Maximum number of snapping relaxation iterations. Should stop
    // before upon reaching a correct mesh.
```

```
    nRelaxIter          3;

    // Number of smoothing iterations of surface normals
    nSmoothSurfaceNormals   1;

    // Number of smoothing iterations of interior mesh movement direction
    nSmoothNormals      3;

    // Smooth layer thickness over surface patches
    nSmoothThickness    2;

    // Stop layer growth on highly warped cells
    maxFaceThicknessRatio   0.5;

    // Reduce layer growth where ratio thickness to medial
    // distance is large
    maxThicknessToMedialRatio   1;

    // Angle used to pick up medial axis points
    // Note: changed(corrected) w.r.t 17x! 90 degrees corresponds to 130 in 17x.
    minMedianAxisAngle      90;

    // Create buffer region for new layer terminations
    nBufferCellsNoExtrude       0;

    // Overall max number of layer addition iterations. The mesher will exit
    // if it reaches this number of iterations; possibly with an illegal
    // mesh.
    nLayerIter          50;
}



// Generic mesh quality settings. At any undoable phase these determine
// where to undo.
meshQualityControls
{
    //- Maximum non-orthogonality allowed. Set to 180 to disable.
    maxNonOrtho         65;
```

```
//- Max skewness allowed. Set to <0 to disable.
maxBoundarySkewness     20;
maxInternalSkewness     4;

//- Max concaveness allowed. Is angle (in degrees) below which concavity
//    is allowed. 0 is straight face, <0 would be convex face.
//    Set to 180 to disable.
maxConcave              80;

//- Minimum pyramid volume. Is absolute volume of cell pyramid.
//    Set to a sensible fraction of the smallest cell volume expected.
//    Set to very negative number (e.g. -1E30) to disable.
minVol                  1e-13;

//- Minimum quality of the tet formed by the face-centre
//    and variable base point minimum decomposition triangles and
//    the cell centre. This has to be a positive number for tracking
//    to work. Set to very negative number (e.g. -1E30) to
//    disable.
//        <0 = inside out tet,
//          0 = flat tet
//          1 = regular tet
minTetQuality           -1; // 1e-30;

//- Minimum face area. Set to <0 to disable.
minArea                 -1;

//- Minimum face twist. Set to <-1 to disable. dot product of face normal
//    and face centre triangles normal
minTwist                0.01;

//- Minimum normalised cell determinant
//    1 = hex, <= 0 = folded or flattened illegal cell
minDeterminant          0.001;

//- minFaceWeight (0 -> 0.5)
minFaceWeight           0.05;

//- minVolRatio (0 -> 1)
minVolRatio             0.01;
```

```
        //must be >0 for Fluent compatibility
        minTriangleTwist        -1;


        // Advanced

        //- Number of error distribution iterations
        nSmoothScale            4;
        //- Amount to scale back displacement at error points
        errorReduction          0.75;

        // Optional : some meshing phases allow usage of relaxed rules.
        // See e.g. addLayersControls::nRelaxedIter.
        relaxed
        {
            //- Maximum non-orthogonality allowed. Set to 180 to disable.
            maxNonOrtho         75;
        }
}

// Advanced
// Merge tolerance. Is fraction of overall bounding box of initial mesh.
// Note: the write tolerance needs to be higher than this.
mergeTolerance              1e-6;
```

A.9. surfaceFeatureExtractDict

```
/*--------------------------------*- C++ -*----------------------------------*\
| =========                 |                                                 |
| \\      /  F ield         | OpenFOAM: The Open Source CFD Toolbox           |
|  \\    /   O peration     | Version:  4.0                                   |
|   \\  /    A nd           | Web:      www.OpenFOAM.org                      |
|    \\/     M anipulation  |                                                 |
\*---------------------------------------------------------------------------*/
FoamFile
{
    version     2.0;
    format      ascii;
    class       dictionary;
    object      surfaceFeatureExtractDict;
}
// * * * * * * * * * * * * * * * * * * * * * * * * * * * * * * * * * * * * //

buffer.stl
{
    extractionMethod    extractFromSurface;

    extractFromSurfaceCoeffs
    {
        // Mark edges whose adjacent surface normals are at an angle less
        // than includedAngle as features
        // - 0    : selects no edges
        // - 180: selects all edges
        includedAngle   180;
    }

    // Write options
    writeFeatureEdgeMesh    yes;
}

contour.stl
{
    extractionMethod    extractFromSurface;

    extractFromSurfaceCoeffs
```

```
    {
        // Mark edges whose adjacent surface normals are at an angle less
        // than includedAngle as features
        // - 0    : selects no edges
        // - 180: selects all edges
        includedAngle           180;
    }

    // Write options
    writeFeatureEdgeMesh      yes;
}
```

A.10. topoSetDict

```
/*--------------------------------*- C++ -*----------------------------------*\
| =========                 |                                                 |
| \\      /  F ield         | OpenFOAM: The Open Source CFD Toolbox           |
|  \\    /   O peration     | Version:  4.0                                   |
|   \\  /    A nd           | Web:      www.OpenFOAM.org                      |
|    \\/     M anipulation  |                                                 |
\*---------------------------------------------------------------------------*/
FoamFile
{
    version     2.0;
    format      ascii;
    class       dictionary;
    object      topoSetDict;
}
// * * * * * * * * * * * * * * * * * * * * * * * * * * * * * * * * * * * * //

actions
(
    {
        name    ConiferBox;
        type    cellSet;
        action  new;
        source  surfaceToCell;
         sourceInfo
         {
             file            "ConiferBox.stl";
             outsidePoints   ((1000 1000 1000)) ;
             includeCut      false;
             includeInside   true;
             includeOutside  false;
             nearDistance    -1;
             curvature       0.9;
         }
    }

    {
        name    DeciduousBox;
        type    cellSet;
```

```
        action      new;
        source      surfaceToCell;
        sourceInfo
        {
            file                "DeciduousBox.stl";
            outsidePoints       ((1000 1000 1000)) ;
            includeCut          false;
            includeInside       true;
            includeOutside      false;
            nearDistance        -1;
            curvature           0.9;
        }
    }

    {
        name        MixedBox;
        type        cellSet;
        action      new;
        source      surfaceToCell;
        sourceInfo
        {
            file                "MixedBox.stl";
            outsidePoints       ((1000 1000 1000)) ;
            includeCut          false;
            includeInside       true;
            includeOutside      false;
            nearDistance        -1;
            curvature           0.9;
        }
    }
);
```

B. constant

B.1. porosityProperties

```
/*--------------------------------*- C++ -*----------------------------------*\
| =========                 |                                                 |
| \\      /  F ield         | OpenFOAM: The Open Source CFD Toolbox           |
|  \\    /   O peration     | Version:  4.0                                   |
|   \\  /    A nd           | Web:      www.OpenFOAM.org                      |
|    \\/     M anipulation  |                                                 |
\*---------------------------------------------------------------------------*/
FoamFile
{
    version     2.0;
    format      ascii;
    class       dictionary;
    location    "constant";
    object      porosityProperties;
}
// * * * * * * * * * * * * * * * * * * * * * * * * * * * * * * * * * * * * //

Conifer
{
    type            DarcyForchheimer;
    active          yes;
    cellZone        ConiferBox;

    DarcyForchheimerCoeffs
    {
        d           (0 0 0);
        f           (0.6478 0.6478 0.6478);

        coordinateSystem
        {
            type            cartesian;
            origin          (0 0 0);
            coordinateRotation
            {
                type        axesRotation;
```

```
            e1          (1 0 0);
            e2          (0 1 0);
        }
    }
}

Deciduous
{
    type            DarcyForchheimer;
    active          yes;
    cellZone        DeciduousBox;

    DarcyForchheimerCoeffs
    {
        d           (0 0 0);
        f           (0.75725 0.75725 0.75725);

        coordinateSystem
        {
            type            cartesian;
            origin          (0 0 0);
            coordinateRotation
            {
                type        axesRotation;
                e1          (1 0 0);
                e2          (0 1 0);
            }
        }
    }
}

Mixed
{
    type            DarcyForchheimer;
    active          yes;
    cellZone        MixedBox;

    DarcyForchheimerCoeffs
    {
```

```
        d               (0 0 0);
        f               (0.702525 0.702525 0.702525);

        coordinateSystem
        {
            type                cartesian;
            origin              (0 0 0);
            coordinateRotation
            {
                type            axesRotation;
                e1              (1 0 0);
                e2              (0 1 0);
            }
        }
    }
}
```

B.2. transportProperties

```
/*--------------------------------*- C++ -*----------------------------------*\
| =========                 |                                                 |
| \\      /  F ield         | OpenFOAM: The Open Source CFD Toolbox           |
|  \\    /   O peration     | Version:  4.0                                   |
|   \\  /    A nd           | Web:      www.OpenFOAM.org                      |
|    \\/     M anipulation  |                                                 |
\*---------------------------------------------------------------------------*/
FoamFile
{
    version     2.0;
    format      ascii;
    class       dictionary;
    object      transportProperties;
}
// * * * * * * * * * * * * * * * * * * * * * * * * * * * * * * * * * * * * //

transportModel  Newtonian;

nu              [0 2 -1 0 0 0 0] 1.5e-05;
```

B.3. turbulenceProperties

```
/*--------------------------------*- C++ -*----------------------------------*\
| =========                 |                                                 |
| \\      /  F ield         | OpenFOAM: The Open Source CFD Toolbox           |
|  \\    /   O peration     | Version:  4.0                                   |
|   \\  /    A nd           | Web:      www.OpenFOAM.org                      |
|    \\/     M anipulation  |                                                 |
\*---------------------------------------------------------------------------*/
FoamFile
{
    version     2.0;
    format      ascii;
    class       dictionary;
    location    "constant";
    object      RASProperties;
}
// * * * * * * * * * * * * * * * * * * * * * * * * * * * * * * * * * * * * //

simulationType RAS;

RAS
{
    RASModel        kEpsilon;

    turbulence      on;

    printCoeffs     on;
}
```

C. boundary conditions and initial conditions

C.1. ABLConditions

```
/*--------------------------------*- C++ -*----------------------------------*\
| =========                 |                                                 |
| \\      /  F ield         | OpenFOAM: The Open Source CFD Toolbox           |
|  \\    /   O peration     | Version:  4.0                                   |
|   \\  /    A nd           | Web:      www.OpenFOAM.org                      |
|    \\/     M anipulation  |                                                 |
\*---------------------------------------------------------------------------*/
```

```
Uref            1.885;
Zref            100;
zDir            (0 0 1);
flowDir         (-1 0 0);
z0              uniform         1.25;
zGround         uniform         0;
value           $internalField;
```

C.2. initialConditions

```
/*--------------------------------*- C++ -*----------------------------------*\
| =========                 |                                                 |
| \\      /  F ield         | OpenFOAM: The Open Source CFD Toolbox           |
|  \\    /   O peration     | Version:  4.0                                   |
|   \\  /    A nd           | Web:      www.OpenFOAM.org                      |
|    \\/     M anipulation  |                                                 |
\*---------------------------------------------------------------------------*/
```

```
flowVelocity        (-1.0 0 0);
pressure            0;
turbulentKE         0.015;
turbulentEpsilon    0.000116;
```

C.3. epsilon

```
/*--------------------------------*- C++ -*----------------------------------*\
| =========                 |                                                 |
| \\      /  F ield         | OpenFOAM: The Open Source CFD Toolbox           |
|  \\    /   O peration     | Version:  4.0                                   |
|   \\  /    A nd           | Web:      www.OpenFOAM.org                      |
|    \\/     M anipulation  |                                                 |
\*---------------------------------------------------------------------------*/
FoamFile
{
    version     2.0;
    format      ascii;
    class       volScalarField;
    location    "0";
    object      epsilon;
}
// * * * * * * * * * * * * * * * * * * * * * * * * * * * * * * * * * * * * //

dimensions      [0 2 -3 0 0 0 0];

#include        "include/initialConditions"

internalField   uniform $turbulentEpsilon;

boundaryField
{
    east
    {
        type            atmBoundaryLayerInletEpsilon;
        #include        "include/ABLConditions"
    }
    west
    {
        type            zeroGradient;
    }
    north
    {
        type            symmetryPlane;
    }
```

```
    south
    {
        type            symmetryPlane;
    }
    sky
    {
        type            symmetryPlane;
    }
    gwangneungBuffer
    {
        type            epsilonWallFunction;
        Cmu             0.09;
        kappa           0.4;
        E               9.8;
        value           $internalField;
    }
    gwangneung
    {
        type            epsilonWallFunction;
        Cmu             0.09;
        kappa           0.4;
        E               9.8;
        value           $internalField;
    }
}
```

C.4. k

```
/*--------------------------------*- C++ -*----------------------------------*\
| =========                 |                                                 |
| \\      /  F ield         | OpenFOAM: The Open Source CFD Toolbox           |
|  \\    /   O peration     | Version:  4.0                                   |
|   \\  /    A nd           | Web:      www.OpenFOAM.org                      |
|    \\/     M anipulation  |                                                 |
\*---------------------------------------------------------------------------*/
FoamFile
{
    version     2.0;
    format      ascii;
    class       volScalarField;
    location    "0";
    object      k;
}
// * * * * * * * * * * * * * * * * * * * * * * * * * * * * * * * * * * * * //

dimensions      [0 2 -2 0 0 0 0];
#include        "include/initialConditions"
internalField   uniform $turbulentKE;

boundaryField
{
    east
    {
        type            atmBoundaryLayerInletK;
        #include        "include/ABLConditions"
    }
    west
    {
        type            zeroGradient;
    }
    north
    {
        type            symmetryPlane;
    }
    south
    {
```

```
        type            symmetryPlane;
    }
    sky
    {
        type            symmetryPlane;
    }
    gwangneungBuffer
    {
        type            kqRWallFunction;
        value           uniform 0.0;
    }
    gwangneung
    {
        type            kqRWallFunction;
        value           uniform 0.0;
    }
}
```

C.5. nut

```
/*--------------------------------*- C++ -*----------------------------------*\
| =========                 |                                                 |
| \\      /  F ield         | OpenFOAM: The Open Source CFD Toolbox           |
|  \\    /   O peration     | Version:  4.0                                   |
|   \\  /    A nd           | Web:      www.OpenFOAM.org                      |
|    \\/     M anipulation  |                                                 |
\*---------------------------------------------------------------------------*/
FoamFile
{
    version     2.0;
    format      ascii;
    class       volScalarField;
    lcoation    "0";
    object      nut;
}
// * * * * * * * * * * * * * * * * * * * * * * * * * * * * * * * * * * * * //

dimensions      [0 2 -1 0 0 0 0];
internalField   uniform 0;
boundaryField
{
    #include "include/ABLConditions"

    east
    {
        type            calculated;
        value           uniform 0;
    }
    west
    {
        type            calculated;
        value           uniform 0;
    }
    north
    {
        type            symmetryPlane;
    }
    south
```

```
    {
        type            symmetryPlane;
    }
    sky
    {
        type            symmetryPlane;
    }
    gwangneungBuffer
    {
        type            nutkAtmRoughWallFunction;
        z0              $z0;
        value           uniform  0.0;
    }
    gwangneung
    {
        type            nutkAtmRoughWallFunction;
        z0              $z0;
        value           uniform  0.0;
    }
}
```

C.6. p

```
/*--------------------------------*- C++ -*----------------------------------*\
| =========                 |                                                 |
| \\      /  F ield         | OpenFOAM: The Open Source CFD Toolbox           |
|  \\    /   O peration     | Version:  4.0                                   |
|   \\  /    A nd           | Web:      www.OpenFOAM.org                      |
|    \\/     M anipulation  |                                                 |
\*---------------------------------------------------------------------------*/
FoamFile
{
    version     2.0;
    format      ascii;
    class       volScalarField;
    object      p;
}
// * * * * * * * * * * * * * * * * * * * * * * * * * * * * * * * * * * * * //

dimensions      [0 2 -2 0 0 0 0];
#include        "include/initialConditions"
internalField   uniform $pressure;

boundaryField
{
    east
    {
        type            zeroGradient;
    }
    west
    {
        type            fixedValue;
        value           $internalField;
    }
    north
    {
        type            symmetryPlane;
    }
    south
    {
        type            symmetryPlane;
```

```
    }
    sky
    {
        type            symmetryPlane;
    }
    gwangneungBuffer
    {
        type            zeroGradient;
    }
    gwangneung
    {
        type            zeroGradient;
    }
}
```

C.7. U

```
/*--------------------------------*- C++ -*----------------------------------*\
| =========                 |                                                 |
| \\      /  F ield         | OpenFOAM: The Open Source CFD Toolbox           |
|  \\    /   O peration     | Version:  4.0                                   |
|   \\  /    A nd           | Web:      www.OpenFOAM.org                      |
|    \\/     M anipulation  |                                                 |
\*---------------------------------------------------------------------------*/
FoamFile
{
    version     2.0;
    format      ascii;
    class       volVectorField;
    object      U;
}
// * * * * * * * * * * * * * * * * * * * * * * * * * * * * * * * * * * * * //

#include        "include/initialConditions"
dimensions      [0 1 -1 0 0 0 0];
internalField   uniform  $flowVelocity;

boundaryField
{
    east
    {
        type            atmBoundaryLayerInletVelocity;
        #include        "include/ABLConditions"
    }
    west
    {
        type            zeroGradient;
    }
    north
    {
        type            symmetryPlane;
    }
    south
    {
        type            symmetryPlane;
```

```
    }
    sky
    {
        type            symmetryPlane;
    }
    gwangneungBuffer
    {
        type            noSlip;
    }
    gwangneung
    {
        type            noSlip;
    }
}
```

국 문 초 록

산악지역에서의 정확한 기상정보 관측, 산불이나 산사태와 같은 산악재해의 예측 및 오염물질의 확산을 예측하기 위해서는 기상환경 관측소의 설치가 중요하다. 세계기상기구(WMO, World Meteorological Organization)과 캐나다 산림청(CFS, Canada Forest Service) 등에서는 숲의 경계에서부터 수고의 10배 이상 이격하여 설치하거나 수고보다 10 m 이상 높게 설치할 것을 권장하고 있다. 하지만 국내 기상관측소 설치 기준은 평지에 대한 설치방법만을 제시하고 있을 뿐, 산악지역에 대한 설치방법은 제시하고 있지 않다. 또한 외국의 산악기상관측소 설치 기준에서 제안하고 있는 수고보다 20배 이상 넓은 개벌지 또는 수고보다 10 m 이상 높은 관측소를 설치하는 것은 비용 및 안전적인 측면 이외에도 충분히 넓은 개벌지의 확보가 어렵기 때문에 현실적이지 않다. 따라서 국내 실정에 맞는 산악기상관측소 설치 방법에 대한 연구가 필요하다. 기상관측시스템의 적정 높이 및 기상관측시스템이 설치되는 개벌지의 적정 크기는 주변 수목의 종류, 수고, 개벌지의 크기 등 다양한 환경조건에서의 개벌지 내 풍환경을 바탕으로 결정되어야 하는데, 현장실험을 통해 산악지역 내 풍환경을 분석할 경우 실험 환경을 통제하기 어렵고 개벌지의 크기와 같은 실험 조건을 다양하게 구성하는데 어려움이 있다. 이러한 현장실험의 단점을 극복하기 위하여 많은 연구자들이 3차원 CFD 시뮬레이션 기법을 활용하고 있으며, 본 연구에서도 CFD를 이용하여 산악지역 내 기상관측타워의 적정

설치방법을 제안하고자 하였다.

2장에서는 논문에 대한 기틀을 다지고 연구 방법론의 적정성을 평가하기 위하여 수 킬로미터 규모의 수평 해상도를 가지는 중규모(mesoscale)의 기상현상을 예측하기 위한 중규모 기상예측 모델링 기법, 100 m 이하의 수평 해상도를 가지는 상세규모(microscale)의 기상현상을 예측하기 위한 중규모 기상예측 모델링 기법, 수목이 기류에 미치는 영향에 대한 연구사 검토를 실시하였다.

3장에서는 상용 CFD 소프트웨어를 이용하여 산악지역에서의 풍환경을 모의할 수 있는 3차원 microscale CFD 모델을 개발하고 수목의 공기저항성을 적용하는 방법을 제안하였다. 상용 CFD 소프트웨어를 이용하여 수목의 공기 저항성을 적용하는 방법은 모델을 설계하는 과정에서 산악지역에 분포하고 있는 수목의 캐노피 영역을 구분하여 설계하는 방법과 수목의 캐노피 영역이 구분되지 않고 설계된 3차원 CFD 모델에 대해서 연산 과정에서 UDF(User defined function)을 이용하는 방법을 제안하였다. 수목의 캐노피 영역을 구분하는 방법은 모델을 설계하는 과정에서 숲 영역에 대한 왜곡이 발생하기 때문에 UDF를 이용하여 캐노피 영역이 위치하는 격자에 수목의 공극저항계수를 적용하는 방법이 적절한 것으로 판단하였다.

그리고 4장에서는 오픈소스 CFD 소프트웨어를 이용하여 산악지역에서의 풍환경을 모의할 수 있는 3차원 microscale CFD 모델을 개발하고 수목의 공기저항성을 적용하는 방법을 제안하였다. 우선적으로 대상지역에 분포하고 있는 숲 영역에 대해서 도메인을 구분하지 않고

3차원 산악지역 모델을 설계하였다. 이후 설계된 모델의 숲 영역에 해당하는 격자들을 따로 그룹지어 수목의 공극저항계수를 적용하는 코드를 개발하였다. 이렇게 3장과 4장에서 개발된 CFD 시뮬레이션 모델들은 현장에서 관측된 풍환경 데이터를 이용하여 검증하였으며 모델의 신뢰도를 확보하였다.

5장에서는 오픈소스 CFD 소프트웨어를 이용하여 수목의 종류, 수목의 공기역학적 공극저항계수 및 수고, 개벌지의 크기 등 다양한 환경조건에서 개벌지 안에서의 풍환경을 분석하였다. 이렇게 분석된 개벌지 안에서의 풍환경 데이터를 이용하여 수목이 분포하고 있는 산악지역에서 수목의 물리적 특성에 따라서 풍환경을 관측함에 있어 적절한 관측 높이 및 적절한 개벌지의 크기를 제안하였다. 또한 이렇게 제시된 적절한 관측 높이 및 개벌지의 크기를 구축하지 못하는 경우에 주변 수목의 영향을 받지 않는 기준 풍속을 추정하기 위한 환산계수를 도출하여 제시하였다.

주요어: 산악기상관측소 설치방법, 산악기상망, 산악지역 모델링,
수목 공극저항, 오픈소스 CFD, 전산유체역학

학 번: 2014-30403